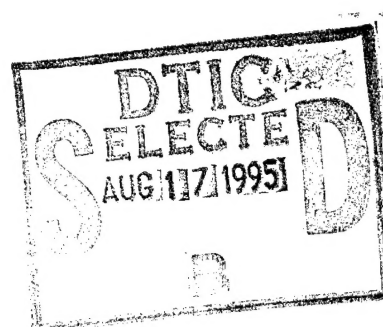


# NAVAL POSTGRADUATE SCHOOL

## Monterey, California



## THESIS

### TRANSIENT DETECTION USING WAVELETS

by

Jorge Antonio Fernandes da Rocha Pitta

March, 1995

Thesis Advisor:

Ralph Hippenstiel

Thesis Co-Advisor:

Monique Fargues

Approved for public release; distribution is unlimited.

DTIC QUALITY INSPECTED 3

19950816 089

REPORT DOCUMENTATION PAGE			Form Approved OMB No. 0704	
Public reporting burden for this collection of information is estimated to average 1 hour per response, including the time for reviewing instruction, searching existing data sources, gathering and maintaining the data needed, and completing and reviewing the collection of information. Send comments regarding this burden estimate or any other aspect of this collection of information, including suggestions for reducing this burden, to Washington headquarters Services, Directorate for Information Operations and Reports, 1215 Jefferson Davis Highway, Suite 1204, Arlington, VA 22202-4302, and to the Office of Management and Budget, Paperwork Reduction Project (0704-0188) Washington DC 20503.				
1. AGENCY USE ONLY (Leave blank)		2. REPORT DATE March, 1995		3. REPORT TYPE AND DATES COVERED Master's Thesis
4. TITLE AND SUBTITLE TRANSIENT DETECTION USING WAVELETS			5. FUNDING NUMBERS	
6. AUTHOR Jorge Antonio Fernandes da Rocha Pitta				
7. PERFORMING ORGANIZATION NAME(S) AND ADDRESS(ES) Naval Postgraduate School Monterey CA 93943-5000			8. PERFORMING ORGANIZATION REPORT NUMBER	
9. SPONSORING/MONITORING AGENCY NAME(S) AND ADDRESS(ES)			10. SPONSORING/MONITORING AGENCY REPORT NUMBER Naval Postgraduate School	
11. SUPPLEMENTARY NOTES The views expressed in this thesis are those of the author and do not reflect the official policy or position of the Department of Defense or the U.S. Government.				
12a. DISTRIBUTION/AVAILABILITY STATEMENT Approved for public release; distribution unlimited			12b. DISTRIBUTION CODE	
13. ABSTRACT  The analysis of transient signals using classical techniques is frequently not satisfactory. The Fourier analysis is based on stationarity of the signal, and transients are non-stationary. A new technique for the analysis of this type of signal, called the Wavelet Transform, was applied to artificial and real signals. A brief theoretical comparison between the Short Time Fourier Transform and the Wavelet Transform is introduced. A multiresolution analysis approach for implementing the transform was used. Computer code for the Discrete Wavelet Transform was implemented. Different types of wavelets to use as basis functions were evaluated.				
14. SUBJECT TERMS Wavelet, Transient Detection, Discrete Wavelet Transform.			15. NUMBER OF PAGES 148	
			16. PRICE CODE	
17. SECURITY CLASSIFICATION OF REPORT Unclassified	18. SECURITY CLASSIFICATION OF THIS PAGE Unclassified	19. SECURITY CLASSIFICATION OF ABSTRACT Unclassified	20. LIMITATION OF ABSTRACT UL	

NSN 7540-01-280-5500

Prescribed by ANSI Std. Z39-18

Standard Form 298 (Rev. 2-89)



Approved for public release; distribution is unlimited.

## TRANSIENT DETECTION USING WAVELETS

Jorge Antonio Fernandes da Rocha Pitta  
Lieutenant Commander, Brazilian Navy  
BSEE, Brazilian Naval Academy, 1982

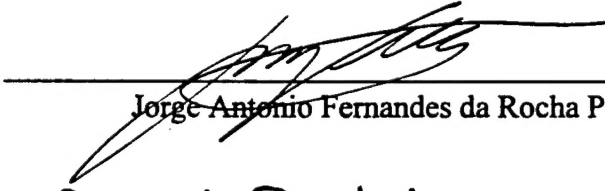
Submitted in partial fulfillment  
of the requirements for the degree of

## MASTER OF SCIENCE IN ELECTRICAL ENGINEERING

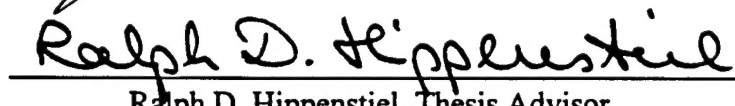
from the

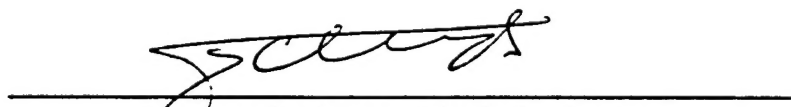
NAVAL POSTGRADUATE SCHOOL  
March, 1995

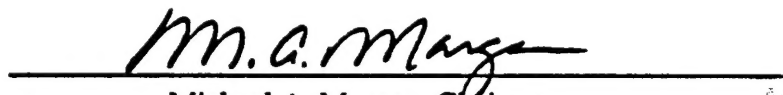
Author:

  
Jorge Antonio Fernandes da Rocha Pitta

Approved by:

  
Ralph D. Hippenstiel, Thesis Advisor

  
Menique P. Fargues, Thesis Co-Advisor

  
Michael A. Morgan, Chairman  
Department of Electrical and Computer Engineering

Accession For	
NTIS CLEAR	<input checked="checked" type="checkbox"/>
DTIC TAB	<input type="checkbox"/>
Unannounced	<input type="checkbox"/>
Justification	
By	
Distribution	
Availability Code	
Page	Author
A-1	





## ABSTRACT

The analysis of transient signals using classical techniques is frequently not satisfactory. The Fourier analysis is based on stationarity of the signal, and transients are non-stationary. A new technique for the analysis of this type of signal, called the Wavelet Transform, was applied to artificial and real signals. A brief theoretical comparison between the Short Time Fourier Transform and the Wavelet Transform is introduced. A multiresolution analysis approach for implementing the transform was used. Computer code for the Discrete Wavelet Transform was implemented. Different types of wavelets to use as basis functions were evaluated.



## TABLE OF CONTENTS

I. INTRODUCTION .....	1
II. TRANSIENT SIGNAL ANALYSIS .....	3
A. THE SHORT TIME FOURIER TRANSFORM ( STFT ) .....	3
1. The Continuous STFT .....	3
2. The Discrete-Time STFT .....	5
B. THE WAVELET TRANSFORM .....	7
1. The Continuous Wavelet Transform .....	9
2. The Discrete Wavelet Transform .....	10
3. Multiresolution Signal Analysis .....	14
a. The Scaling Function and the Scaling Coefficients .....	18
b. Scaling and Wavelet Functions Regularity .....	20
c. The Frequency Domain .....	20
4. Filter Banks and the Discrete Wavelet Transform .....	21
III. WAVELET SIGNAL PROCESSING .....	27
A. INTRODUCTION .....	27
B. MOTHER WAVELETS .....	27
C. THE SIMULATION PHASE .....	32
1. Application of the DWT to Artificial Signals .....	34
2. Evaluation of the DWT for the Artificial Signals .....	43
D. THE TEST PHASE .....	43
1. Metallic Sound Transients. ....	43
2. Radar Pulses .....	44

3. Turn-On / Turn-Off of Push-To-Talk Radios .....	45
IV. CONCLUSIONS .....	67
A. RESULTS .....	67
B. RECOMMENDATIONS FOR FUTURE STUDIES .....	67
APPENDIX A. DEVELOPMENT OF NECESSARY CONDITIONS .....	69
APPENDIX B. DWT OF THE ARTIFICIAL SIGNALS IN NOISE .....	73
APPENDIX C. MATLAB CODES .....	121
LIST OF REFERENCES .....	137
INITIAL DISTRIBUTION LIST .....	139

# I. INTRODUCTION

It is believed that different transmitters have unique signatures, that is, the *transient or turn on-turn off* response is unique to a given transmitter or at least to a particular make. In this thesis we will examine this issue. The resulting process algorithms are also useful in other transient signal applications. We will make use of a new analysis technique called the *Wavelet Transform*.

Analysis of stationary signals is a very well studied subject. The researcher can choose among a variety of methods and apply the best technique. However, the study of non-stationary signals, like transients and signals that show a behavior with sharp transitions, presents a challenge. The Fourier Transform method is not appropriate because it uses as basis function the complex exponential that extends over infinite time, while transients are of short duration. In 1946, Gabor [Ref. 1] proposed a modification to the Fourier Transform. A sliding time-window was introduced to the original transform equation with the intention to *look into* the signal by small portions. Assuming that this small portion has a stationary behavior, the analysis of the signal by the Short Time Fourier Transform (STFT) is appropriate. Other methods such as the Instantaneous Power Spectrum and the Wigner-Ville Distribution [Ref. 11], have also been developed but have similar limitations as the STFT.

The purpose of this thesis is to investigate the use of the Wavelet Transform for the estimation / classification of certain transient signals. The results may be adapted to problems related to acoustic and electromagnetic transients.



## II. TRANSIENT SIGNAL ANALYSIS

### A. THE SHORT TIME FOURIER TRANSFORM ( STFT )

#### 1. The Continuous STFT

The Standard Fourier Transform of a signal is defined as

$$X(\Omega) = \int_{-\infty}^{\infty} x(t)e^{-j\Omega t} dt, \quad (2.1)$$

or as

$$X(\Omega) = \langle x(t), e^{+j\Omega t} \rangle. \quad (2.2)$$

Equations 2.1 and 2.2 show that the Fourier coefficients are computed as inner products of the signal with a complex exponential basis function of infinite duration. It decomposes the signal into frequency components. If the signal components vary sharply in the time domain, after being transformed these local irregularities are spread out over the entire frequency domain losing their localization. This approach may not be suitable if the signal of interest is non-stationary. However, even non-stationary signals can be assumed to have a stationary behavior for a short time. Based on this assumption, Gabor [Ref. 1] proposed the modification of the Standard Fourier Transform. A window  $g(t)$  of short duration and centered at location  $\tau$  was inserted in Equation 2.1 as follows

$$X(\Omega) = \int_{-\infty}^{\infty} x(t)g(t - \tau)e^{-j\Omega t} dt. \quad (2.3)$$

Equation 2.3 is called *Short Time Fourier Transform* ( STFT ). If the analysis window  $g(t)$  is Gaussian the STFT is called the *Gabor Transform*. The analysis window  $g(t)$  is



considered to be part of the specification of the STFT. The short-time section of  $x(t)$  is the product  $x(t)g(t-\tau)$  and it becomes clear that changing the analysis window will, in general, change all the short-time sections and consequently the STFT [Ref. 3]. A major drawback of the STFT is that  $g(t)$ , as a fixed duration window, is accompanied by a fixed frequency resolution, allowing only a fixed time-frequency resolution [Ref. 2]. This is known as the Heisenberg inequality that states that for a given transform pair

$$\sigma_t \sigma_\Omega \geq \frac{1}{2}, \quad (2.4)$$

where  $\sigma_t$  and  $\sigma_\Omega$  are the root mean square of the variance of the signal over time and frequency respectively. The variances are given by

$$\sigma_t^2 = \frac{\int_{-\infty}^{\infty} t^2 |g(t)|^2 dt}{\int_{-\infty}^{\infty} |g(t)|^2 dt}, \quad (2.5)$$

$$\sigma_\Omega^2 = \frac{\int_{-\infty}^{\infty} \Omega^2 |G(\Omega)|^2 d\Omega}{\int_{-\infty}^{\infty} |G(\Omega)|^2 d\Omega}. \quad (2.6)$$

Hence, either time or frequency resolution can be enhanced at the expense of a poor resolution in the other domain since there is a lower bound for the product given by Equation 2.4. Note that the time-frequency resolution is fixed for the whole time-frequency plane once a window has been selected. Figure 1 shows the tiling of the time-frequency plane for the STFT, where each rectangle represents the basic resolution cell, given by  $\sigma_t \sigma_\Omega$ .

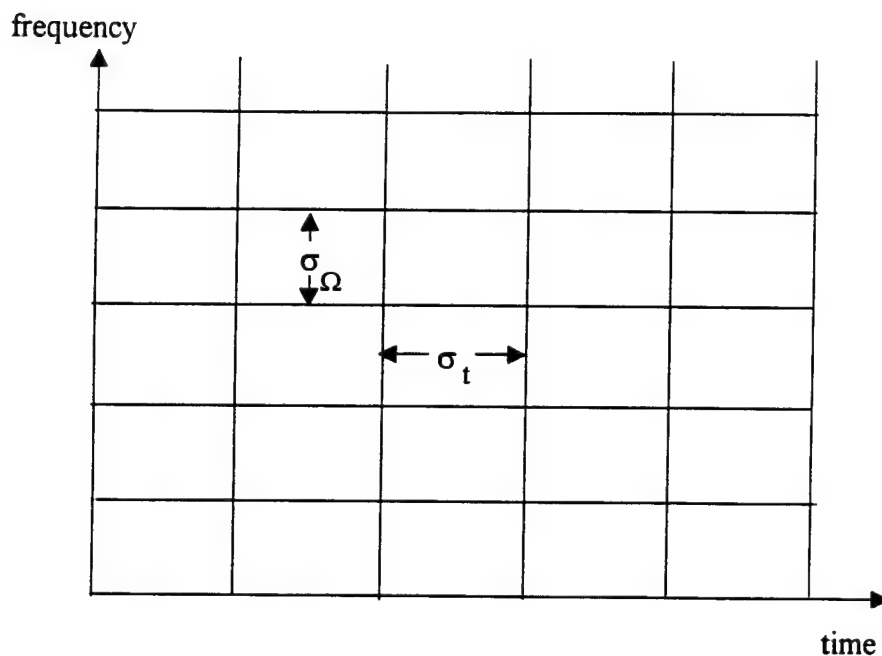


Figure 1. Tiling of the Time-frequency Plane for the STFT

## 2. The Discrete-Time STFT

The discrete-time version of the STFT can be defined as

$$X(k, n) = \sum_{m=-\infty}^{\infty} g(n-m)x(m)e^{-j\frac{2\pi}{N}km}. \quad (2.7)$$

The analysis window  $g(m)$  is considered to be part of the specification of the STFT, and its selection dictates the trade-off between frequency and time resolution. The discrete-time STFT can be viewed as a set of Discrete Fourier Transforms ( DFT ) of short duration. It can also be viewed as the output of a filter bank.

Rewriting Equation 2.7 we have

$$X(k, n) = \sum_{m=-\infty}^{\infty} [x(m)e^{-j\frac{2\pi}{N}km}]g(n-m). \quad (2.8)$$

Equation 2.8 is in the form of the convolution of the sequence  $[x(m)e^{-j\frac{2\pi}{N}km}]$ , with the sequence  $g(m)$ . We can then rewrite Equation 2.8 as

$$X(k, n) = [x(n)e^{-j\frac{2\pi}{N}kn}] * g(n), \quad (2.9)$$

where the symbol "  $*$  " denotes the convolution operator. Thus, the discrete-time STFT can be viewed as a collection of sequences, each corresponding to the frequency components of  $x(n)$  falling within a particular frequency band. Figure 2 illustrates a filter bank operation, where each filter acts as a bandpass filter centered at a selected frequency [Ref. 3].

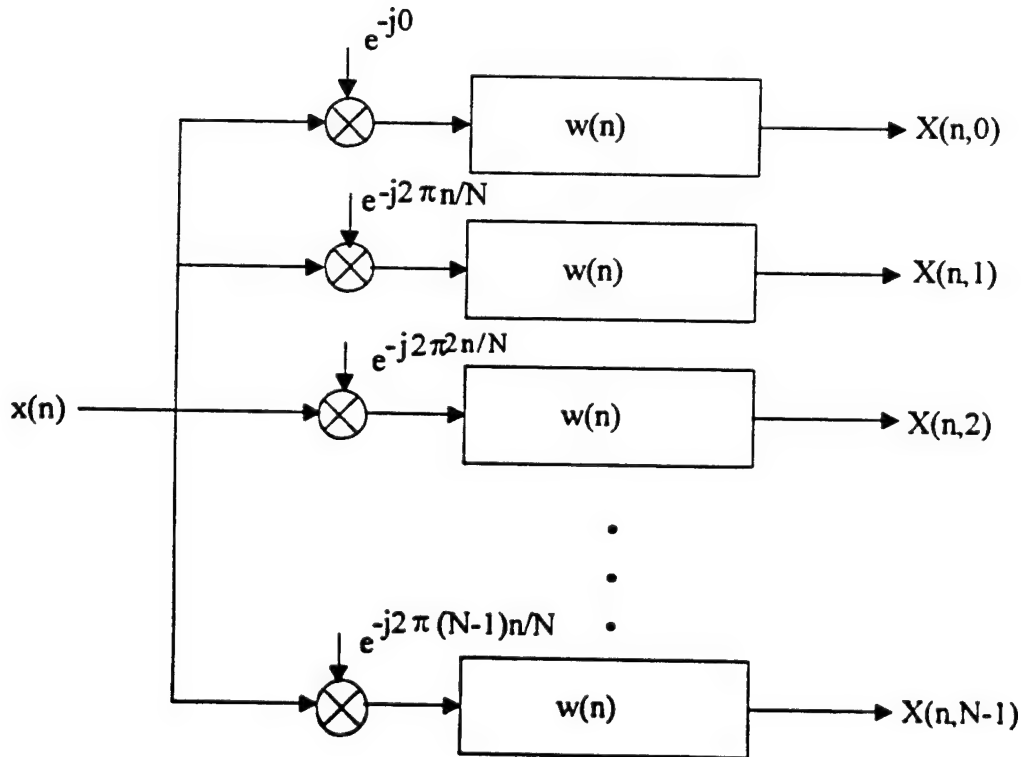


Figure 2. The Discrete-time STFT as a Filter Bank

To overcome the time-frequency resolution constraint of the STFT a new technique was devised to create a basis function to allow a multiresolution analysis. This new technique is known as the *Wavelet Transform*.

## B. THE WAVELET TRANSFORM

To obtain a multiresolution analysis we must allow both resolutions  $\sigma_t$  and  $\sigma_\Omega$  to vary in the time-frequency plane. When the analysis is viewed as a filter bank, the time resolution  $\sigma_t$  increases with the central frequency of the analysis filters, consequently the frequency resolution  $\sigma_\Omega$  is inversely proportional to  $\Omega$ , or

$$\frac{\sigma_\Omega}{\Omega} = c, \quad (2.10)$$

where  $c$  is a constant. The analysis filter bank is then composed of bandpass filters with proportional bandwidth (the *constant Q* analysis). Figure 3 shows a division of the frequency domain for the STFT and the Wavelet Transform.

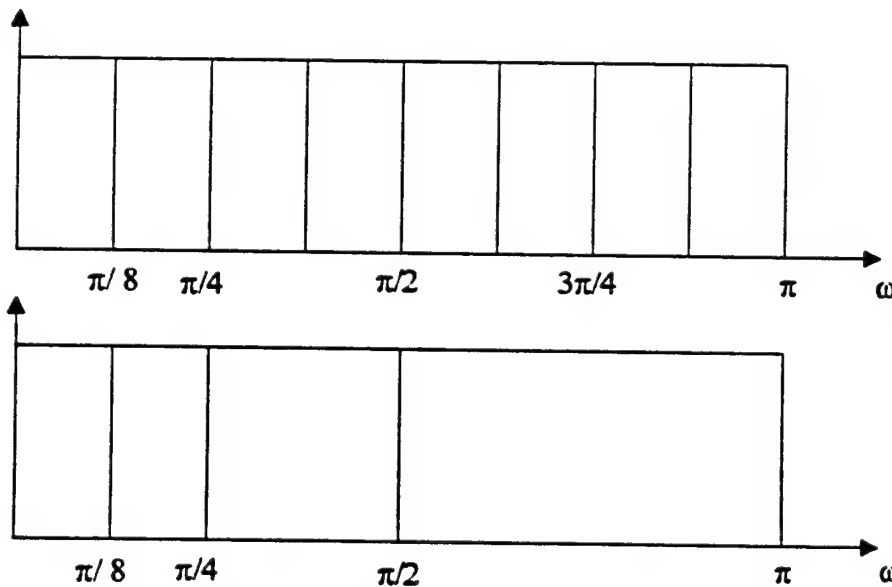


Figure 3. Division of the Frequency-domain for the STFT and the Wavelet Transform

The Wavelet transform is founded on dilations and translations of a basis function known as the *mother wavelet*. The *family* derived from this basis function is of the form

$$\psi_{ab}(t) = \frac{1}{\sqrt{a}} \psi\left(\frac{t-b}{a}\right), \quad (2.11)$$

where  $a$  is the scaling parameter and  $b$  is the shifting or translation parameter. If  $a$  is large then  $\psi_{ab}(t)$  becomes stretched and corresponds to a low frequency function and if  $a$  is small  $\psi_{ab}(t)$  becomes compressed and corresponds to a high frequency function. The dilations and translations present in the wavelet function enable the narrowing and widening of the time-frequency plane. Thus, it is possible to adjust to the characteristics of the analyzed signal [Ref. 5]. Figure 4 shows the tiling of the time-frequency plane for the Wavelet Transform. Figure 5a shows a *mother wavelet function* while Figures 5b, 5c and 5d show examples of its dilations and translations.

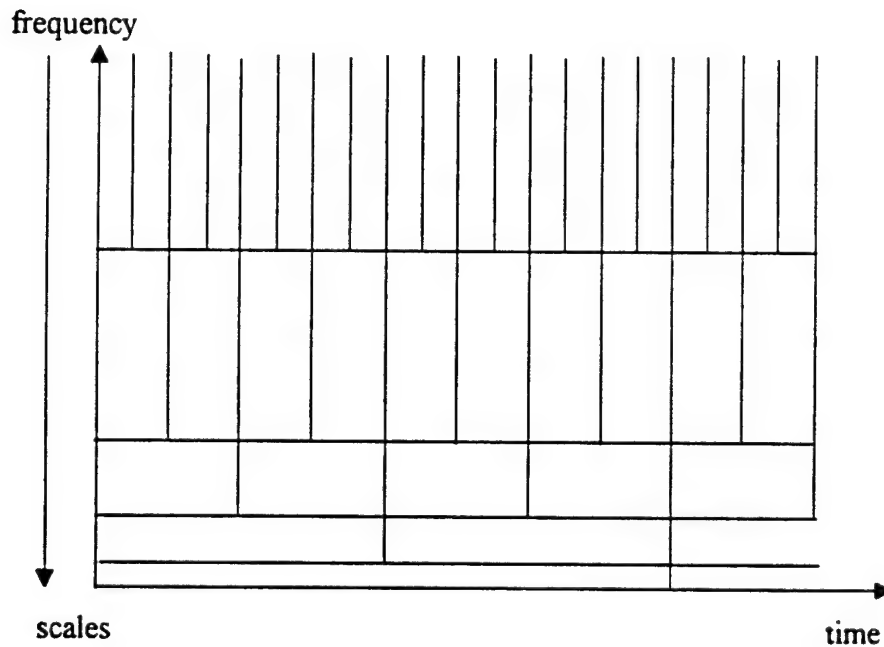


Figure 4. Tiling of the Time-frequency Plane

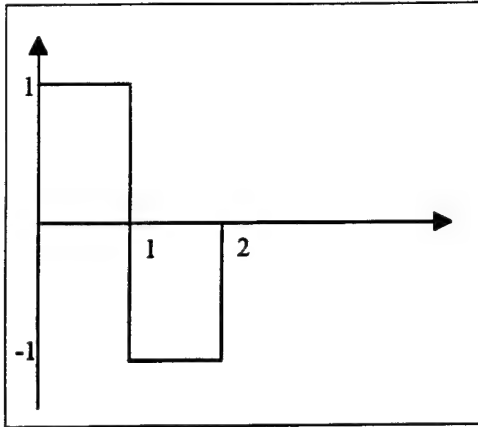


Figure 5a. Haar Wavelet

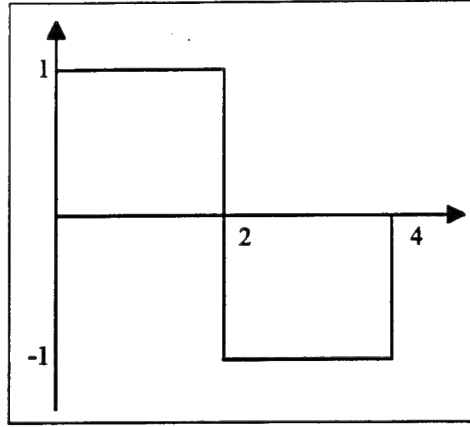


Figure 5b.  $a = 0.5, b = 0$

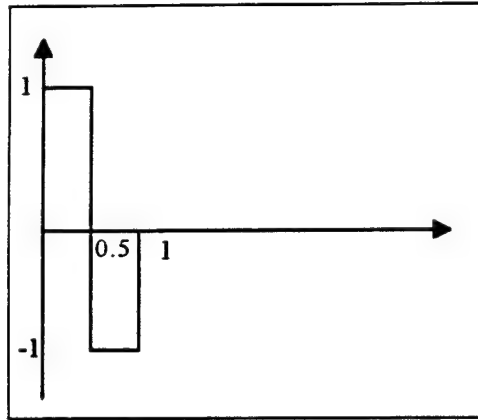


Figure 5c.  $a = 2, b = 1$

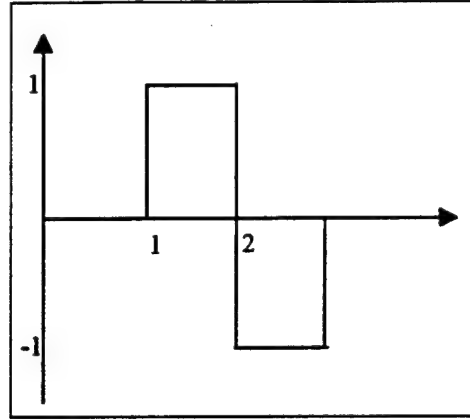


Figure 5d.  $a = 1, b = 1$

Figure 5. Haar Wavelet and Part of its Family

### 1. The Continuous Wavelet Transform

The Continuous Wavelet Transform ( CWT ) can be defined as

$$CWT_x(a, b) = \frac{1}{\sqrt{a}} \int_{-\infty}^{\infty} \psi_{ab}(t)x(t)dt, \quad (2.12)$$

where  $\psi_{ab}(t)$  is given by Equation 2.11 and the term  $1/\sqrt{a}$  is the wavelet energy normalization factor. Equation 2.12 can be written as

$$CWT_x(a, b) = \frac{1}{\sqrt{a}} \langle \psi_{ab}(t), x(t) \rangle, \quad (2.13)$$

The inverse of the Wavelet Transform is given by

$$x(t) = \frac{1}{C_\psi} \int_{-\infty}^{\infty} \int_0^{\infty} CWT_x(a, b) \psi_{ab}(t) \frac{da db}{a^2}, \quad (2.14)$$

where  $C_\psi$  is given by

$$C_\psi = \int_0^{\infty} \frac{|\Psi(\Omega)|^2}{\Omega} d\Omega, \quad (2.15)$$

and  $\Psi(\Omega)$  is the Fourier Transform of  $\psi(t)$ . Equation 2.14 holds only if the wavelet function  $\psi_{ab}(t)$  satisfies the *admissibility* condition. To be an admissible wavelet function, the term  $C_\psi < \infty$ , therefore  $\psi_{ab}(t)$  has zero mean or its DC value is zero ( $\Psi(0) = 0$ ). The function  $\psi_{ab}(t)$  has compact support, hence it acts as the impulse response of a bandpass filter that decays very fast to zero [Ref. 2].

## 2. The Discrete Wavelet Transform

The parameters  $a$  and  $b$  of the *mother wavelet*  $\psi_{ab}(t)$  are continuous variables making the Wavelet Transform very redundant and impractical. Both parameters can be discretized by sampling to obtain a set of discrete wavelet functions. However, if the sampling rate is too high, the transform is close to the continuous transform case and hence it might be redundant. If it is too low, it may not contain the necessary amount of information for reconstructing the original signal. The solution to the problem may be addressed by the use of *frames*. The study of frames was introduced by Duffin and Schaeffer [Ref. 6] and was also addressed by Daubechies [Ref. 7]. Their work provided a general theory that sets the balance for the extreme cases of over and undersampling the

parameters of the Short Time Fourier Transform and the Discrete Wavelet Transform and proved the existence of numerically stable inversion procedures for both transforms.

Let the sampling lattice be

$$a = a_0^{-j}, \quad (2.16)$$

$$b = kb_0 a_0^{-j}, \quad (2.17)$$

where  $j, k \in \mathbb{Z}$ . Equation 2.11 becomes

$$\psi_{ab}(t) = \frac{1}{\sqrt{a}} \psi\left(\frac{t-b}{a}\right) = a^{-1/2} \psi(a^{-1}t - \frac{b}{a}). \quad (2.18)$$

Substituting 2.16 and 2.17 into 2.18 we obtain

$$\psi_{jk}(t) = a_0^{j/2} \psi(a_0^j t - kb_0). \quad (2.19)$$

The set of wavelet functions defined by 2.19 can be considered as a discretized version of the continuous case and we can represent any signal or function  $x(t) \in L^2(R)$  as

$$x(t) = \sum_j \sum_k d_{j,k} \psi_{jk}(t), \quad j, k \in \mathbb{Z}, \quad (2.20)$$

where  $d_{j,k}$  is defined as

$$d_{j,k} = \frac{1}{a_0^{j/2}} \int_{-\infty}^{\infty} x(t) \psi(a_0^j t - kb_0) dt. \quad (2.21)$$

The wavelet basis function cannot be considered a basis for  $L^2(R)$ ; it is called a *frame*. The *frame* does not satisfy Parseval's power theorem and the wavelet expansion may lead to



more than one solution. Daubechies [Ref. 7] showed that, the recovery of  $x(t)$  is possible only if

$$A\|x\|^2 \leq \sum_j \sum_k |d_{j,k}|^2 \leq B\|x\|^2, \quad j, k \in Z, \quad (2.22)$$

where  $A$  and  $B$  are the frame bounds for the frame  $\psi_{jk}(t)$  and  $\|x\|^2 \triangleq \int_{-\infty}^{\infty} |x(t)|^2 dt$ . The set defined by 2.19 is considered a frame only if  $\psi(t)$  satisfies the admissibility condition. Then the frame bounds are constrained by

$$A \leq \frac{\pi}{b_0 \log a_0} \int_{-\infty}^{\infty} \frac{|\Psi(\Omega)|^2 d\Omega}{|\Omega|^2} \leq B, \quad 0 < A \leq B < \infty. \quad (2.23)$$

If  $\psi_{jk}(t)$  is inadmissible it leads to a diverging upper bound ( $B = \infty$ ). The inequalities hold for any  $a_0$  and  $b_0$ . Some definitions are needed before we proceed :

- If  $A = B = 1$  then the frame is named a *tight* frame;
- If the removal of a function leads to an incomplete set, it is an *exact* frame;
- An exact and tight frame constitutes an orthonormal basis [Ref. 7].

For the set of functions defined by 2.19 to be considered a basis for  $L^2(R)$  it has to satisfy the definitions above and, therefore, the *tightest* set  $\psi_{jk}(t)$  is the *orthonormal* set.

Let the set  $\psi_{jk}(t)$  be a set of orthonormal wavelets then

$$\int \psi_{jk}(t) \psi_{j'k'}(t) dt = \begin{cases} 1, & j = j', \quad k = k' \\ 0, & \text{otherwise.} \end{cases} \quad (2.24)$$

Both indices are orthonormal in time within any scale  $j$  and also across all other scales [Ref. 2].

For practical purposes  $a_0 = 2$  and  $b_0 = 1$ , leading to what is called a *dyadic* or *octave* lattice [Ref. 2, 4, 7]. Figure 6 shows the *dyadic* or *octave* sampling lattice.

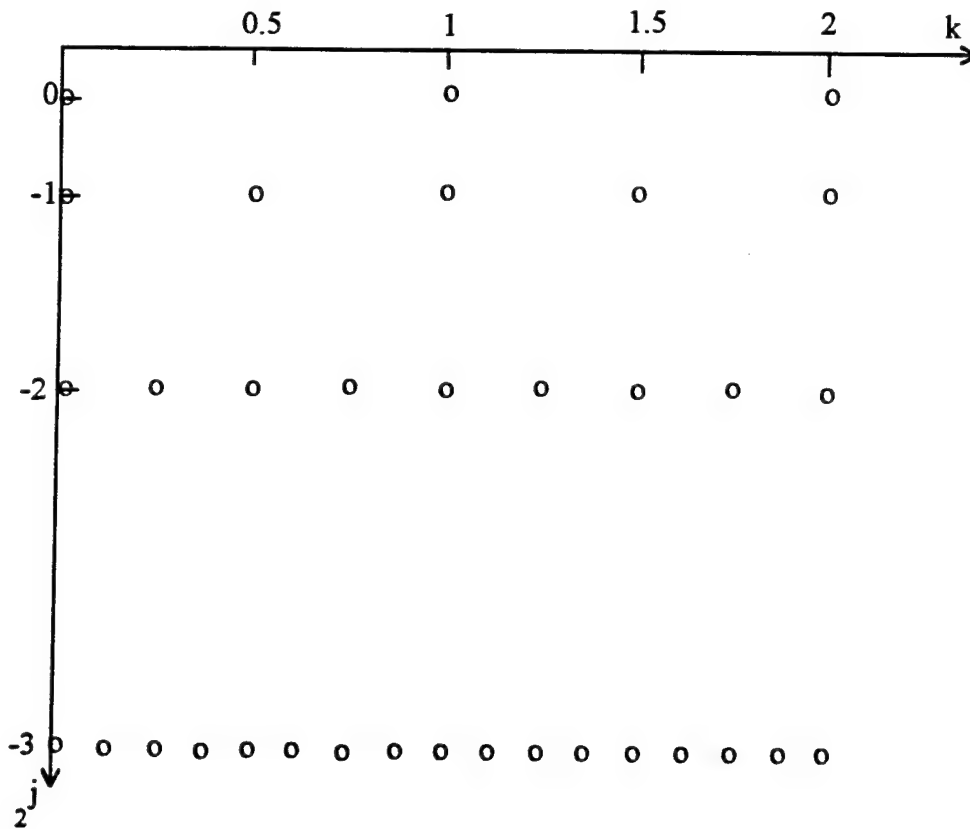


Figure 6. Sampling Dyadic Lattice for the DWT

If we substitute the values  $a_0 = 2$  and  $b_0 = 1$  in Equation 2.19 we have

$$\psi_{jk}(t) = 2^{j/2} \psi(2^j t - k). \quad (2.25)$$

Mathematical and practical perceptions of the wavelet transform can be better understood by using the concept of *multiresolution* to define the effects of changing scales [Ref. 8].

### 3. Multiresolution Signal Analysis

Multiresolution analysis of  $L^2(R)$  is defined as a sequence of closed subspace  $V_j$  of  $L^2(R)$ ,  $j \in Z$  that satisfy the following properties [Ref. 9]:

➤ Containment

$$\dots V_{-2} \subset V_{-1} \subset V_0 \subset V_1 \subset V_2 \dots ;$$

$\leftarrow \text{coarser} \qquad \text{finer} \rightarrow$

➤ Completeness

$$\bigcap V_j = \{0\} \text{ for } j \in Z, \text{ (i.e., there is no intersection of subspaces),}$$

$$\bigcup V_j = L^2(R) \text{ for } j \in Z, \text{ (i.e., the union of subspaces is equal to } L^2(R)\text{);}$$

➤ Scaling

$$x(t) \in V_j \Leftrightarrow x(2t) \in V_{j+1} \text{ for any function } x \in L^2(R);$$

➤ Shift or translation

$$x(t) \in V_0 \Leftrightarrow x(t+k) \in V_0 \text{ for any function } x \in L^2(R), k \in Z;$$

➤ A function  $\varphi(t) \in V_0$  exists such that, for  $\forall m \in Z$ , the set defined by

$$\varphi_{jk}(t) = 2^{j/2} \varphi(2^j t - k) \text{ forms an orthonormal basis for } V_j. \quad (2.26)$$

The functions defined by 2.26 are called *scaling functions*, since they are scaled versions of functions in  $L^2(R)$ . From the above definition for multiresolution analysis, it can be said

that the function  $\varphi(t)$  in  $L^2(\mathbb{R})$  is the limit of the approximations  $\varphi_j(t) \in V_j$  as  $j$  approaches infinity [Ref. 5] or

$$\varphi(t) = \lim_{j \rightarrow \infty} \varphi_{jk}(t).$$

The variable  $j$  is called a *scale factor*. For  $j > 0$ ,  $\varphi_{jk}(t)$  narrows, and consequently  $V_j$  is wider, being able to represent finer detail. If  $j < 0$ ,  $\varphi_{jk}(t)$  stretches,  $V_j$  is narrower and the resolution is coarser. Let  $\varphi(t) \in V_0$  be a scaling function; then its translations  $\varphi(t-k)$  span  $V_0$ . Let  $\varphi(2t-k)$  be dilations of  $\varphi(t-k)$  in  $V_0$ . We know that  $V_0 \subset V_1$  then  $\varphi(2t-k)$  span  $V_1$ . Therefore,  $\varphi(t)$  can be presented as a linear combination of translations of  $\varphi(2t)$  as

$$\varphi(t) = \sum_k h_0(k) \varphi(2t-k), \quad k \in \mathbb{Z}. \quad (2.27)$$

Equation 2.27 is known as *dilation* or *fundamental* equation and  $h_0(k)$  are the *scaling function coefficients*. We will see later that  $h_0(k)$  can be interpreted as a FIR filter. The space  $L^2(\mathbb{R})$  can be represented via a Venn diagram as shown in Figure 7.

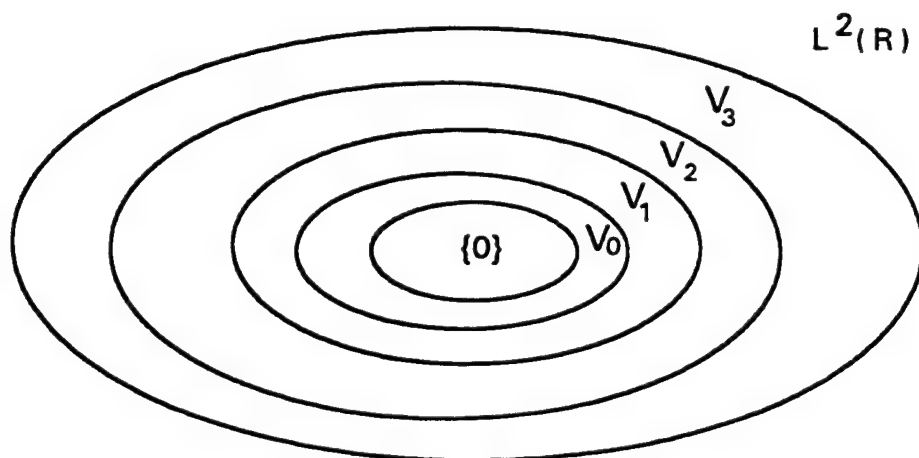


Figure 7. Multiresolution Representation of  $L^2(\mathbb{R})$

Another way of graphically representing  $L^2(R)$  is shown in Figure 8.

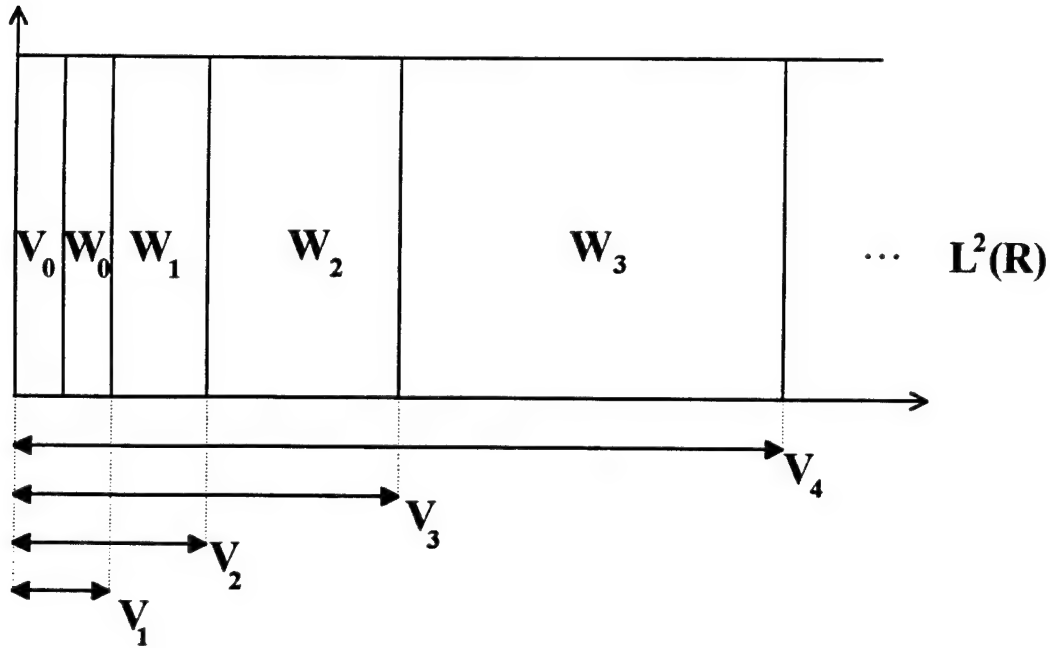


Figure 8. Multiresolution Representation of  $L^2(R)$

Note in Figure 8 that the areas denoted by  $W_0, W_1, W_2, W_3$  etc., are the difference spaces between  $(V_1, V_0), (V_2, V_1), (V_3, V_2), (V_4, V_3)$ , respectively. The idea can be extended to an arbitrary  $W_j$ . The spaces  $W_j$  are defined to be the orthogonal complement of the spaces  $V_j$ , with respect to  $V_{j+1}$  [Ref. 5] that is

$$V_{j+1} = V_j \oplus W_j, \quad (2.28)$$

$$V_j \perp W_j. \quad (2.29)$$

Where the symbol " $\oplus$ " stands for direct sum. This means that each element of  $V_{j+1}$  can be written as the sum of an element of  $W_j$  and an element of  $V_j$ . A subspace  $W_j$  provides the necessary *detail* information to go from subspace  $V_j$  to  $V_{j+1}$ . The direct sum of all the possibly infinite spaces is equal to  $L^2(R)$  [Ref. 10].

Let  $\psi(t)$ , as defined by Equation 2.25, be an element of any given subspace  $W_j$ . The subspace  $W_j$  is itself a subspace of  $V_{j+1}$ . Therefore,  $\psi(t)$  can be written as a linear combination of translations of  $\phi(t)$

$$\psi(t) = \sum_k h_1(k) \phi(2t - k), \quad k \in Z, \quad (2.30)$$

where  $h_1(k)$  represents the *wavelet coefficients* that can be used as a high pass Finite Impulse Response (FIR) filter. These coefficients are related to the scaling coefficients, as they span two orthogonal spaces, they must also be orthogonal. Note that both equations are derived from a common term and differ only by the coefficients  $h_0(k)$  and  $h_1(k)$ . Hence, orthogonality can be achieved by requiring that

$$\langle h_0(k), h_1(k) \rangle = 0. \quad (2.31)$$

Assuming that the number of coefficients defining  $h_0(k)$  and  $h_1(k)$  is even and

$$h_1(k) = (-1)^k h_0(N - 1 - k), \quad (2.32)$$

where  $N$  is the number of coefficients, then the inner product of the coefficients is equal to

$$\sum_{k=0}^{N-1} h_0(k) h_1(k) = \sum_{k=0}^{N-1} h_0(k) (-1)^k h_0(N - 1 - k). \quad (2.33)$$

The expansion of 2.33 is equal to zero. Therefore, the space  $L^2(R)$  is spanned by a linear combination of functions in the subspace  $V_0$  and functions in subspaces  $W_0$  to  $W_j$ . As a consequence, any function  $x(t)$  in  $L^2(R)$  can be written as

$$x(t) = \sum_{k=-\infty}^{\infty} a_k \phi_k(t) + \sum_{j=1}^{\infty} \sum_{k=-\infty}^{\infty} d_{jk} \psi_{jk}(t). \quad (2.34)$$

Equation 2.34 is an expansion in terms of scaling and wavelet functions. The coefficients  $a_k$  and  $d_{jk}$  are the *Discrete Wavelet Transform coefficients*. They completely describe the original signal and are defined as:

$$a_k = \langle x(t), \phi_k(k) \rangle = \int_{-\infty}^{\infty} x(t) \phi_k(t) dt, \quad (2.35)$$

$$d_{jk} = \langle x(t), \psi_{jk}(t) \rangle = \int_{-\infty}^{\infty} x(t) \psi_{jk}(t) dt. \quad (2.36)$$

Where  $\phi_k(t)$  and  $\psi_{jk}(t)$  are real functions. If the scaling and the wavelet functions form an orthonormal basis, Parseval's power theorem holds. For the expansion defined by 2.34, Parseval's theorem is

$$\int |x(t)|^2 dt = \sum_{k=-\infty}^{\infty} |a_k|^2 + \sum_{j=1}^{\infty} \sum_{k=-\infty}^{\infty} |d_{jk}|^2. \quad (2.37)$$

If the functions are orthonormal and have compact support (finite duration), the desired time localization in all scales is achieved [Ref. 8, 10].

#### **a. The Scaling Function and the Scaling Coefficients**

The coefficients  $h_0(k)$  in Equation 2.27 have to be chosen carefully in order to generate scaling functions that have compact support (finite duration). They must satisfy some necessary conditions to ensure this compact support [Ref. 10, 11, 12]. The development of these conditions are provided in Appendix A.

1. The sum of the scaling coefficients must be equal to two

$$\sum_{n=0}^{N-1} h_0(n) = 2. \quad (2.38)$$

2. If a solution to 2.27 exists, and  $\int \varphi(t) dt \neq 0$ , and  $\int |\varphi(t)|^2 dt = 1$ , and an integer number of translations of  $\varphi(t)$  are orthogonal to each other, as defined by

$$\langle \varphi(t) \varphi_k(t) \rangle = \int \varphi(t) \varphi(t-k) dt = \delta(k) = \begin{cases} 1, & k=0 \\ 0, & \text{else} \end{cases}$$

then

$$\sum_{n=0}^{N-1} h_0(n) h_0(n-2k) = 2\delta(k). \quad (2.39)$$

3. The sum of the squares of the coefficients is equal to two.

Let  $k = 0$ , Equation 2.39 reduces to

$$\sum_{n=0}^{N-1} |h_0(n)|^2 = 2. \quad (2.40)$$

4. The individual sums of the odd and even terms of  $h_0(n)$  is equal to one

$$S_1 + S_2 = 2, \quad (2.41)$$

where

$$S_1 = \sum_{n=0}^{N-1} h_0(2n), \quad (2.42)$$

and

$$S_2 = \sum_{n=0}^{N-1} h_0(2n+1). \quad (2.43)$$



### b. Scaling and Wavelet Functions Regularity

The  $N$  number of scaling function coefficients has to be even. These coefficients have to satisfy the linear constraint determined by Equation 2.38 and the  $\frac{N}{2}$  bilinear constraints determined by Equation 2.39. This leaves  $\frac{N}{2} - 1$  degrees of freedom for choosing them. That will guarantee the existence of the scaling function, and the set derived from it will be orthonormal [Ref. 10].

The degrees of freedom in the scaling function coefficients determine how *regular* the function will be. Regularity or smoothness of a function is defined by the number of times that a function can be differentiated. In other words, a regular scaling or wavelet function can be defined as a function with compact support in time and reasonably localized in frequency.

### c. The Frequency Domain

The Discrete Fourier transform of Equation 2.27 is defined as

$$H(\omega) = \sum_{k=-\infty}^{\infty} h_0(k) e^{-j\omega k}. \quad (2.44)$$

It turns out that a solution to Equation 2.27 exists only if  $H(0) = 2$ , or the DC gain of the FIR filter equals two.

If the integer translates of Equation 2.27 are orthogonal, then the constraint defined by Equation 2.39 is true, if and only if

$$|H(\omega)|^2 + |H(\omega + \pi)|^2 = 4. \quad (2.45)$$

Equation 2.45 is equivalent to a Finite Impulse Response (FIR) filter and is called a Quadrature Mirror Filter (QMF) [Ref. 10, 18]. This allows the implementation of the Discrete Wavelet Transform via a Filter Bank technique.

#### 4. Filter Banks and the Discrete Wavelet Transform

The multiresolution analysis introduced in the previous section can be implemented by applying a technique called Pyramid decomposition, or Mallat's algorithm [Ref. 13]. The algorithm does not include the use of scaling or wavelet functions; only the scaling and the wavelet coefficients need to be considered. We derive the basic relationship between the expansion coefficients at a lower scale in terms of those at a higher scale. Reproducing the fundamental equation

$$\varphi(t) = \sum_k h_0(k) \varphi(2t - k), \quad k \in \mathbb{Z}. \quad (2.46)$$

Next, we dilate and translate Equation 2.46 to obtain

$$\begin{aligned} \varphi(2^j t - n) &= \sum_k h_0(k) \varphi(2(2^j t - n) - k) = \\ &= \sum_k h_0(k) \varphi(2^{j+1} t - 2n - k). \end{aligned} \quad (2.47)$$

Let  $m = 2n + k$  or  $k = m - 2n$ , substituting into Equation 2.47

$$\varphi(2^j t - n) = \sum_m h_0(m - 2n) \varphi(2^{j+1} t - m). \quad (2.48)$$

Let  $V_j$  be the subspace spanned by  $\varphi(2^j t - k)$  then

$$x(t) \in V_{j+1} \Rightarrow x(t) = \sum_k a_{jk} \varphi(2^{j+1} t - k). \quad (2.49)$$

Consequently  $x(t)$  can be expressed in terms of scaling functions and no wavelets. At one immediately lower scale, the wavelets will provide the necessary *detail* not available in

that scale space and for a lower resolution the *detail* has to be accounted for. Therefore, the wavelets have to be included in Equation 2.49, which is now rewritten as

$$x(t) = \sum_k a_{jk} 2^{j/2} \phi(2^j t - k) + \sum_k d_{jk} 2^{j/2} \psi(2^j t - k). \quad (2.50)$$

Where the term  $2^{j/2}$  is the normalization for the various scales, and the terms  $a_{jk}$  and  $d_{jk}$  are the discrete wavelet transform coefficients. Note that  $x(t)$  belongs to  $V_{j+1}$  and  $\phi(2^j t - k)$  and  $\psi(2^j t - k)$  belong to  $V_j$ . If we substitute Equation 2.26 into Equation 2.50 we obtain

$$x(t) = \sum_k a_{jk} \phi_{jk}(t) + \sum_k d_{jk} \psi_{jk}(t), \quad k \in \mathbb{Z}. \quad (2.51)$$

The discrete wavelet transform coefficients can be written as

$$a_{jk} = \int_{-\infty}^{\infty} x(t) \phi_{jk}(t) dt. \quad (2.52)$$

Substituting Equations 2.26 and 2.48 into Equation 2.52 leads to

$$a_{jk} = \int_{-\infty}^{\infty} x(t) \sum_m h_0(m - 2k) 2^{(j+1)/2} \phi(2^{j+1} t - m) dt,$$

or

$$a_{jk} = \sum_m h_0(m - 2k) \int_{-\infty}^{\infty} x(t) 2^{(j+1)/2} \phi(2^{j+1} t - m) dt. \quad (2.53)$$

Note that the integrand of Equation 2.53 is the discrete wavelet transform coefficient of the scale  $j + 1$ , which leads to the following relation

$$a_{jk} = \sum_m h_0(m - 2k) a_{j+1,k}. \quad (2.54)$$

The analogous relationship for  $d_{jk}$  is of the form

$$d_{jk} = \sum_m h_1(m - 2k) a_{j+1,k}. \quad (2.55)$$

Therefore, the scaling and wavelet coefficients at a given scale  $j$  are obtained by convolving the coefficients at that scale with  $h_0(-m)$  and  $h_1(-m)$ , and then decimating to produce the expansion coefficients at scale  $j - 1$ . This is equivalent of filtering the  $j^{\text{th}}$  scale coefficients with two FIR filters. The impulse responses are  $h_0(-m)$  and  $h_1(-m)$ . After decimation or down sampling, the next coarser scaling coefficients are obtained [Ref. 10]. Figure 9 shows the implementation of Equations 2.52 and 2.53 for three levels of analysis. The notation LP stands for the lowpass FIR filter (i.e., the weights  $h_0(-m)$ ) and HP stands for the highpass FIR filter (i.e., the weights  $h_1(-m)$ ).

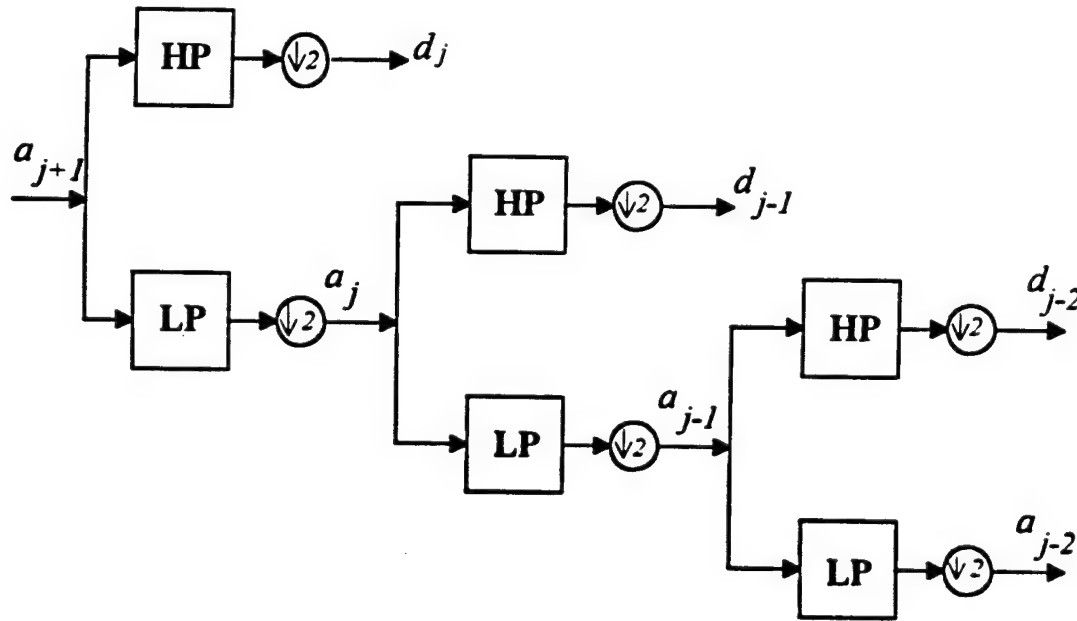


Figure 9. Three levels of Wavelet Transform Analysis

The implementation of the algorithm was done using matrices. An example of a DWT using a four coefficient wavelet is given as follows.

Defining a wavelet coefficient matrix  $A$  as

$$A = \begin{bmatrix} h_0(0) & h_0(1) & h_0(2) & h_0(3) & & & & \\ h_1(0) & h_1(1) & h_1(2) & h_1(3) & & & & \\ & & h_0(0) & h_0(1) & h_0(2) & h_0(3) & & \\ & & h_1(0) & h_1(1) & h_1(2) & h_1(3) & & \\ & & & & \ddots & & & \\ & & & & & h_0(0) & h_0(1) & h_0(2) & h_0(3) \\ & & & & & h_1(0) & h_1(1) & h_1(2) & h_1(3) \\ h_0(2) & h_0(3) & & & & & & h_0(0) & h_0(1) \\ h_1(0) & h_1(1) & & & & & & h_1(2) & h_1(3) \end{bmatrix}$$

The matrix  $A$  is a sparse matrix composed of scaling coefficients  $h_0(m)$ , and wavelet coefficients  $h_1(m)$  as non-zero entries. The blanks indicate zero entries. If we multiply a given signal by the matrix  $A$ , the first row generates one component of the signal convolved with the scaling coefficients. The following odd numbered rows perform the same operation. The even numbered rows generate the convolution of the signal with the wavelet coefficients. Note that there is an offset by two every two rows. This offset by two is the equivalent of a decimation operation. The last two rows wrap around like convolutions with periodic boundary conditions [Ref. 15].

The DWT consists of applying the matrix  $A$  repeatedly to a signal with starting length  $N$  until a stopping criterion is reached. In this thesis, when the number of scaling coefficients was equal to one, we stopped.

As an illustration, let  $x(t)$  be an arbitrary signal of length 16. Applying a DWT to it, we obtain:

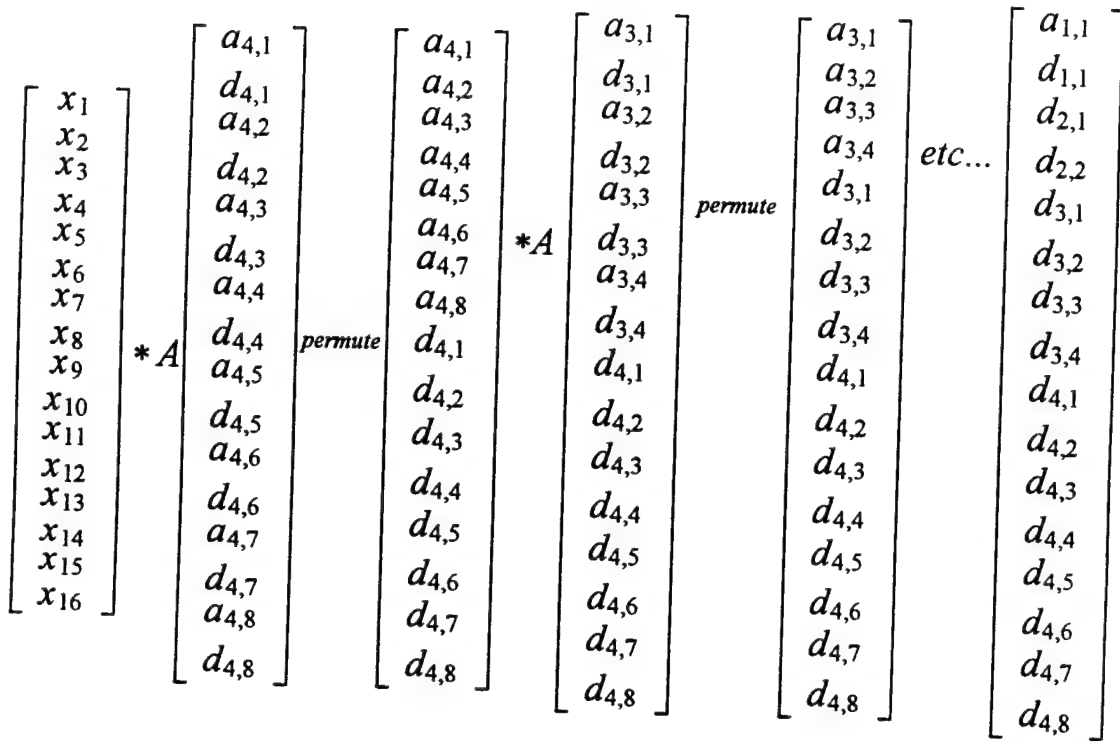


Figure 10. DWT of an Arbitrary Signal  $x(t)$

Note that at each level matrix  $A$  is applied to half of the values of the previous iterations. Once the  $d$  coefficients are generated, they just propagate through all subsequent levels. The DWT can operate only at signals with length equal to a power of two ( $2^n, n \in \mathbb{Z}$ ). These matrices operations are generally carried until there is only one DWT scaling coefficient  $a_{1,1}$ .

The Matlab code used for implementing Mallat's algorithm in this thesis plots the scales of the DWT, with a number of points equal to half of the total length of the signal.



### III. WAVELET SIGNAL PROCESSING

#### A. INTRODUCTION

The Discrete Wavelet Transform was implemented using the Mallat's Pyramid algorithm described in Chapter II.4. All programs for the DWT were written in Matlab® [Ref. 17] and are given in Appendix B. The processing phase was divided in two parts. A *simulation phase* where the DWT was applied to four artificial communication signals, and a *testing phase* where the DWT was applied to three types of real signals. The real signals were composed of transient signals created by metallic objects, radar pulses, and turn-on / turn-off transients of push-to-talk radios. Six types of mother wavelet functions were used to process the signals.

#### B. MOTHER WAVELETS

The Haar wavelet is the simplest type of wavelet basis function. It is very well localized in time, but the frequency localization is poor due to the discontinuities in the time domain. Figure 11 shows the Haar wavelet.

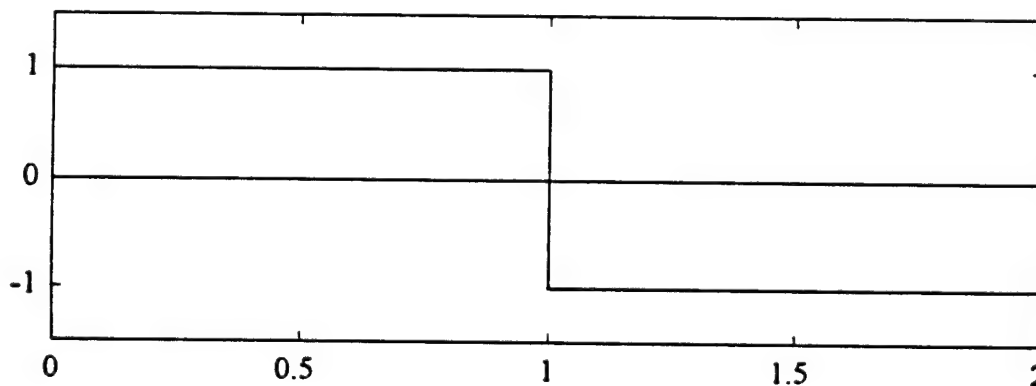


Figure 11. The Haar Wavelet

Figure 12 shows the one-sided spectrum of the Haar wavelet and its dilations. Note that the spectral sidelobes produce a poor frequency localization.



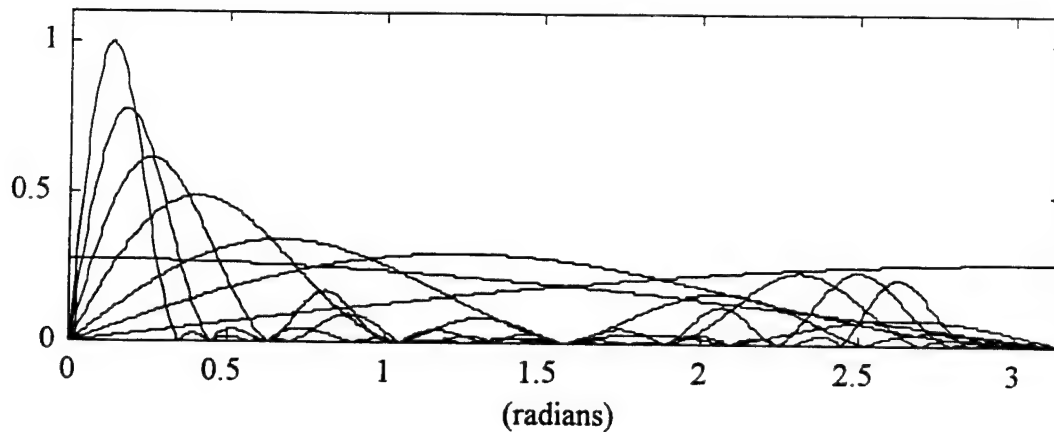


Figure 12. One Sided Spectrum of the Haar Wavelet and its Dilations

The Daubechies' scaling and wavelet functions are the most popular functions for use in DWT. Daubechies' scaling coefficients satisfy all necessary conditions. The wavelets are highly regular. They have compact support in time and their use in the DWT leads to a reasonable localization in frequency. The regularity of this type of wavelets increases linearly with the length of the FIR filter [Ref. 2]. Daubechies' wavelets are identified by the number of their coefficients, e.g., a four coefficient wavelet is called *Fourth Order Daubechies* or *Daubechies four*. In this thesis, the short notation *Daub(n)* is used to denote the  $n^{\text{th}}$  order Daubechies filter. Figures 13, 14, and 15 show the fourth, twelfth and twentieth order Daubechies' wavelets, respectively.

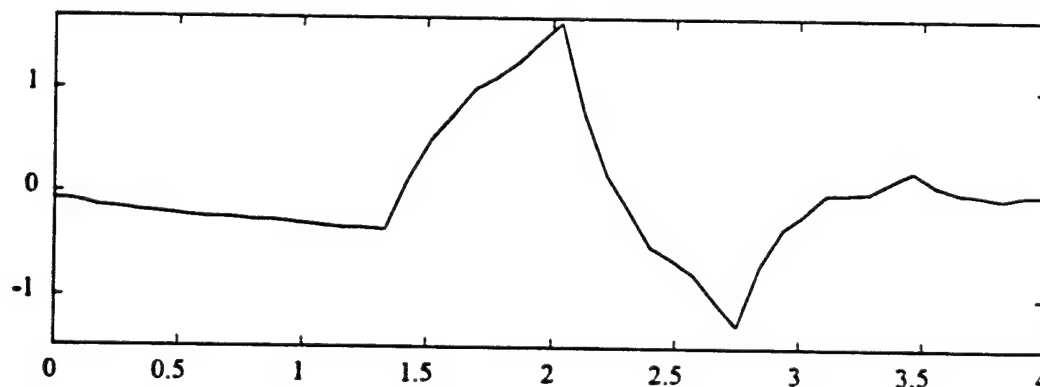


Figure 13. The Fourth Order Daubechies Wavelet

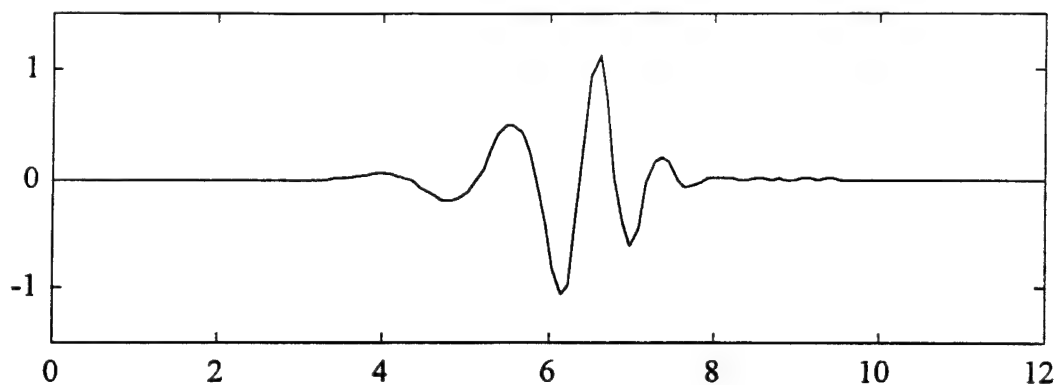


Figure 14. The Twelfth Order Daubechies Wavelet

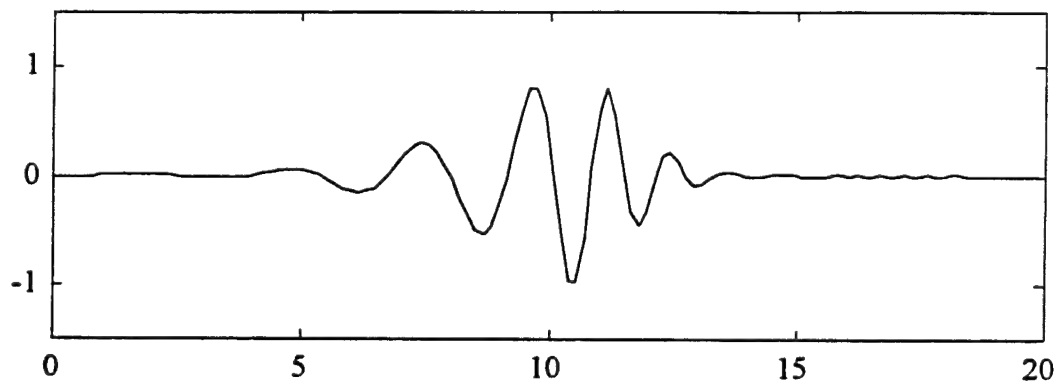


Figure 15. The Twentieth Order Daubechies Wavelet

Note that as the order of the wavelet is increased it becomes smoother. However, if computation speed is a factor then a lower order Daubechies' wavelet might be preferred.

Figures 16, 17, and 18 show the frequency response of Daub4, Daub12 and Daub20 wavelet functions, respectively. Note in Figure 16 the sidelobes around 2.5 radians. Observe that in the subsequent figures these sidelobes are gradually becoming smaller, as the order of the wavelet increases.

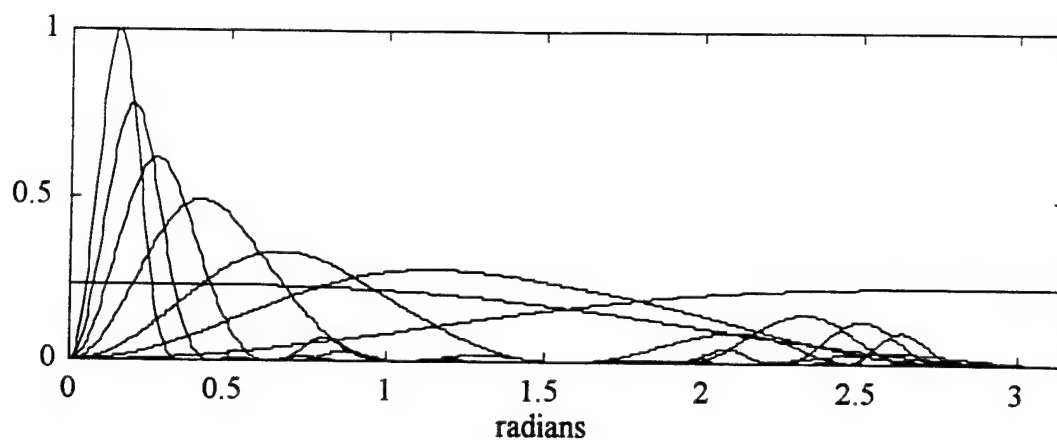


Figure 16. One Sided Spectrum of the Daub4 Wavelet and its Dilations

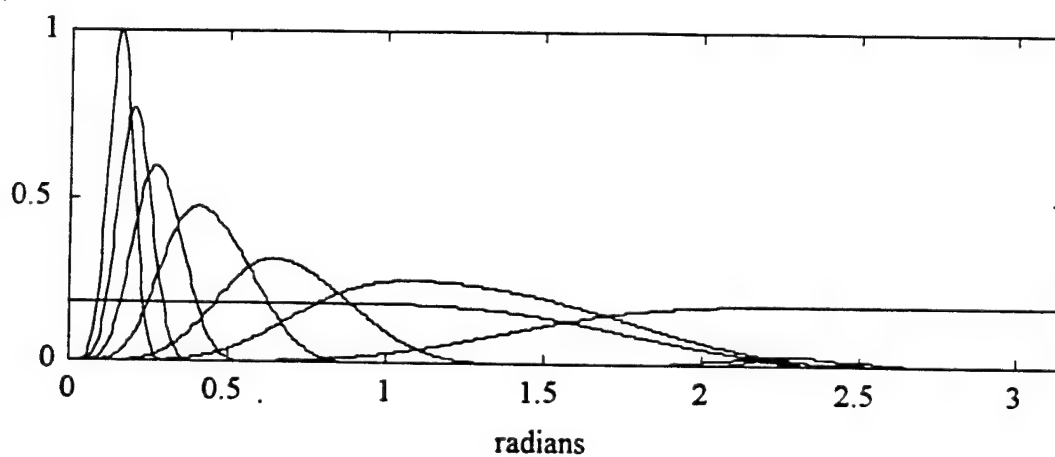


Figure 17. One Sided Spectrum of the Daub12 Wavelet and its Dilations

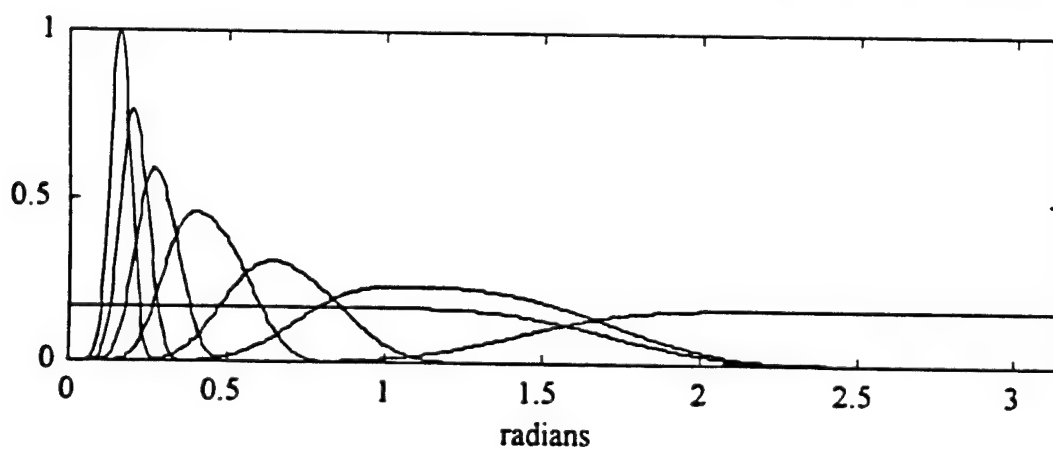


Figure 18. One Sided Spectrum of the Daub20 Wavelet and its Dilations

The Quadratic  $B$ -spline wavelets are piecewise quadratic functions. These wavelets are called the Battle-Lemarié bases [Ref. 14] and are referred to in this thesis as spline functions. The initial scaling function  $\varphi(t)$  is compactly supported. However, the functions  $2^{j/2}\varphi(2^j t - k)$  derived from it are not orthogonal. The spline scaling coefficients do not satisfy all the constraints described in Subsection II.B.3.a. The use of the spline function in the DWT leads to a redundancy in the scales. Transient signal analysis may, sometimes, benefit from this redundancy. These functions have an arbitrarily high number of derivatives [Ref. 7], which makes them extremely regular. Figure 19 shows the four coefficients spline function, and Figure 20 shows the one-sided spectrum of its dilations.

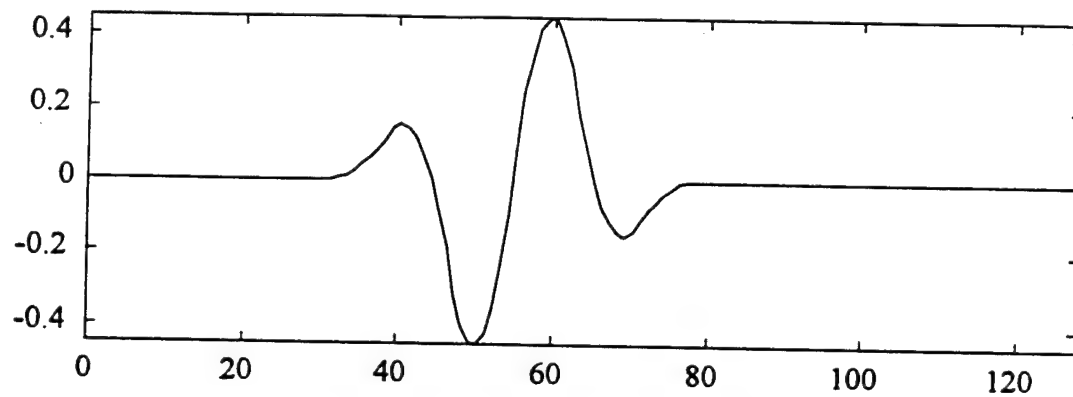


Figure 19. The Fourth Order Spline Wavelet

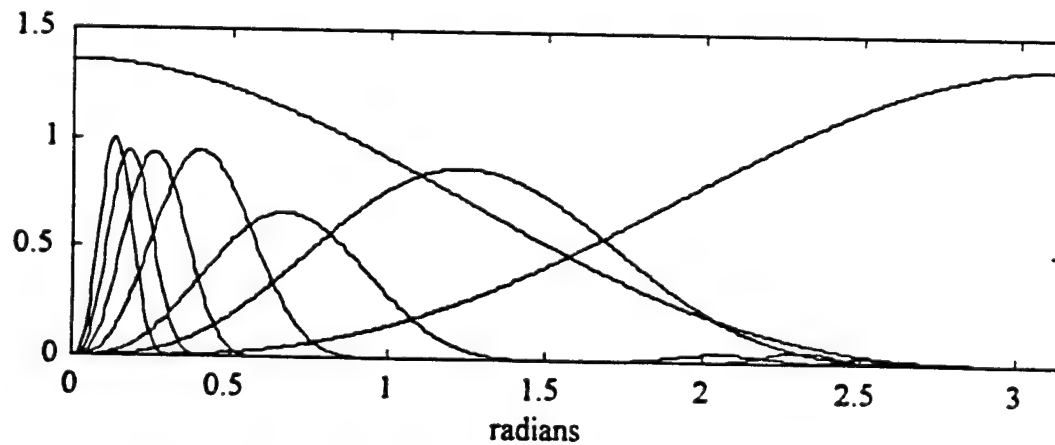


Figure 20. One Sided Spectrum of the Spline Wavelet and its Dilations

The *ad hoc* wavelet is a trial-and-error wavelet function. The of purpose of using it was to find a matching wavelet function. This function would be matched to the signals characteristics and, therefore, enhances the detection of the signal when wavelet transformed.

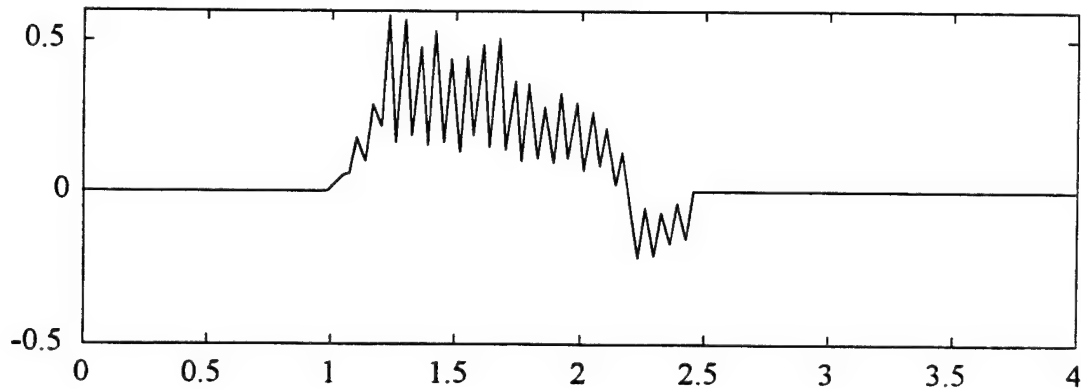


Figure 21. The *ad hoc* Wavelet

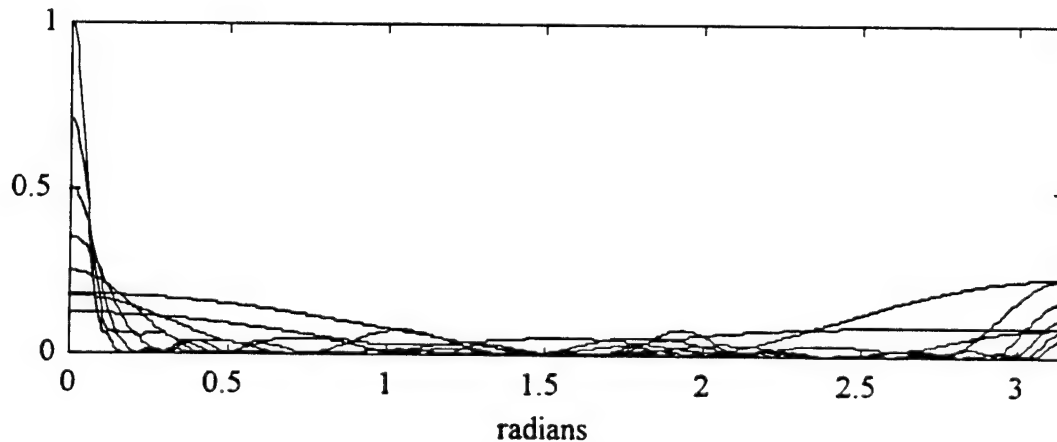


Figure 22. One Sided Spectrum of the *ad hoc* Wavelet and its Dilations

### C. THE SIMULATION PHASE

In this part, four artificial communication signals created by Yayci [Ref. 16] are used as test data. These signals have sharp transitions in time that are exploited via the wavelet transform. They are: Binary Phase Shift Keying (BPSK), On-Off Keying (OOK), Frequency Shift Keying (FSK) and Quadrature Phase Shift Keying (QPSK). They are shown in Figures 23 through 26.

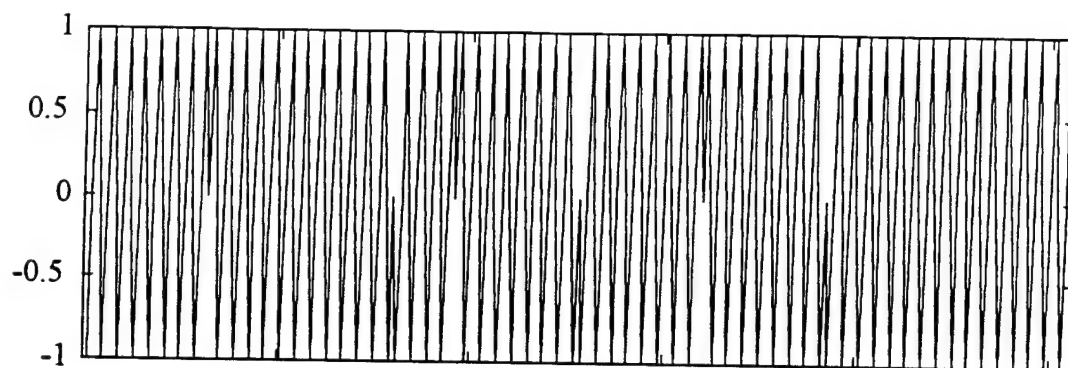


Figure 23. BPSK Signal

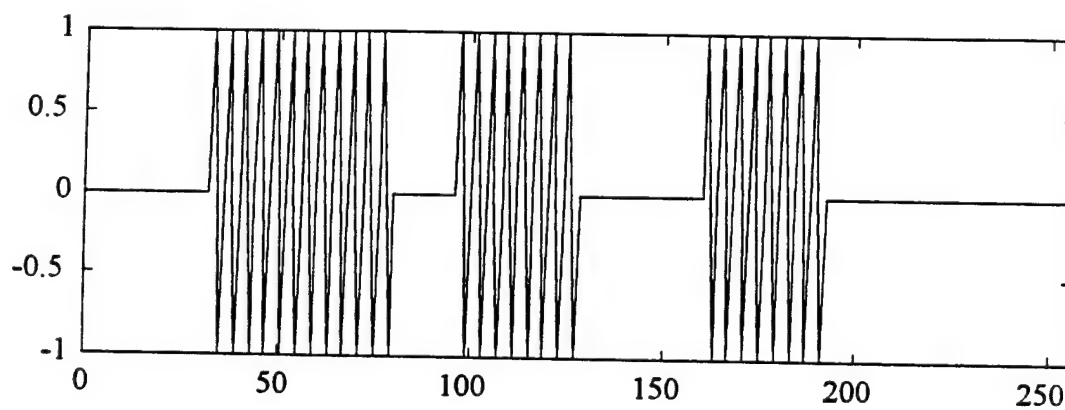


Figure 24. OOK Signal

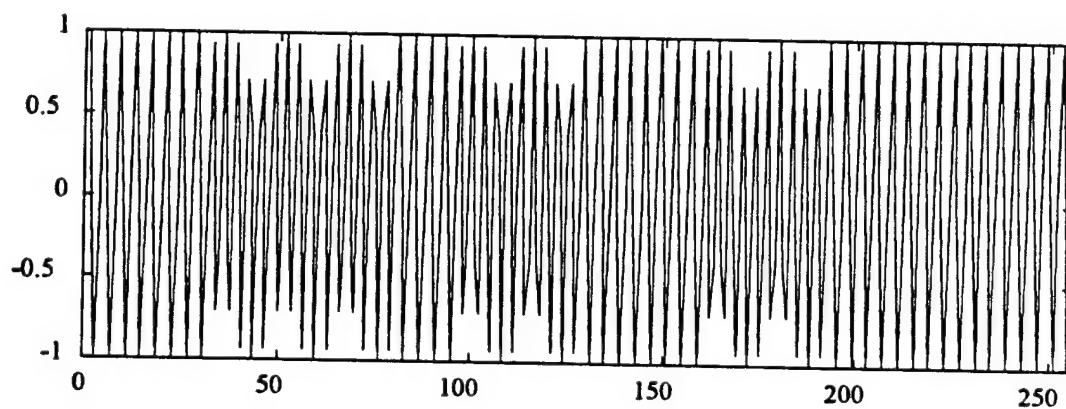


Figure 25. FSK Signal

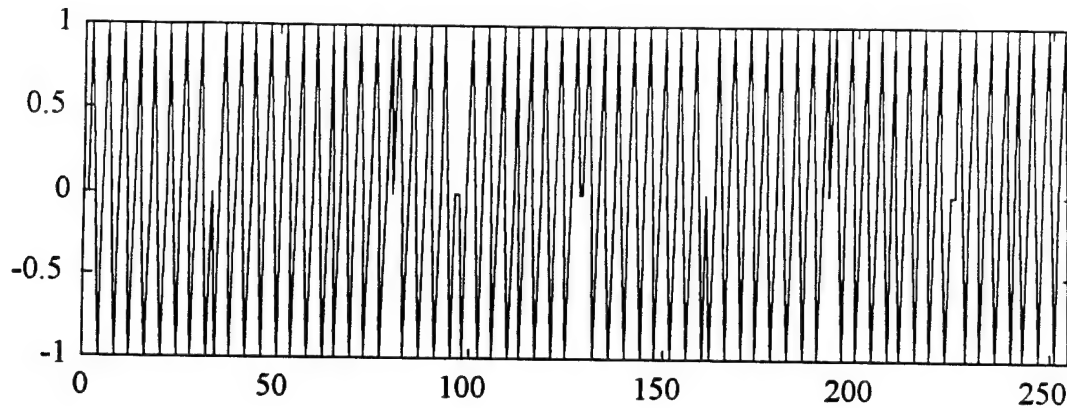


Figure 26. QPSK Signal

### 1. Application of the DWT to Artificial Signals

The DWT was applied to each of the communication signals. The first experiment used noise free signals. Gaussian White Noise (GWN) was added to the signals with six levels of Signal-to-Noise-Ratio (SNR). The SNR levels were 20 dB, 15 dB, 9 dB, 6 dB, 3 dB, and 0 dB. Figures 27 to 33 present the decomposition of the noise free signals. The order of the scales in these plots are reversed, i.e., the first DWT level appears at the end. Only the last four scales are shown because the other ones have few coefficients and little energy. The decompositions for the other levels of SNR are shown in Appendix B.

The transition points of the signals are easily seen in the noise-free case but become harder to identify as the SNR decreases. Preprocessing the noisy signals using differentiation, Hilbert transforms and a combination of these two techniques did not seem to improve the identification of the transients. Differentiating a signal in additive GWN causes the scales to display false peaks. The increase in the order of Daubechies' wavelets improves the probability of identification of the transitions. The *ad hoc* wavelet performs equally well for all cases of GWN. The transitions on the BPSK and the OOK signals can be identified at lower SNR relative to the FSK and QPSK signals. This is, in part, due to the presence of sharper transitions in time.

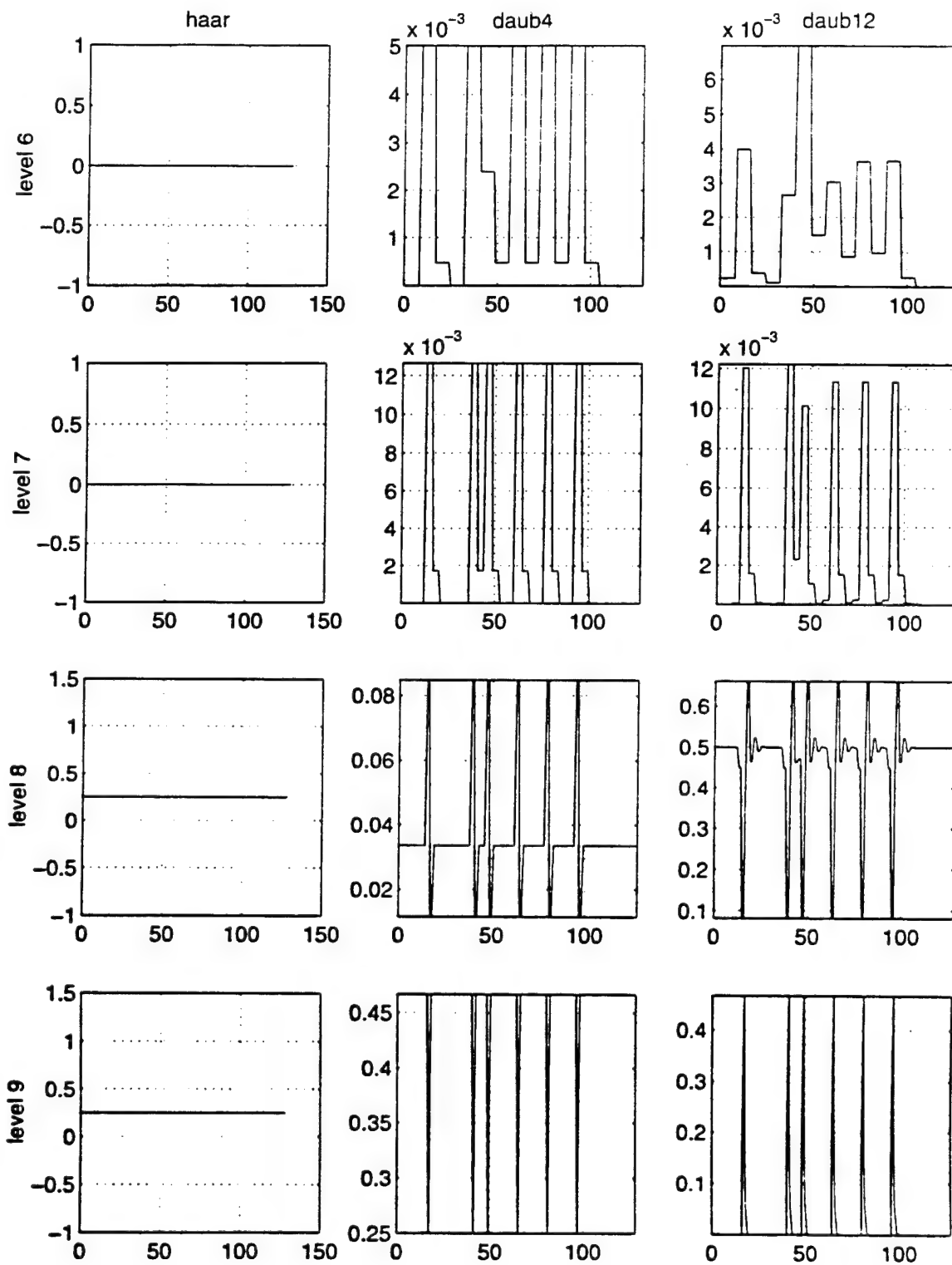


Figure 27. DWT of BPSK



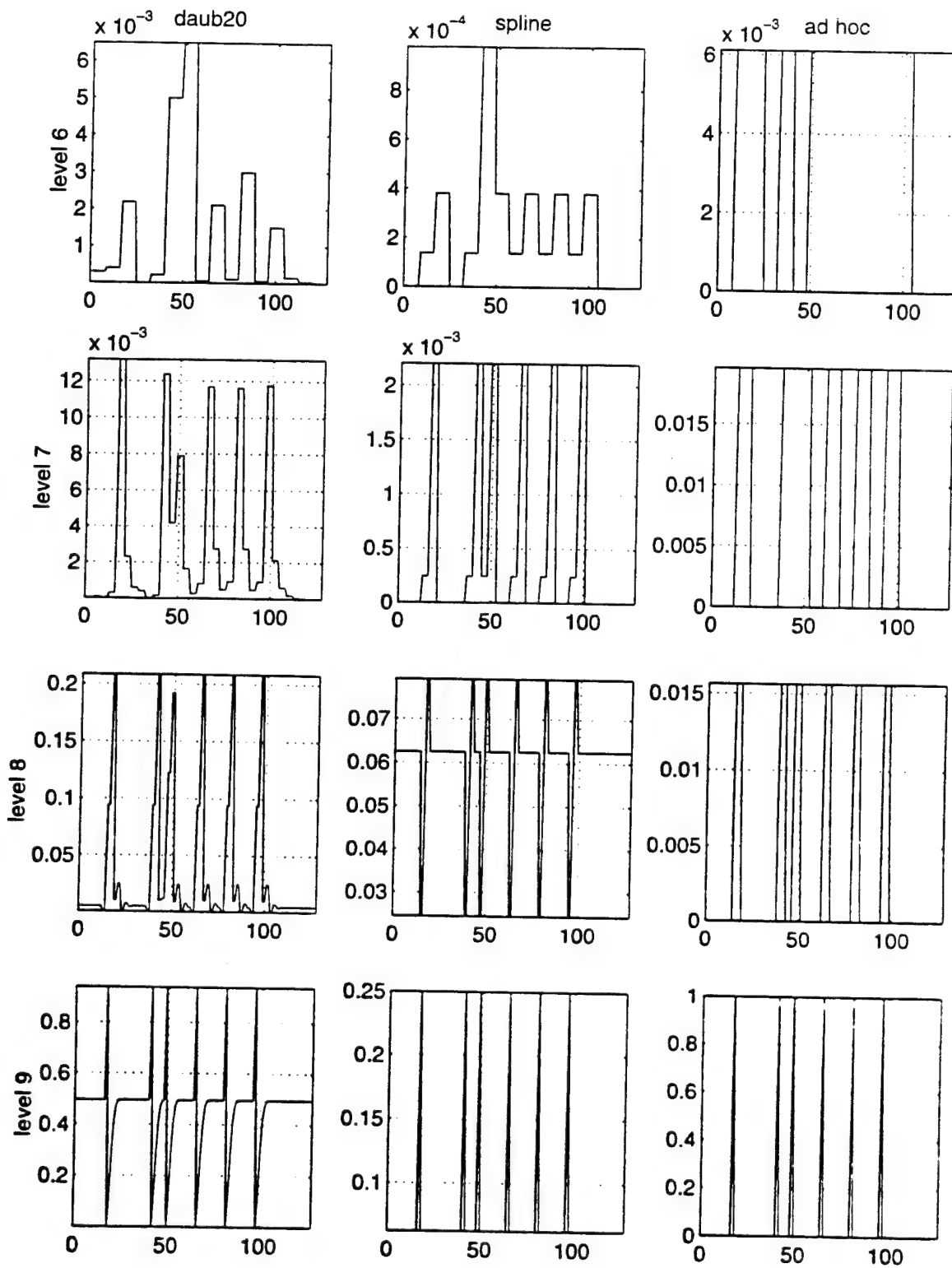


Figure 28. DWT of BPSK

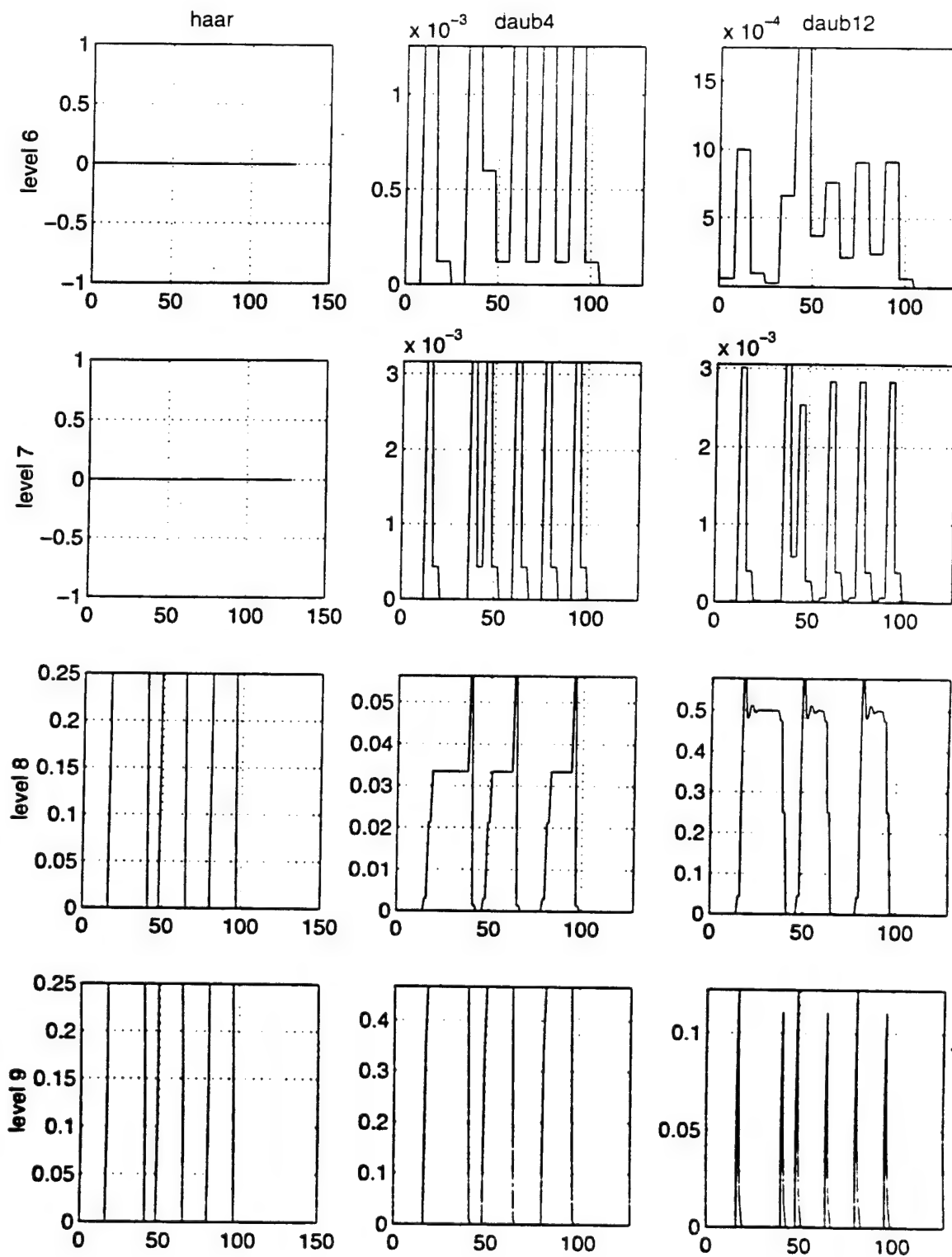


Figure 29. DWT of OOK

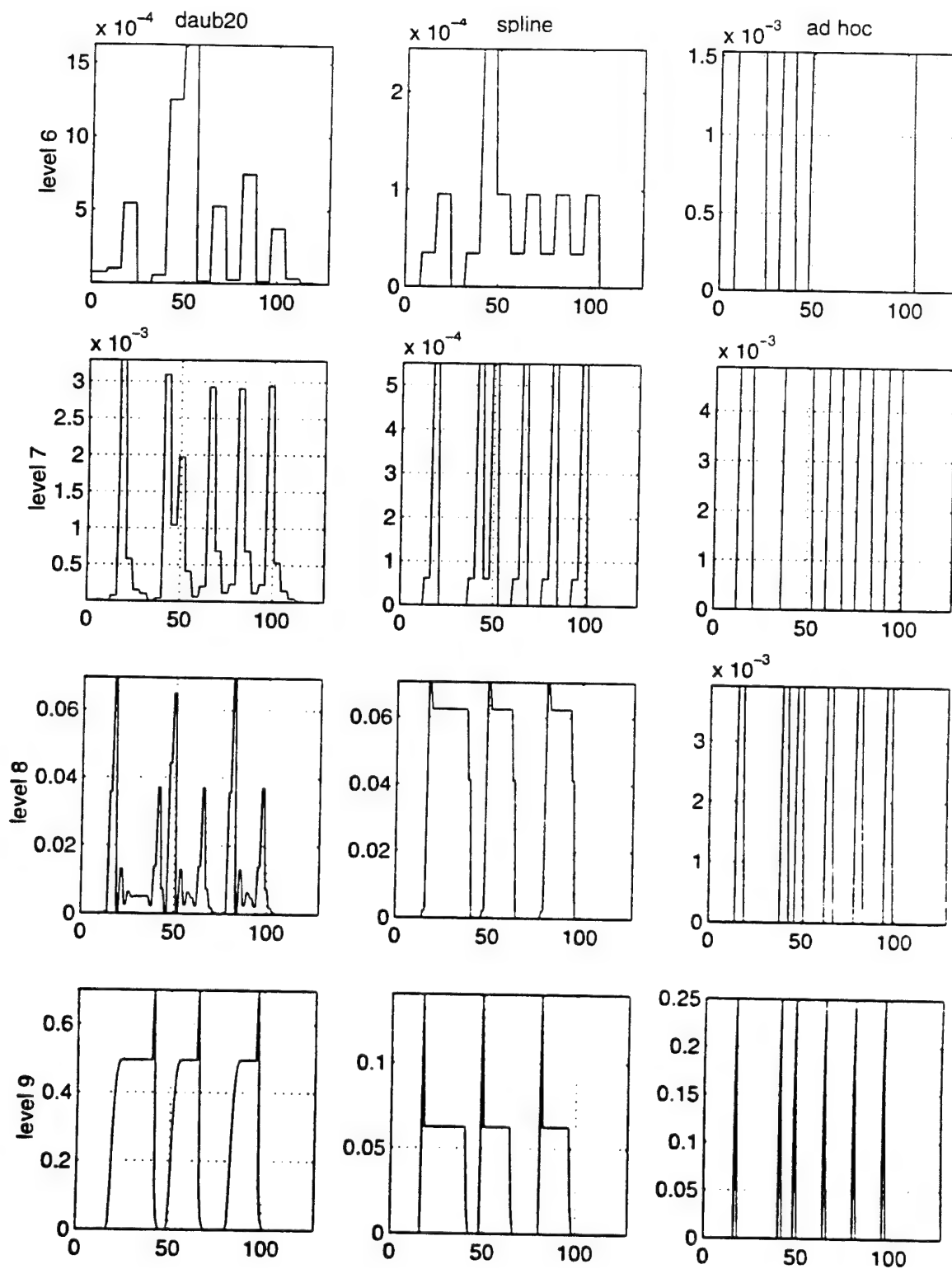


Figure 30. DWT of OOK

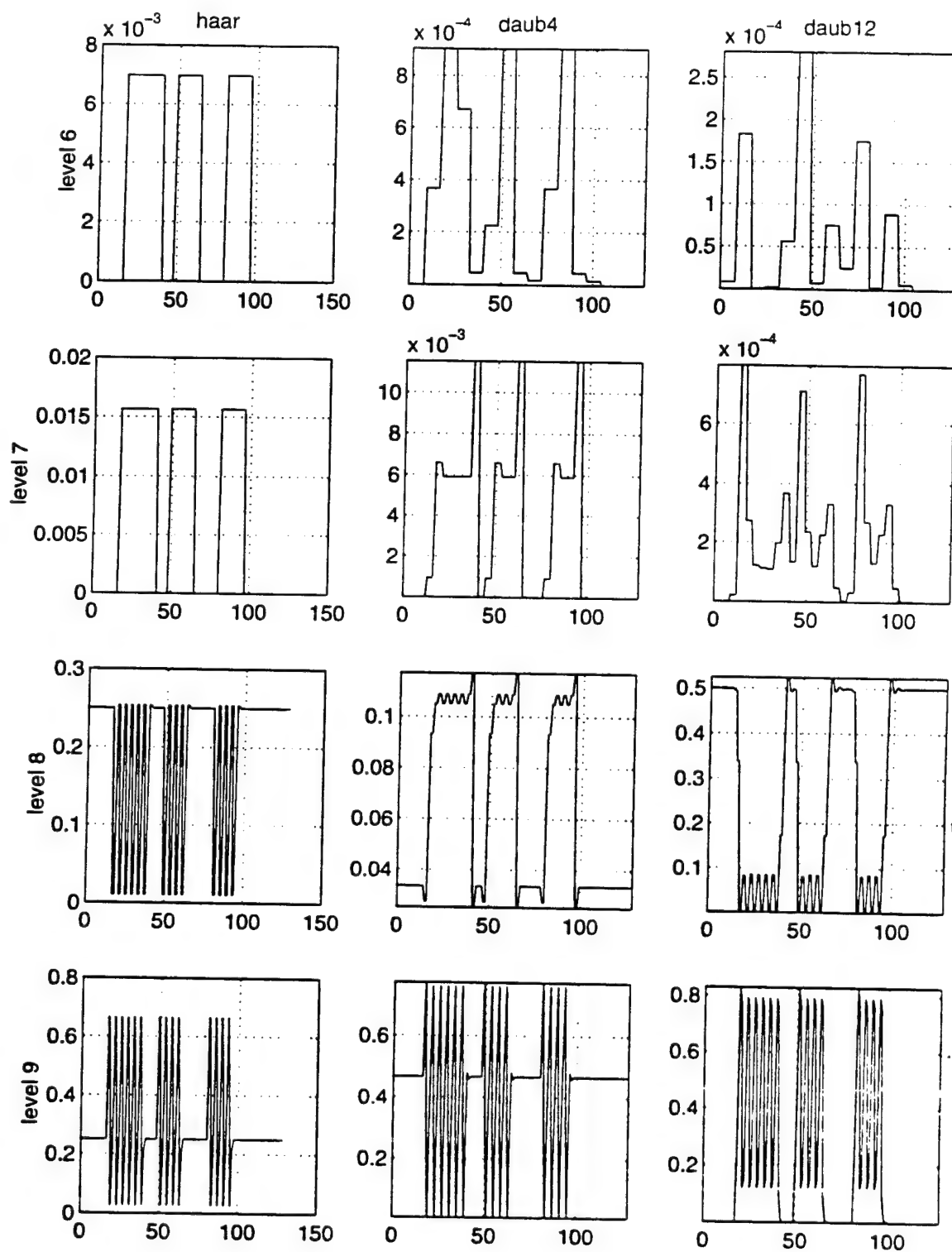


Figure 31. DWT of FSK

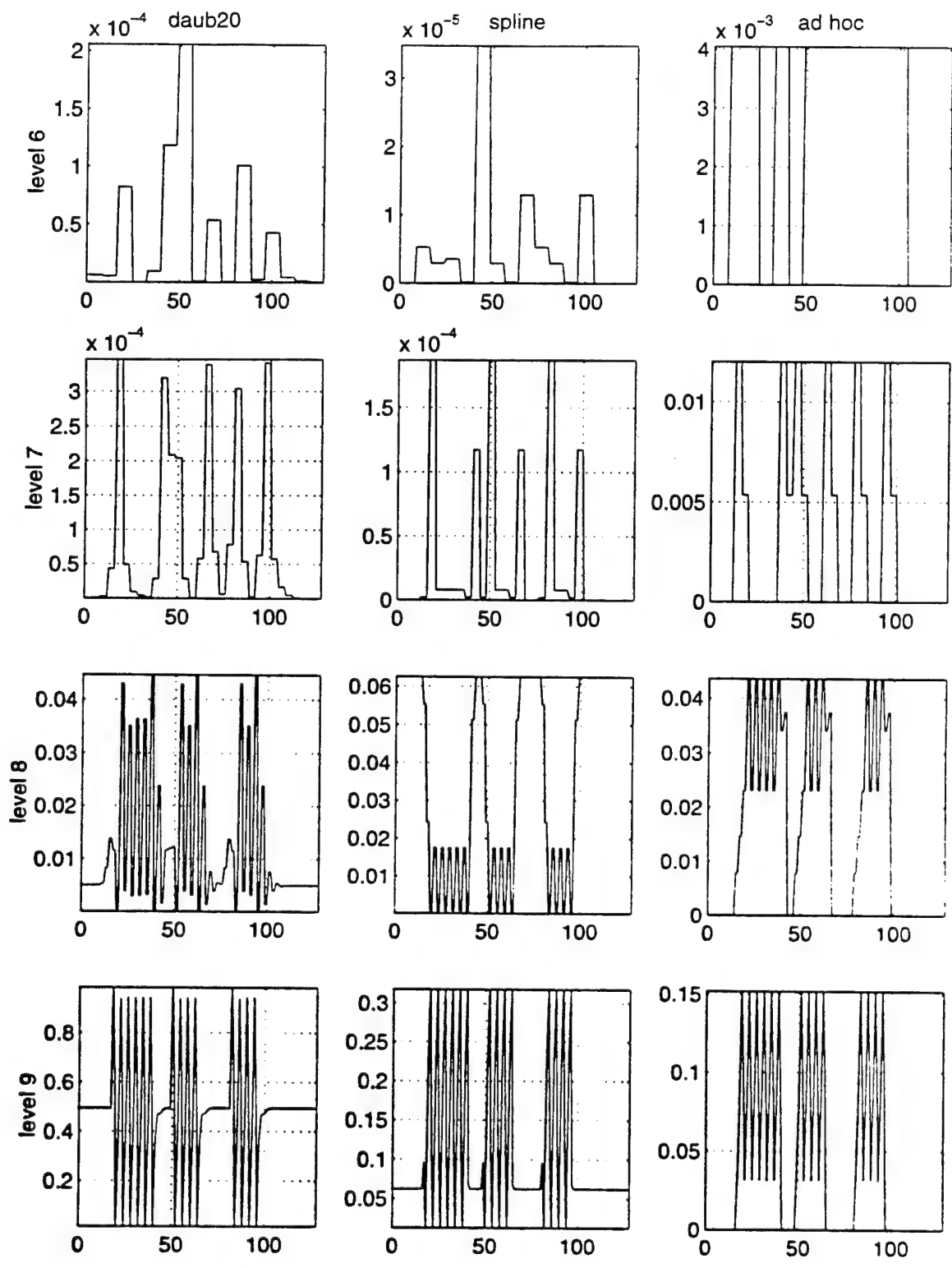


Figure 32. DWT of FSK

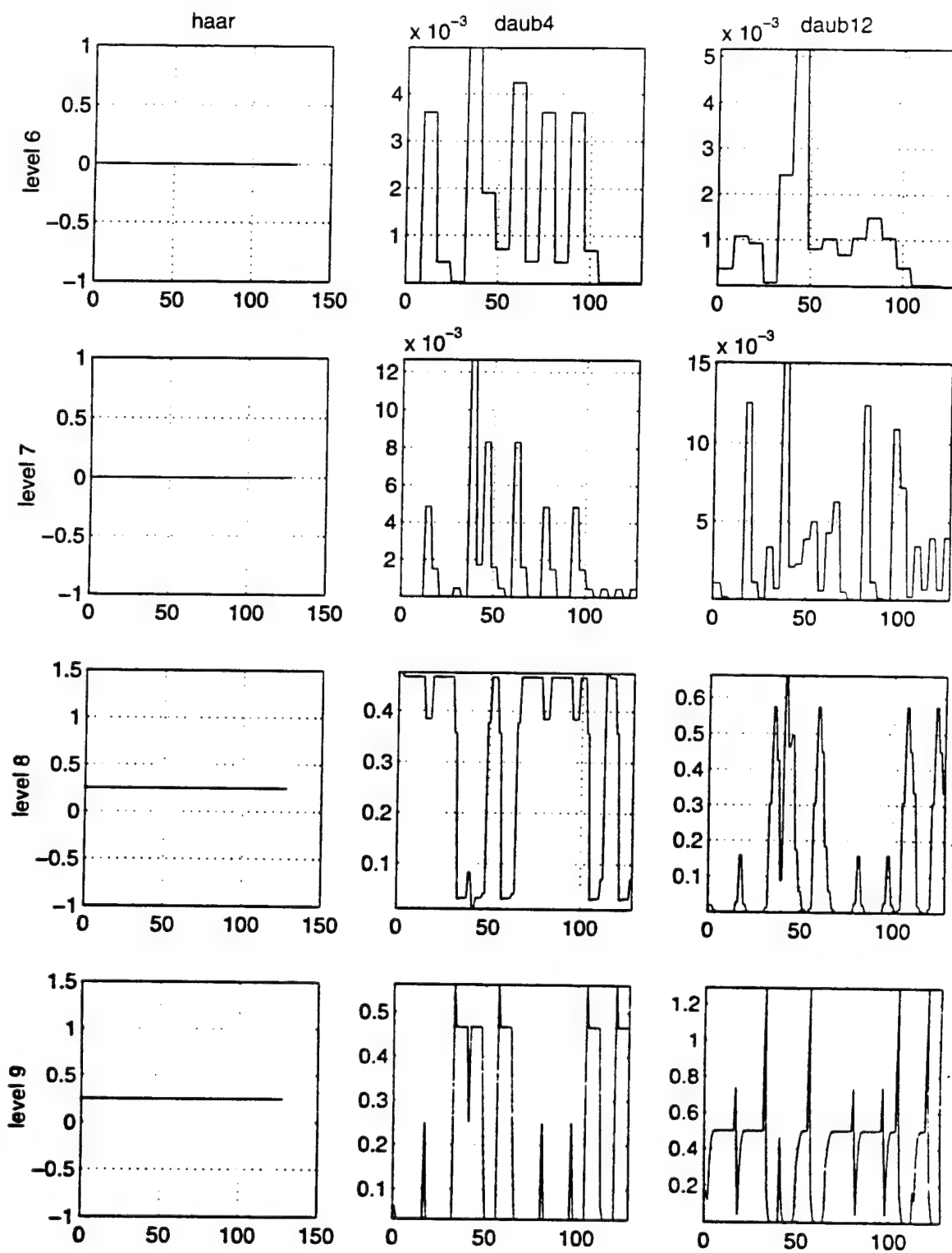


Figure 33. DWT of QPSK



## 2. Evaluation of the DWT for the Artificial Signals

The ability of identifying the transients of the artificial signals embedded in noise was the performance measure for the wavelet functions. The true transient locations were known *a priori*. Therefore, a simple comparison between the peaks shown in the transform domain and the known transition instances was sufficient to determine how well the wavelet function performed. The figures used for comparison are shown in Appendix B. The *ad hoc* wavelet function clearly outperformed the other ones. This wavelet was chosen by trial-and-error, and it produced the strongest peaks at the transition instances. It is possible that its efficiency will be degraded when working with other types of signals. The spline wavelet achieved a reasonable result down to 6 dB of SNR. The twelfth order Daubechies' wavelet presented acceptable results for all signals of interest. Hence, it was chosen to be the basis function for the analysis of the real signals during the test phase.

## D. THE TEST PHASE

This section presents a description of the signals used and their respective transforms. Only the last four scales of the DWT are shown. The signals were divided into three groups of transients: sounds produced by metallic objects, radar pulses, and turn-on / turn-off transients produced by push-to-talk radios. These transient signals are embedded in noise with unknown power levels.

### 1. Metallic Sound Transients

The first group of transient signals was obtained from the sound files directory of the Digital Signal Processing group of the Electrical and Computer Engineering Department Computer Center. There is no documentation on how they were generated or recorded. The length of the transients was cut to the immediate lower power of two. Figures 34.a to 34.c show the time representation of sounds produced by a dropped metallic object on a metallic surface, a gong, and a latch being opened, respectively.



Figure 35 shows the DWT of the last four scales of the metallic sound transients using a Daub12 wavelet.

Each signal has a particular sound. The time representation of the gong and the dropped metallic object show that both signals have an exponential decaying. The sound produced by the latch is clearly different from the other ones, with no particular time behavior.

The DWT of these signals show that the gong and the dropped metallic object sounds have similar characteristics in the transform domain. This is due to their exponential type behavior in the time domain. However, the latch sound has a very particular transformation and the transition instances appear clearly throughout the scales. A preliminary analysis of the plots shows that the sounds produced by the dropped metallic object and the gong can be classified in the same group of transients, while the sound produced by the latch belongs to another group. It is possible to observe these features directly from the time domain plots, maybe due to a high SNR. Hence, a wavelet transform is not necessary. We have seen during the simulation phase that if the SNR is low, the transition instances become harder to identify from the time domain plots. Using a DWT is a good technique to determine these transitions.

Obtaining more metallic sound transients and transforming them, using the DWT for the purpose of their classification into groups, is recommended as a future study.

## **2. Radar Pulses**

Four types of radar pulses were obtained from two types of radar at the Naval Postgraduate School. The first radar recorded was an AN/APS 31-A operating at a center frequency of 9.379 GHz, having a nominal pulse duration of 0.5 microseconds. The other three types of radar pulses were generated by an AN/SPS 64 (V) radar operating at a center frequency of 9.4 GHz and nominal pulse duration of 1.0, 0.5 and 0.15 microseconds. All signals were heterodyned to 500 MHz using a local oscillator and a mixer, then digitized at 2 GHz with 8 bits per sample. There are 64 pulses per record, 8

records for the first type of radar pulse, 15 records for the second, 8 records for the third and 8 records for the fourth. Figures 36.a through 36.d show the first pulse of the first record of each one of the radars. Figures 37 through 44 show the last four scales of the DWT of six pulses of the first record of each radar using the Daub12 wavelet.

The DWT was applied to the first six pulses of each record. Although the pulses inside one record were generated sequentially by the same radar, their DWT scales do not present a particular repeating feature. Therefore, at this point, we could not classify the transformed radar pulses. Statistically, the number of radar pulses that were transformed was not enough to make any assessments. Hence, this is an area where additional research is recommended.

### **3. Turn-On / Turn-Off of Push-To-Talk Radios**

These transient signals were generated by the turn-on and turn-off of six different models of transmitters produced by the same maker. They were collected and recorded by the Naval Security Group Activity, Charleston, SC. Ten samples of each of six push-to-talk Motorola radios were recorded. The carrier frequency of all of them was set to 138.525 MHz. The signals were passed through a 1 MHz bandwidth filter and then digitized with a sampling frequency of 5 MHz and a center frequency of 1.075 MHz. Figures 45.a through 45.f show one sample of the turn-on of each transmitter and Figures 46.a through 46.f show the corresponding transmitter turn-off. The last four scales of the DWT of the turn-on transients, using a Daub12 wavelet, are shown in Figures 47 and 48 and the turn-off transients in Figures 49 and 50.

The localization of the exact moment of the turn-on or turn-off of the transmitter can be extract from the DWT of these transients. Although these signals are sinusoidal, and as such the DWT should not perform well on them, their behavior in the transform domain is different before and after the switching instant. This might be due to the noise present in the records. Denoising the signals before applying the DWT is a possibility and deserves further studies. The transition instances can also be observed from the time

domain plots for most of the signals. If we observe Figure 45.d, the switching instant is difficult to identify, although if we look at Figure 48 the transition instance is observable at levels ten, 11 and 12. A spectrogram of the record in question was performed. Figures 51.a and 51.b show the result of the spectrogram using a hamming window and without a window, respectively. The instant of the switching time can also be observed in both spectrograms. The results of wavelet transforming these signals are inconclusive, since the spectrogram produces a good localization of the transition instant. A feature extraction algorithm based on the energy of each scale for the purpose of classification other than detection was implemented. The results were not satisfactory, since the levels of energy for a given scale seemed to be similar for all records and all transmitters.

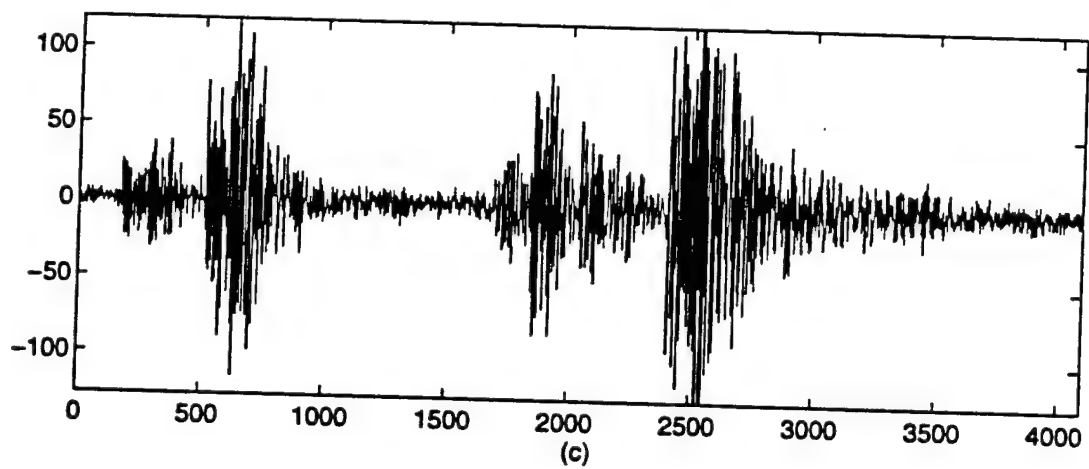
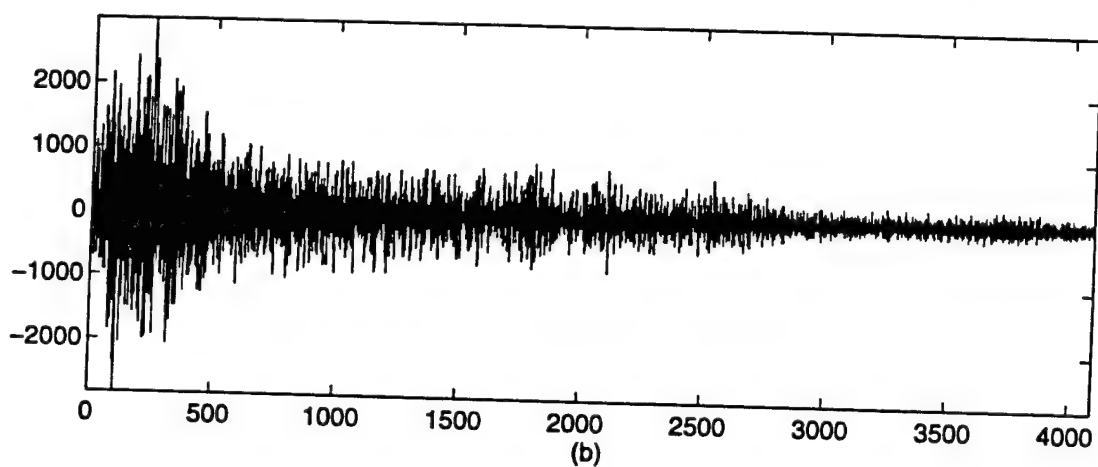
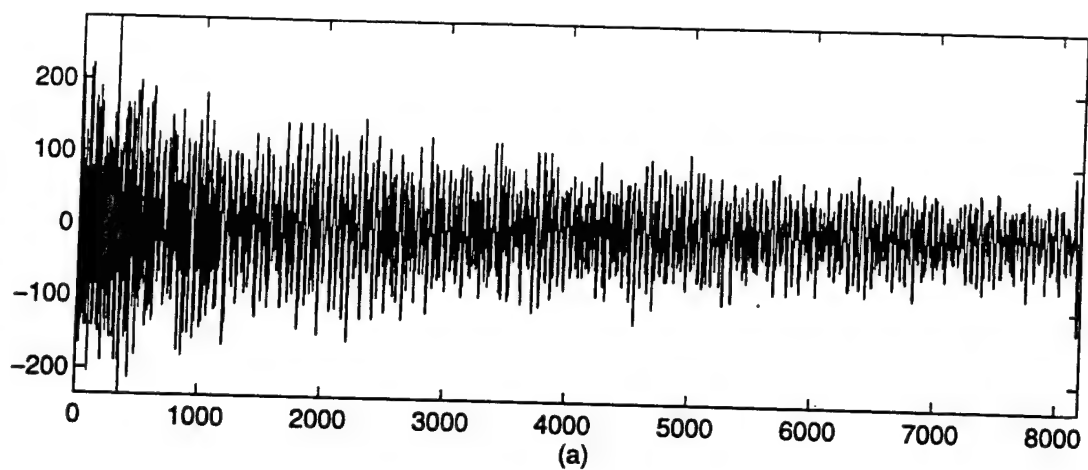


Figure 34. Time Representation of The Metallic Sound Group  
(a) Dropped Metallic Object  
(b) Gong  
(c) Latch

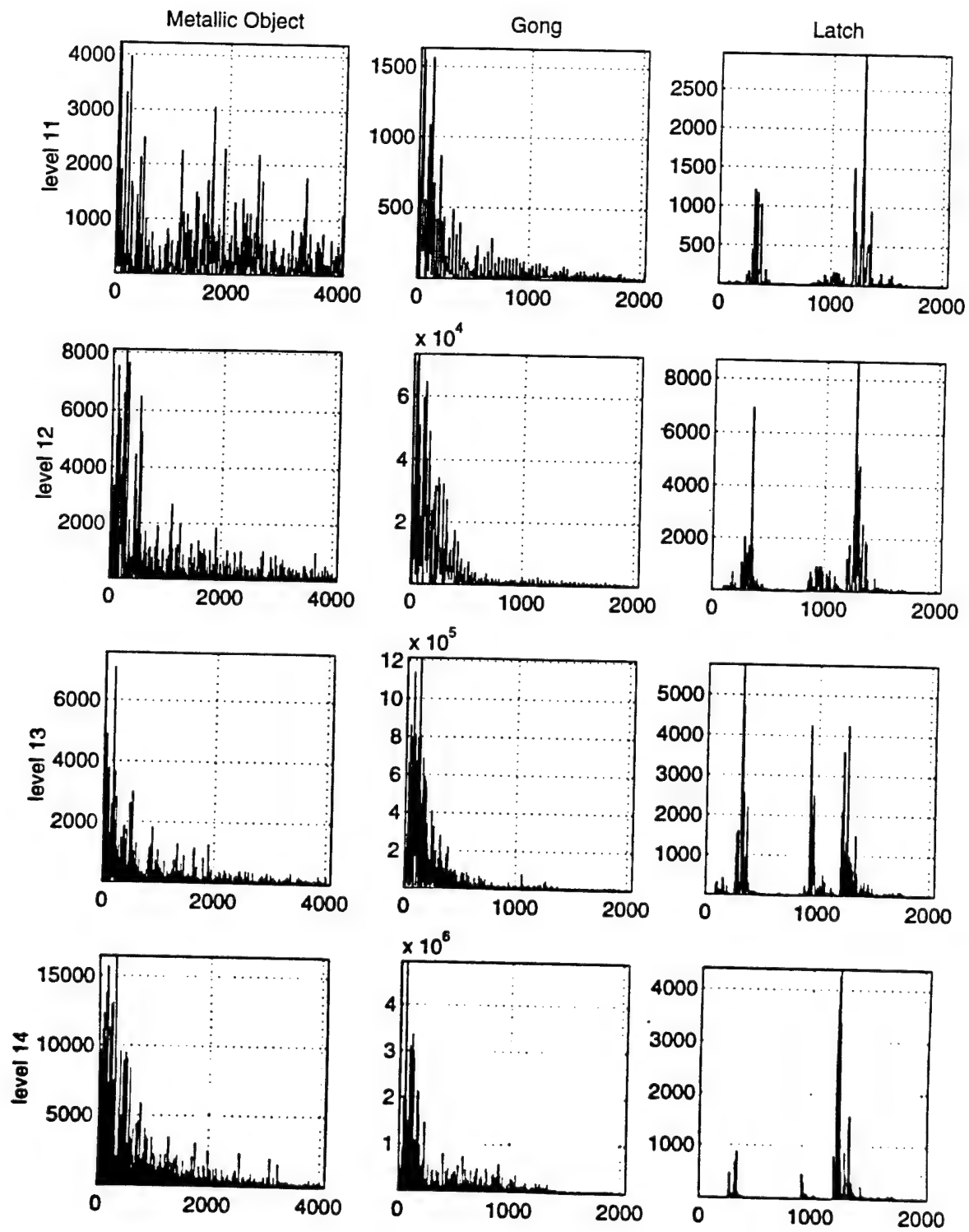


Figure 35. DWT of the Dropped Metallic Object, the Gong and the Latch

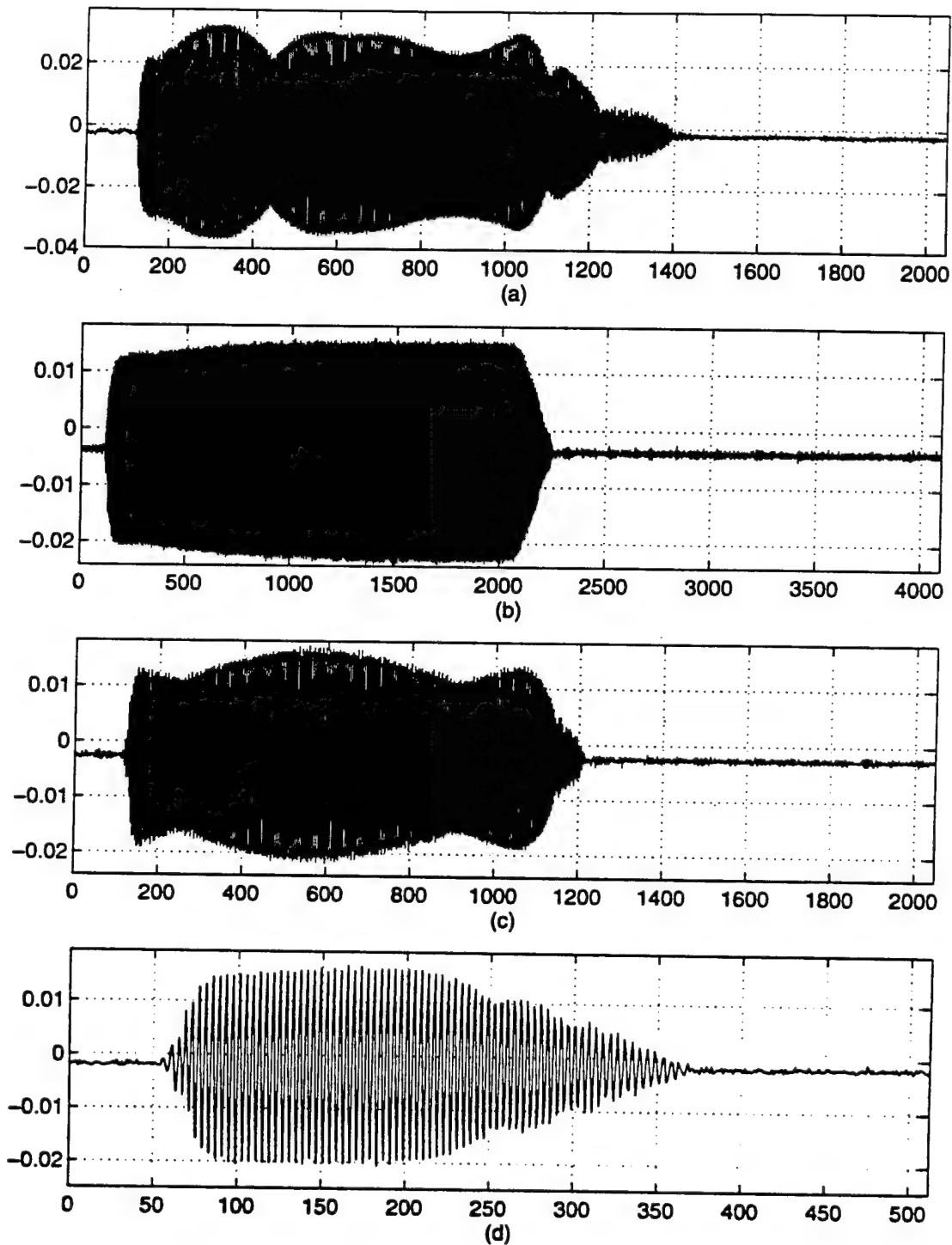


Figure 36. First Pulse of First Record of Radar  
 (a) AN/APS-31A  
 (b) AN/SPS 64(V), 1.0 Microsec., Pulse Duration  
 (c) AN/SPS 64(V), 0.5 Microsec., Pulse Duration  
 (d) AN/SPS 64(V), 0.15 Microsec., Pulse Duration

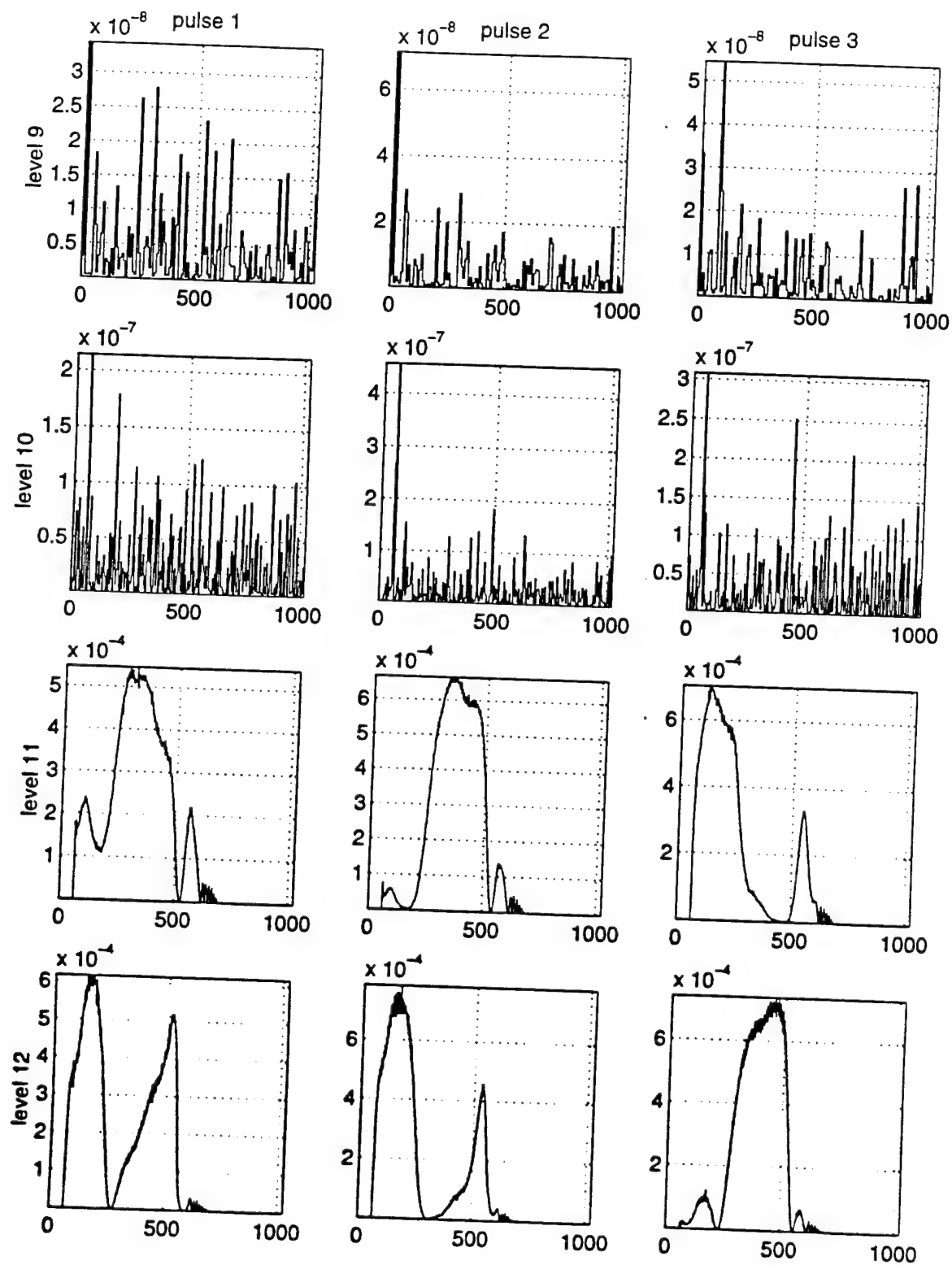


Figure 37. DWT of Pulses 1, 2 and 3 of Radar AN/APS-31A

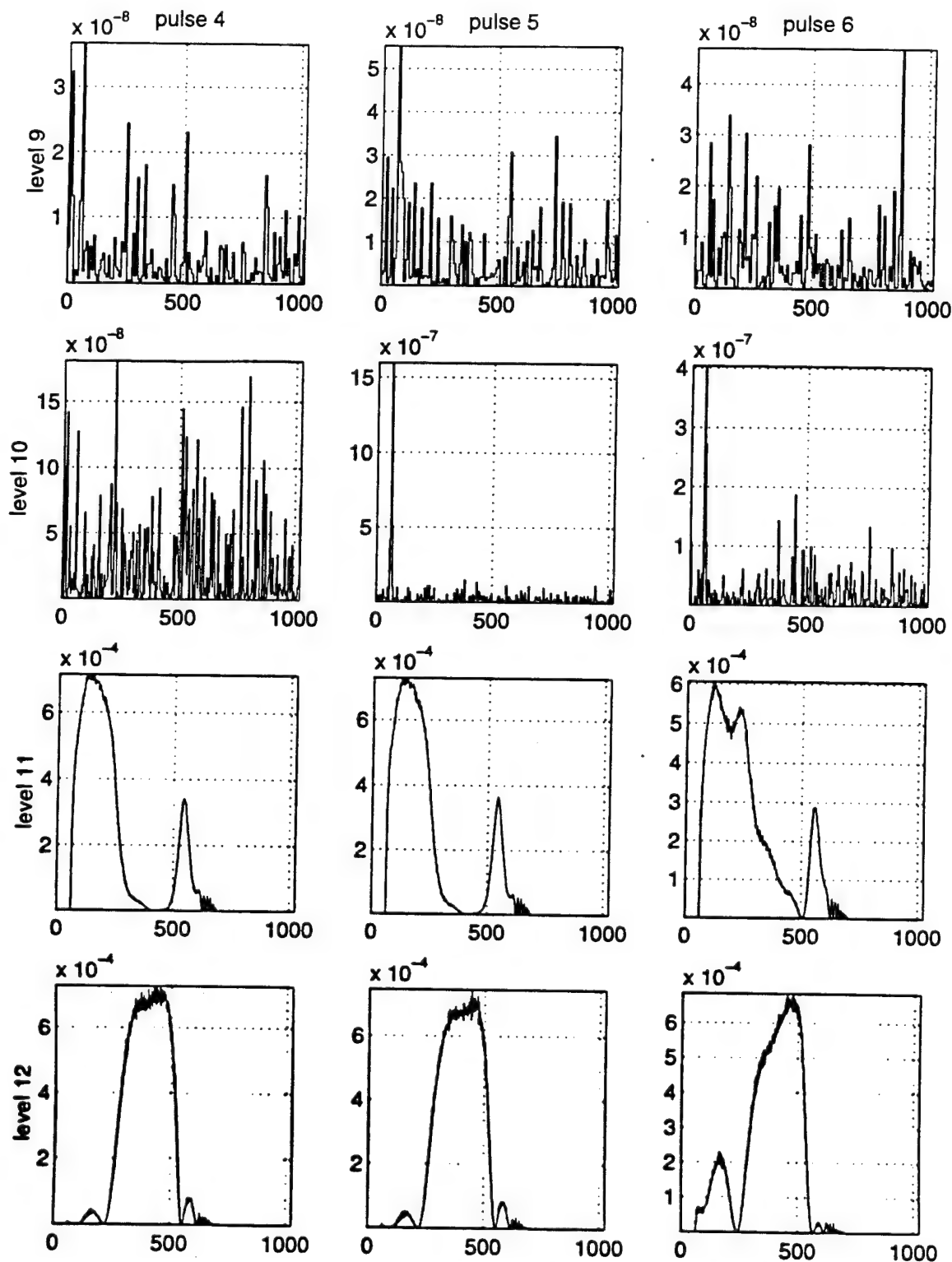


Figure 38. DWT of Pulses 4, 5 and 6 of Radar AN/APS-31A



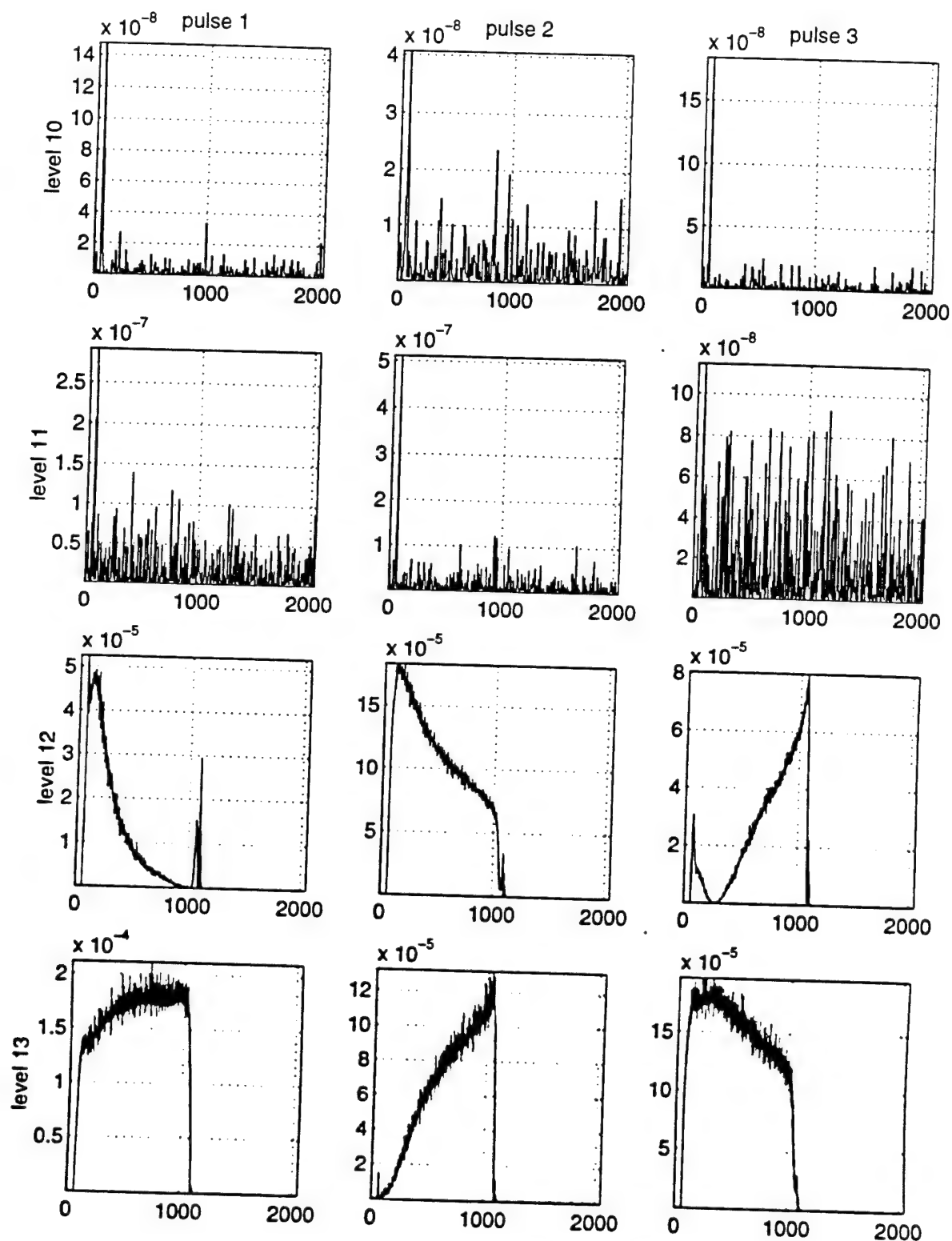


Figure 39. DWT of Pulses 1, 2 and 3 of Radar AN/SPS-64 (V),  
Pulse Duration = 1.0 microsecond

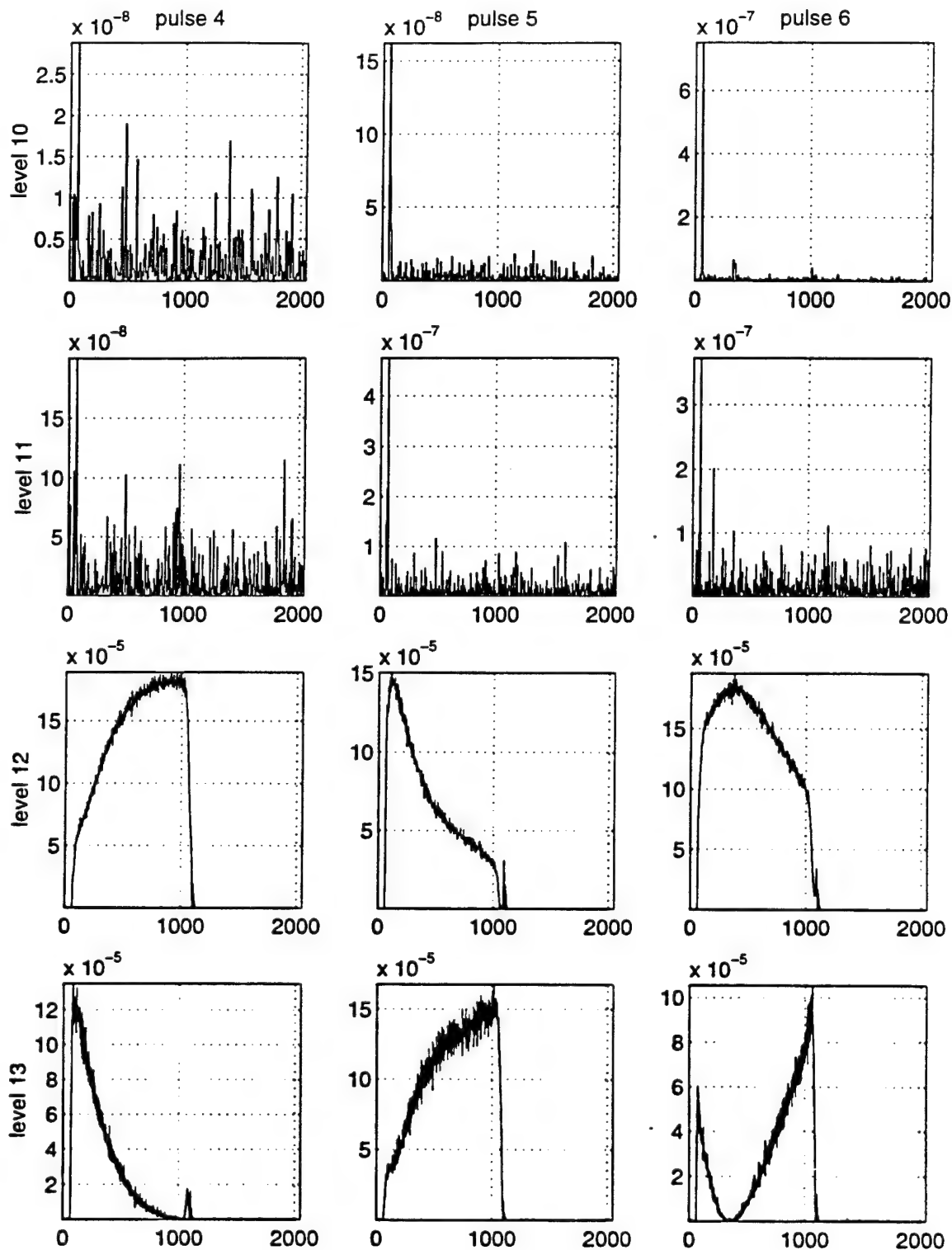


Figure 40. DWT of Pulses 4, 5 and 6 of Radar AN/SPS-64 (V),  
Pulse Duration = 1.0 microsecond

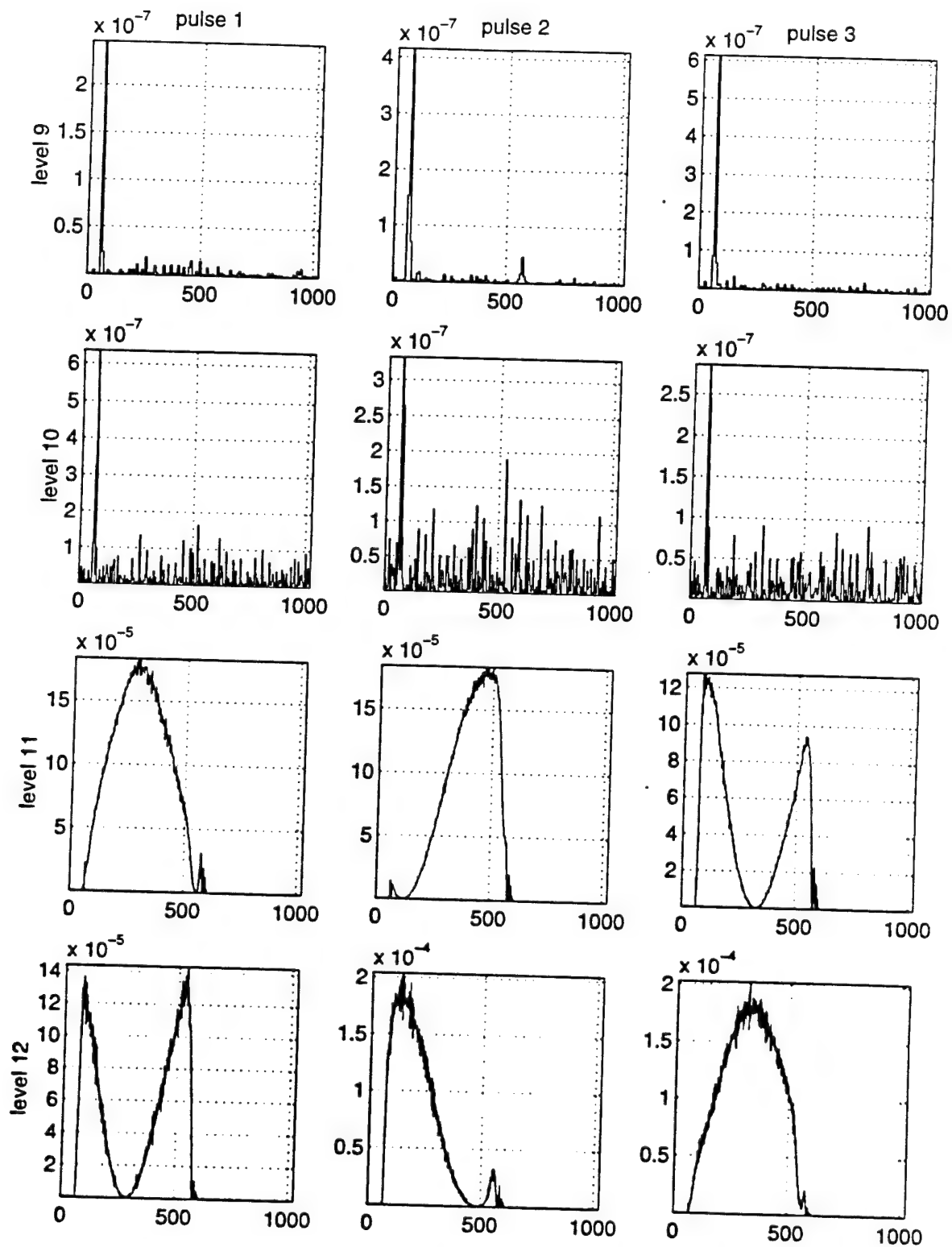


Figure 41. DWT of Pulses 1, 2 and 3 of Radar AN/SPS-64 (V),  
Pulse Duration = 0.5 microseconds

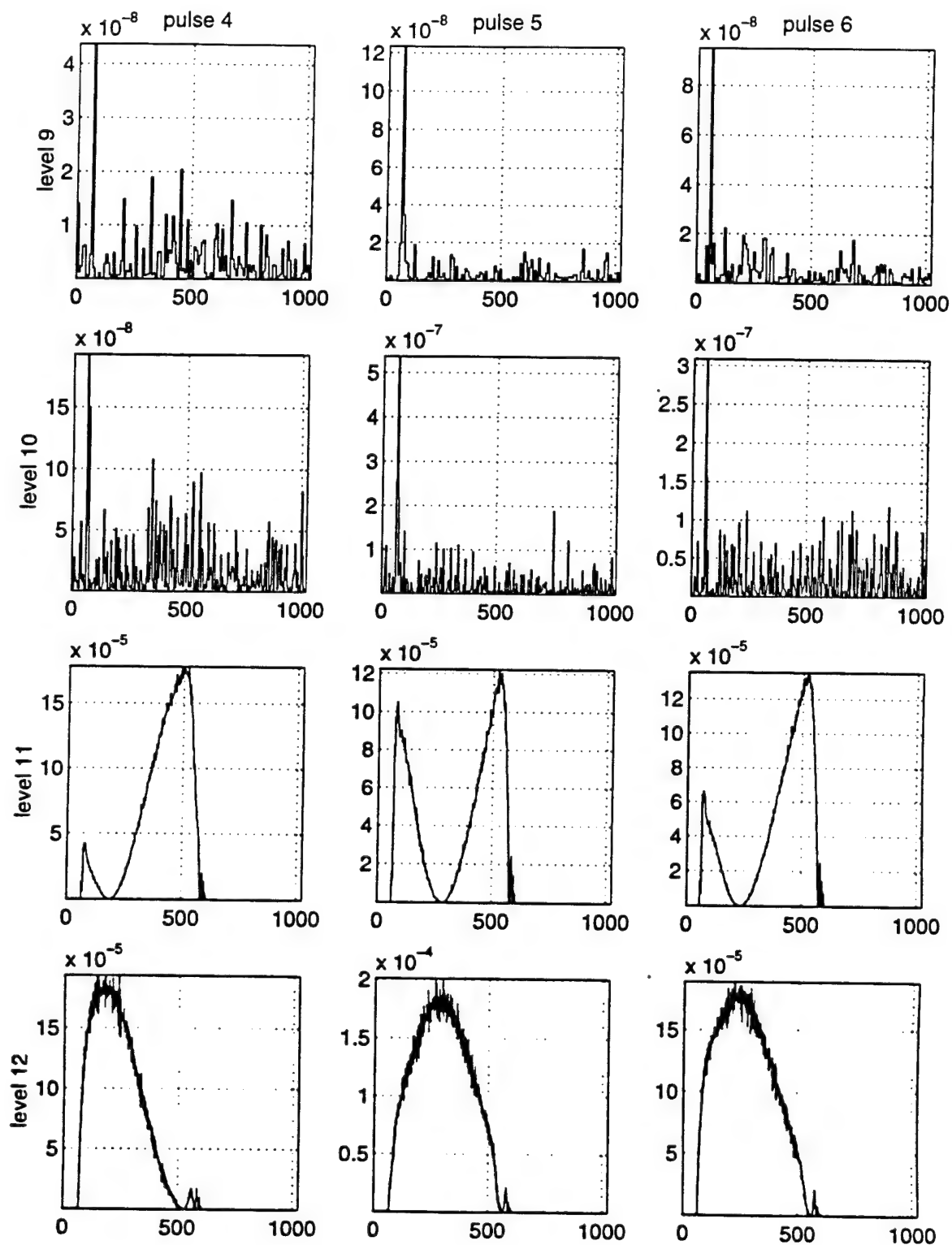


Figure 42. DWT of Pulses 4, 5 and 6 of Radar AN/SPS-64 (V),  
Pulse Duration = 0.5 microseconds

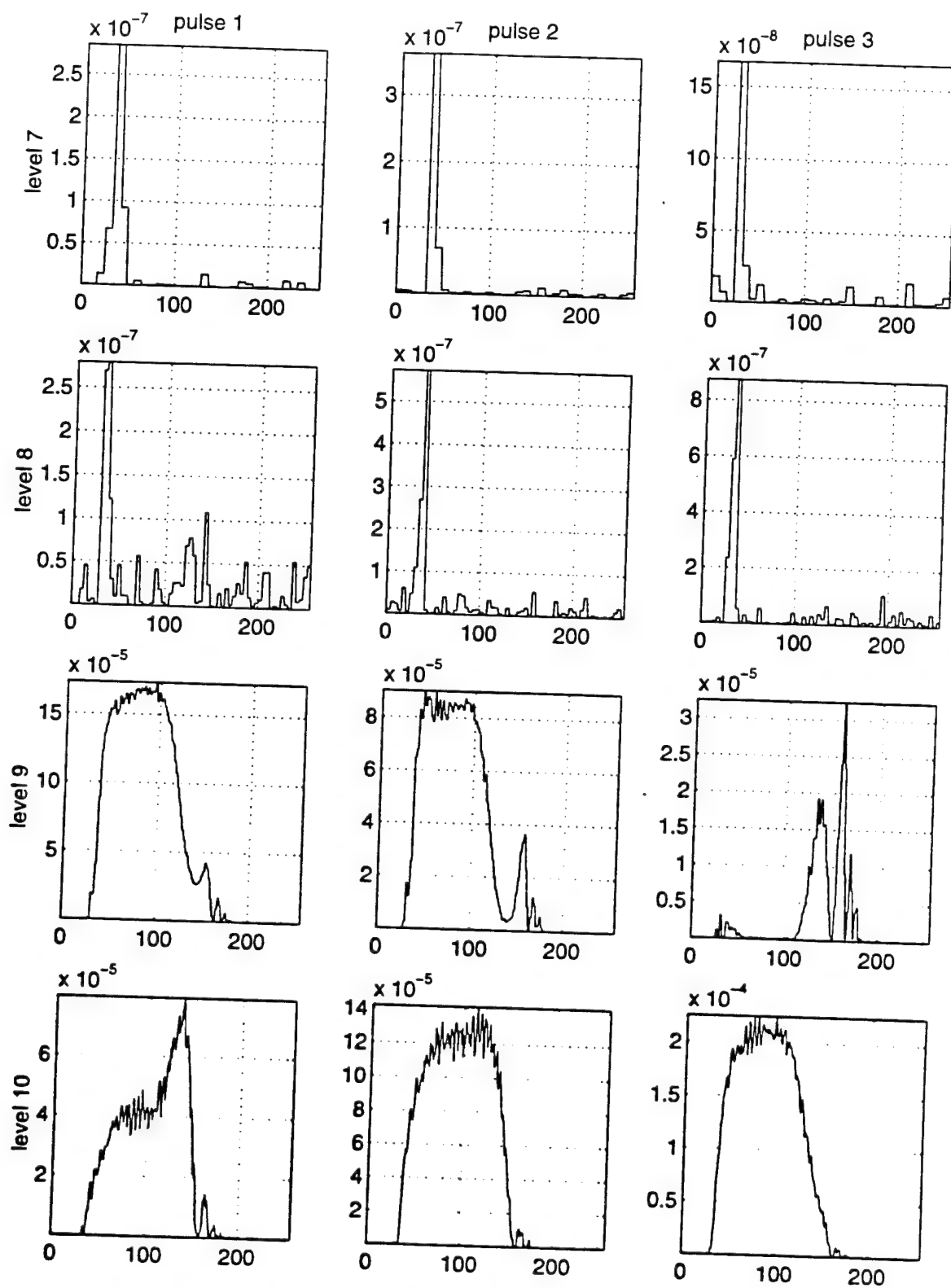


Figure 43. DWT of Pulses 1, 2 and 3 of Radar AN/SPS-64 (V),  
Pulse Duration = 0.15 microseconds

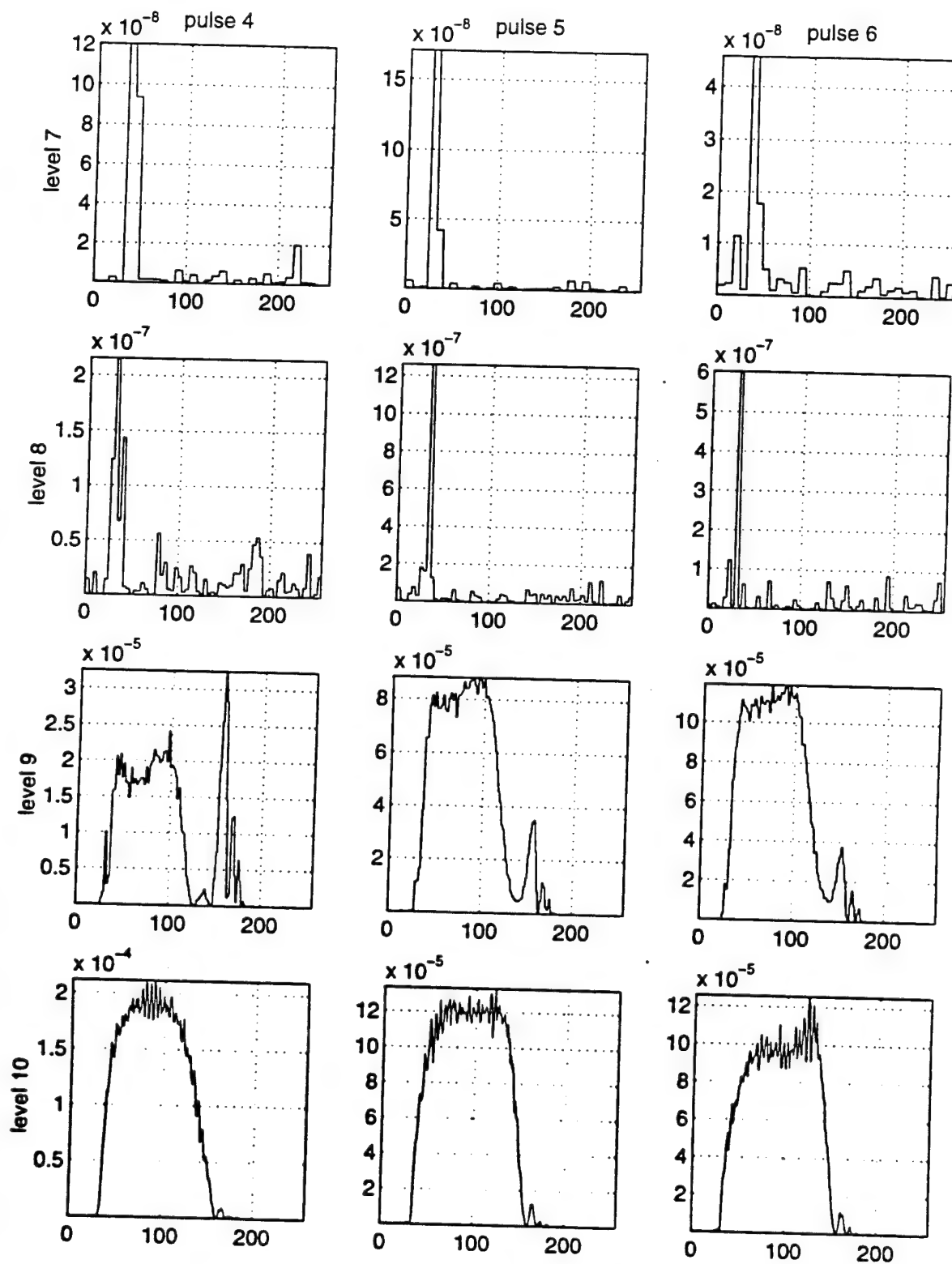


Figure 44. DWT of Pulses 4, 5 and 6 of Radar AN/SPS-64 (V),  
Pulse Duration = 0.15 microseconds

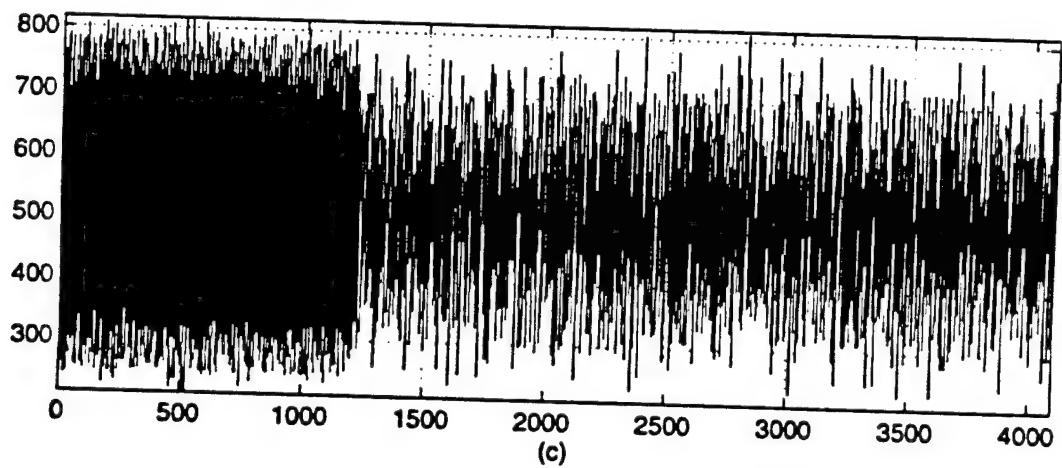
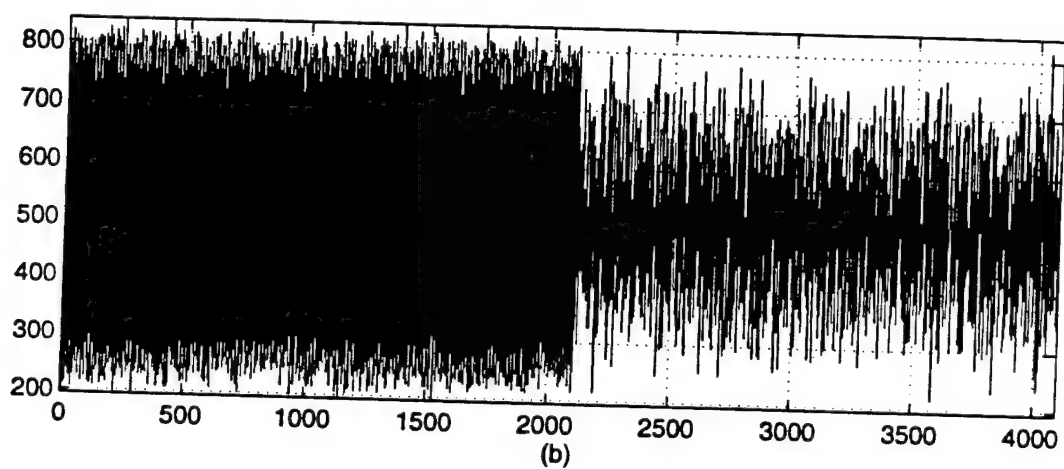
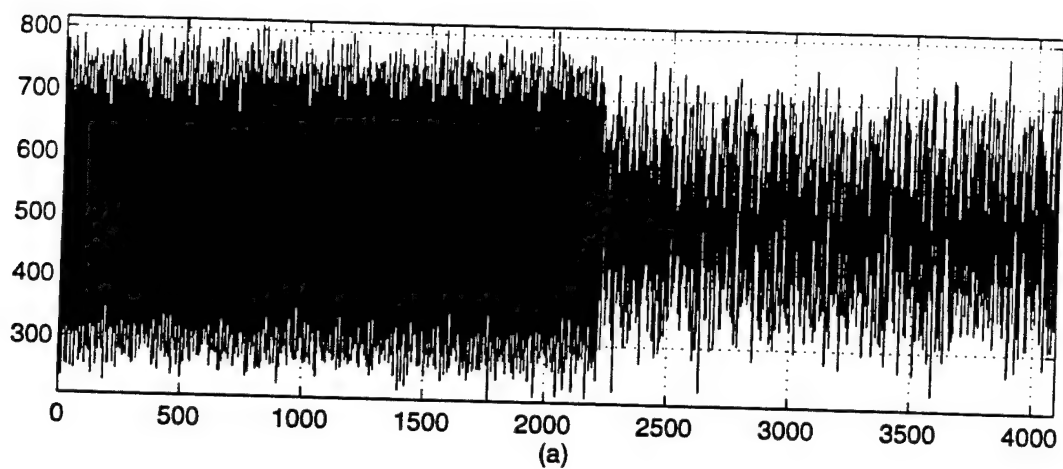


Figure 45. First Record of the Turn-On of:

(a) Transmitter 1

(b) Transmitter 2

(c) Transmitter 3

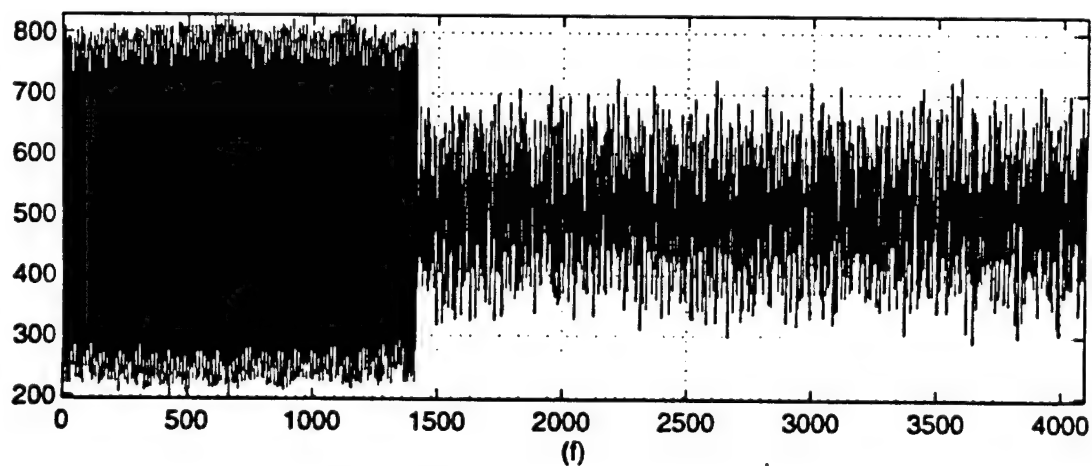
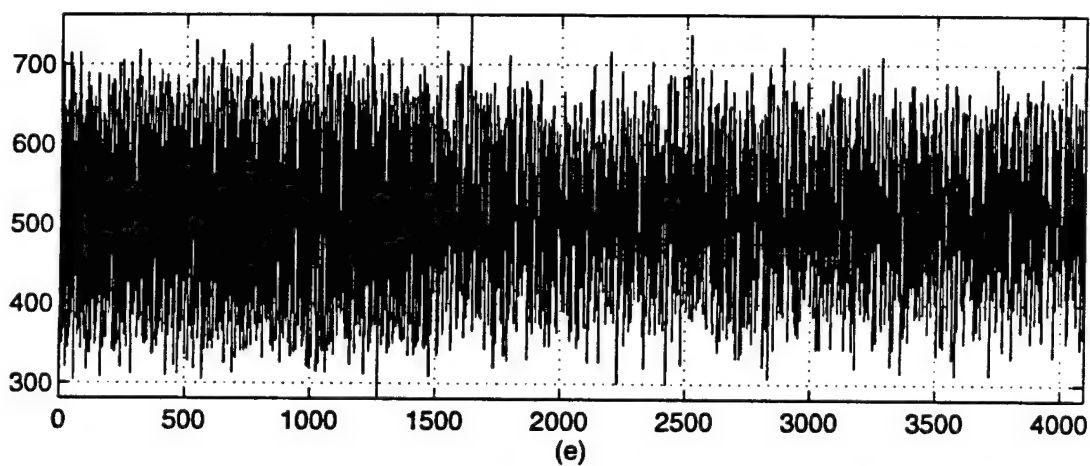
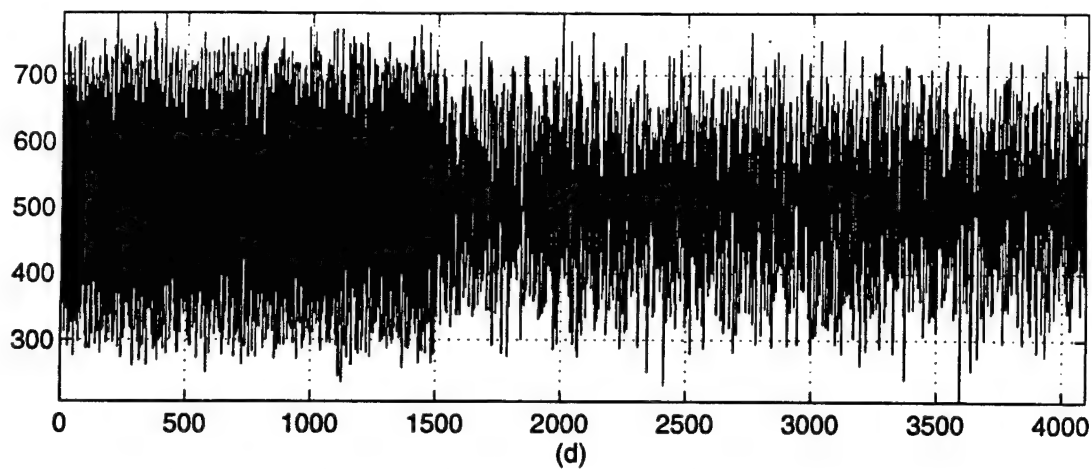


Figure 45. First Record of the Turn-On of:  
(d) Transmitter 4  
(e) Transmitter 5  
(f) Transmitter 6



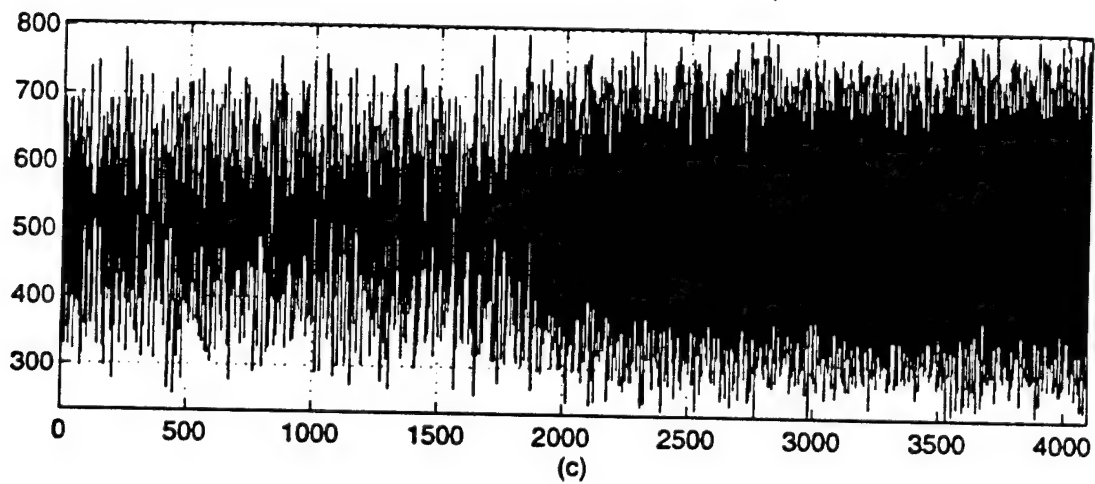
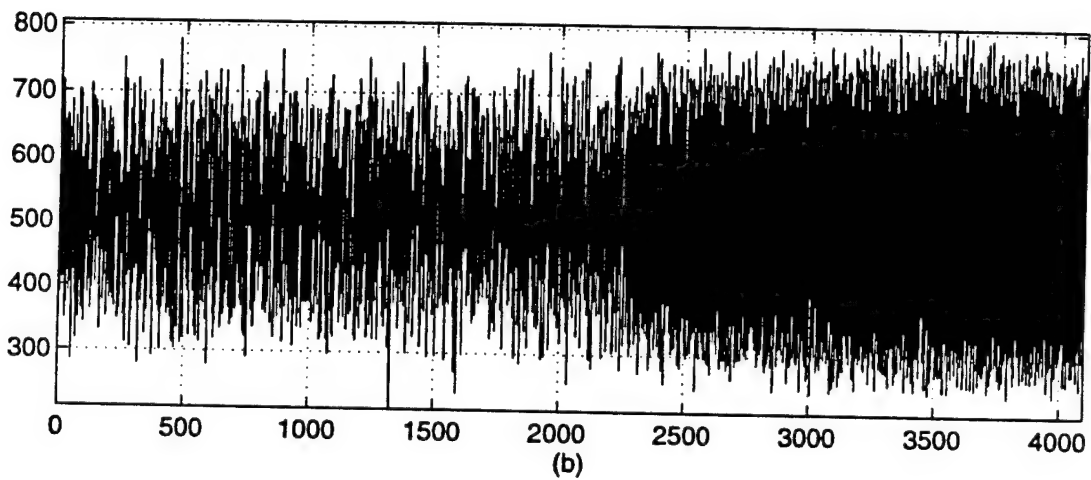
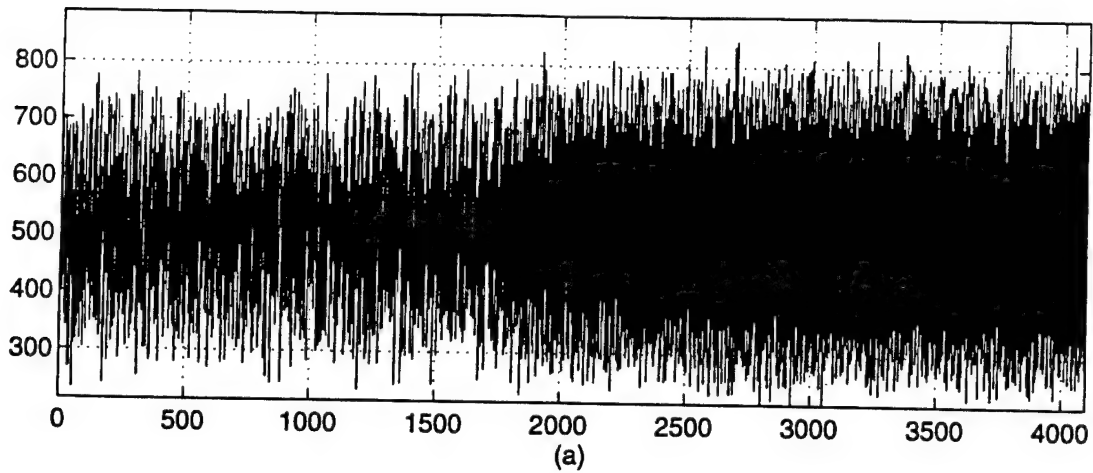


Figure 46. First Record of the Turn-Off of:  
(a) Transmitter 1  
(b) Transmitter 2  
(c) Transmitter 3

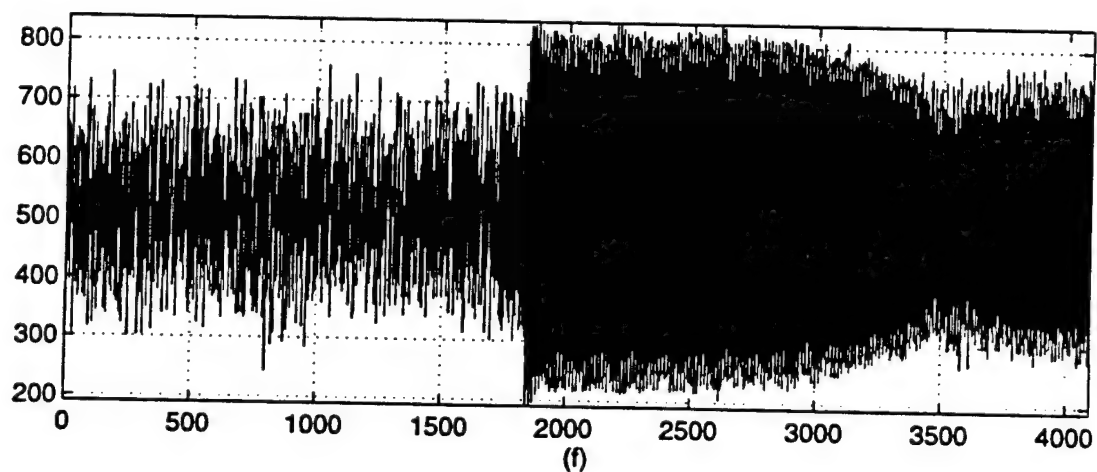
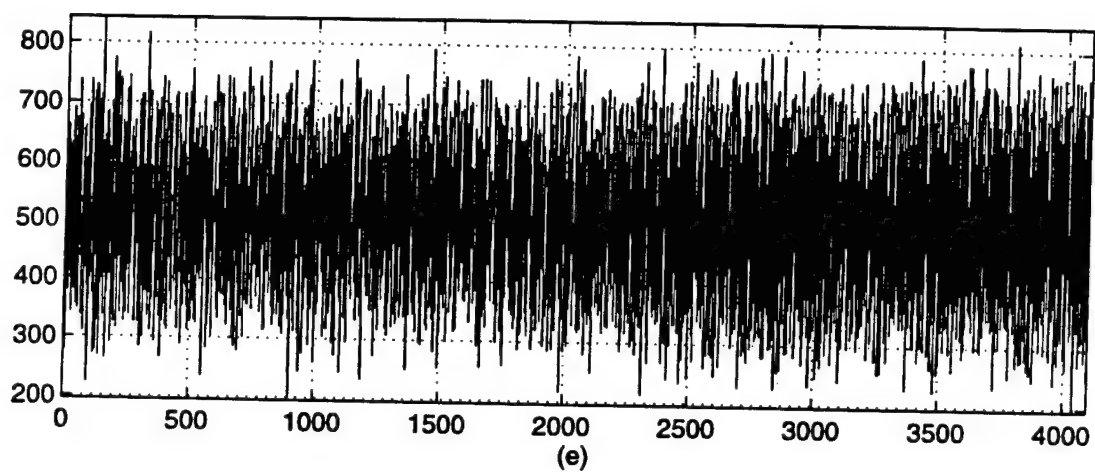
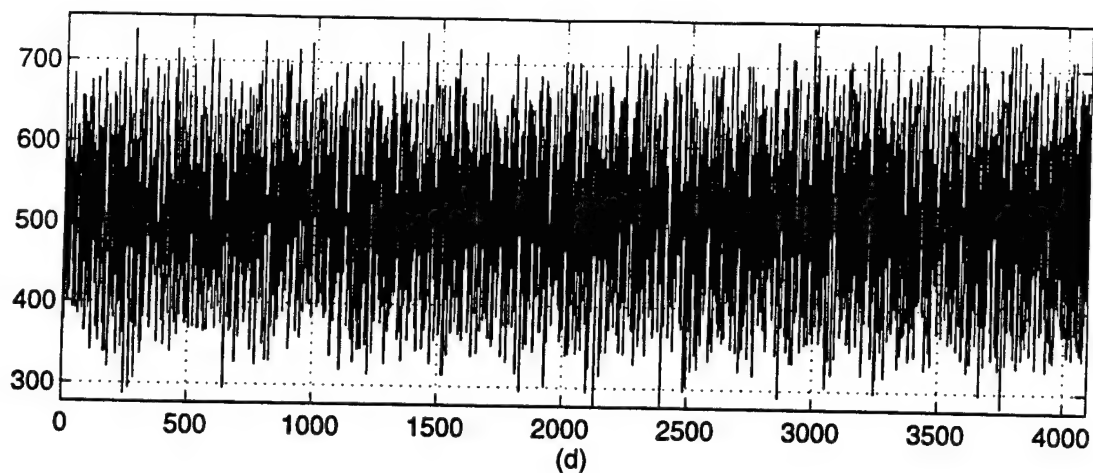


Figure 46. First Record of the Turn-Off of:

(d) Transmitter 4

(e) Transmitter 5

(f) Transmitter 6

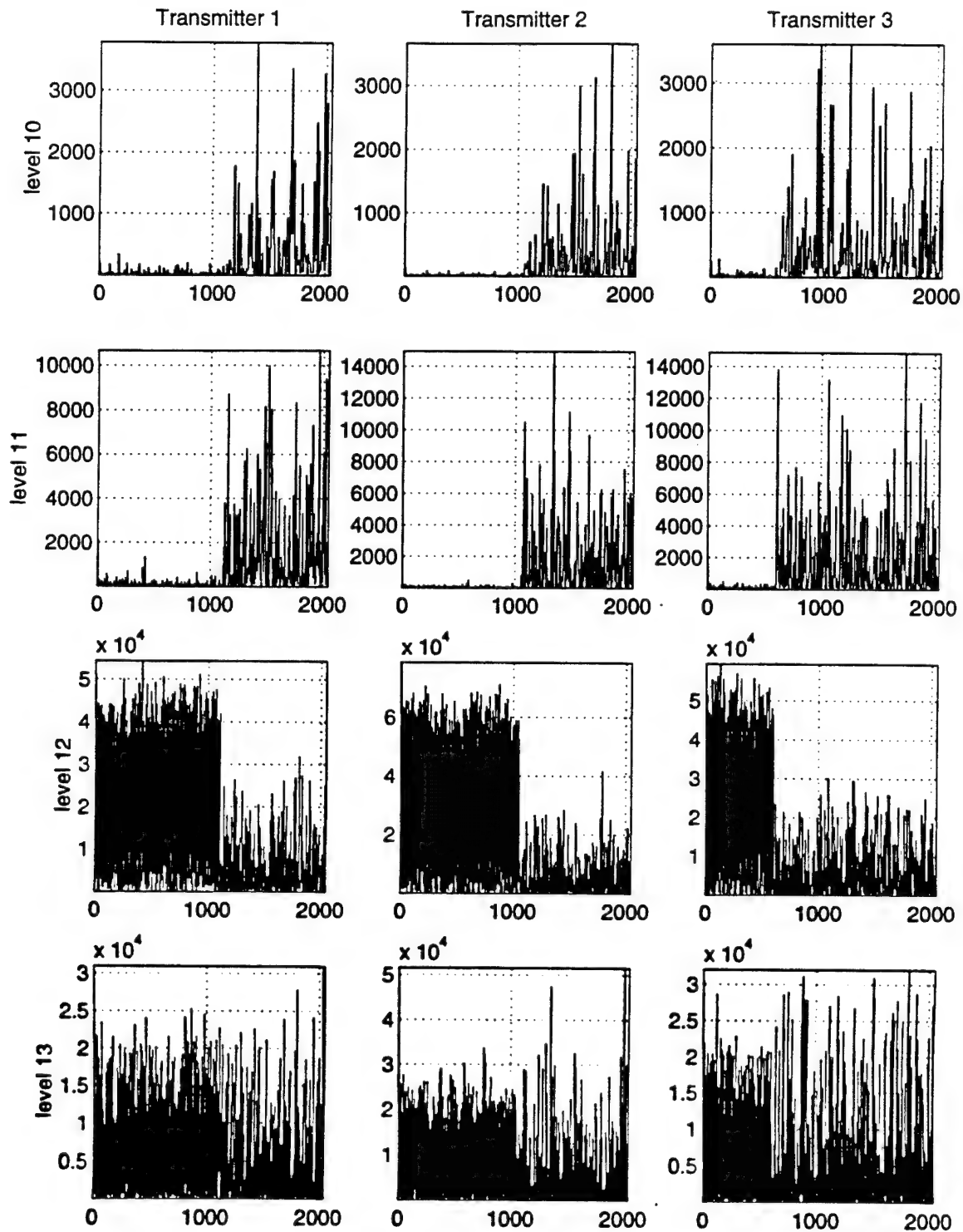


Figure 47. DWT of the First Record of the Turn-On of Transmitters 1, 2 and 3

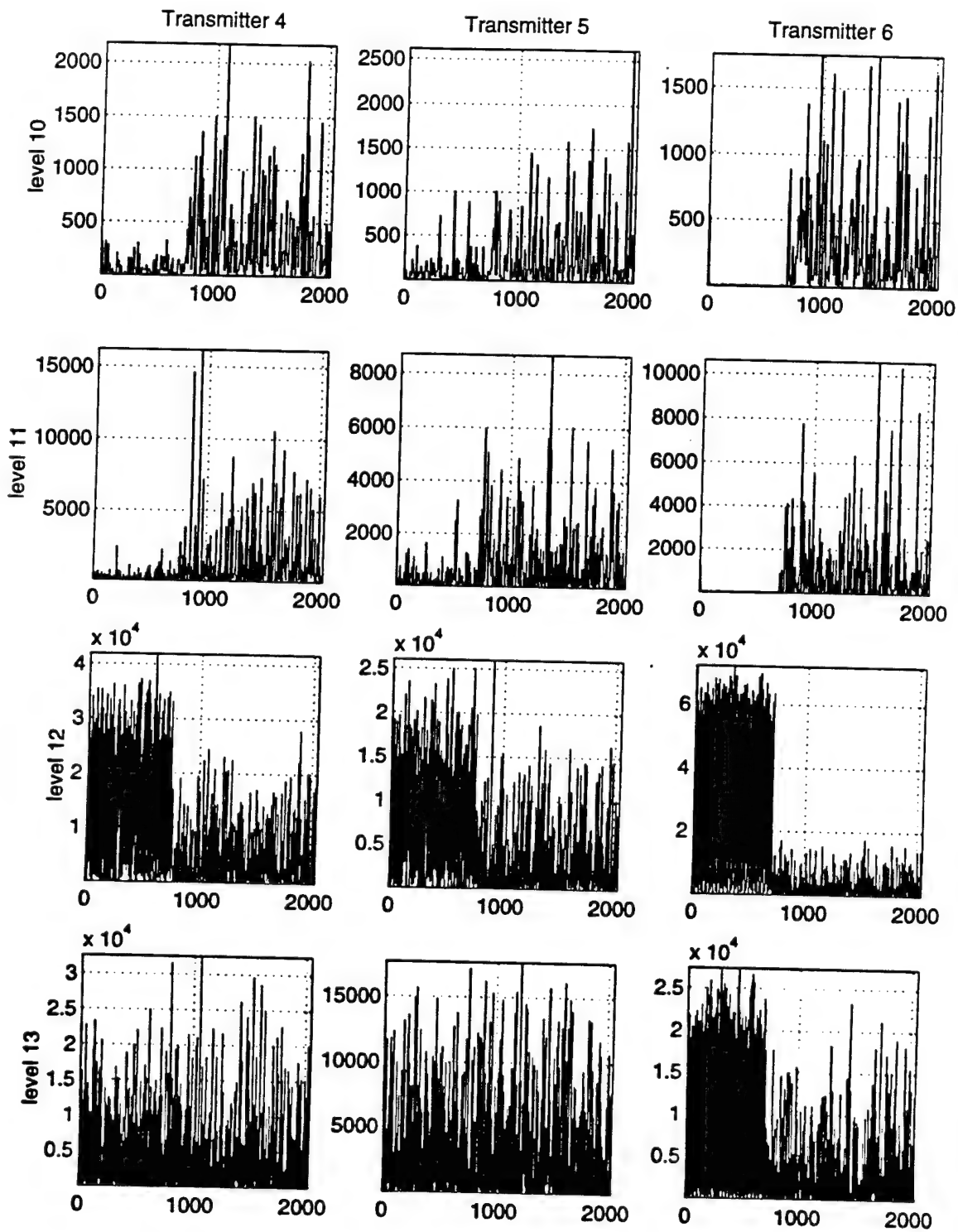


Figure 48. DWT of the First Record of the Turn-On of Transmitters 4, 5 and 6

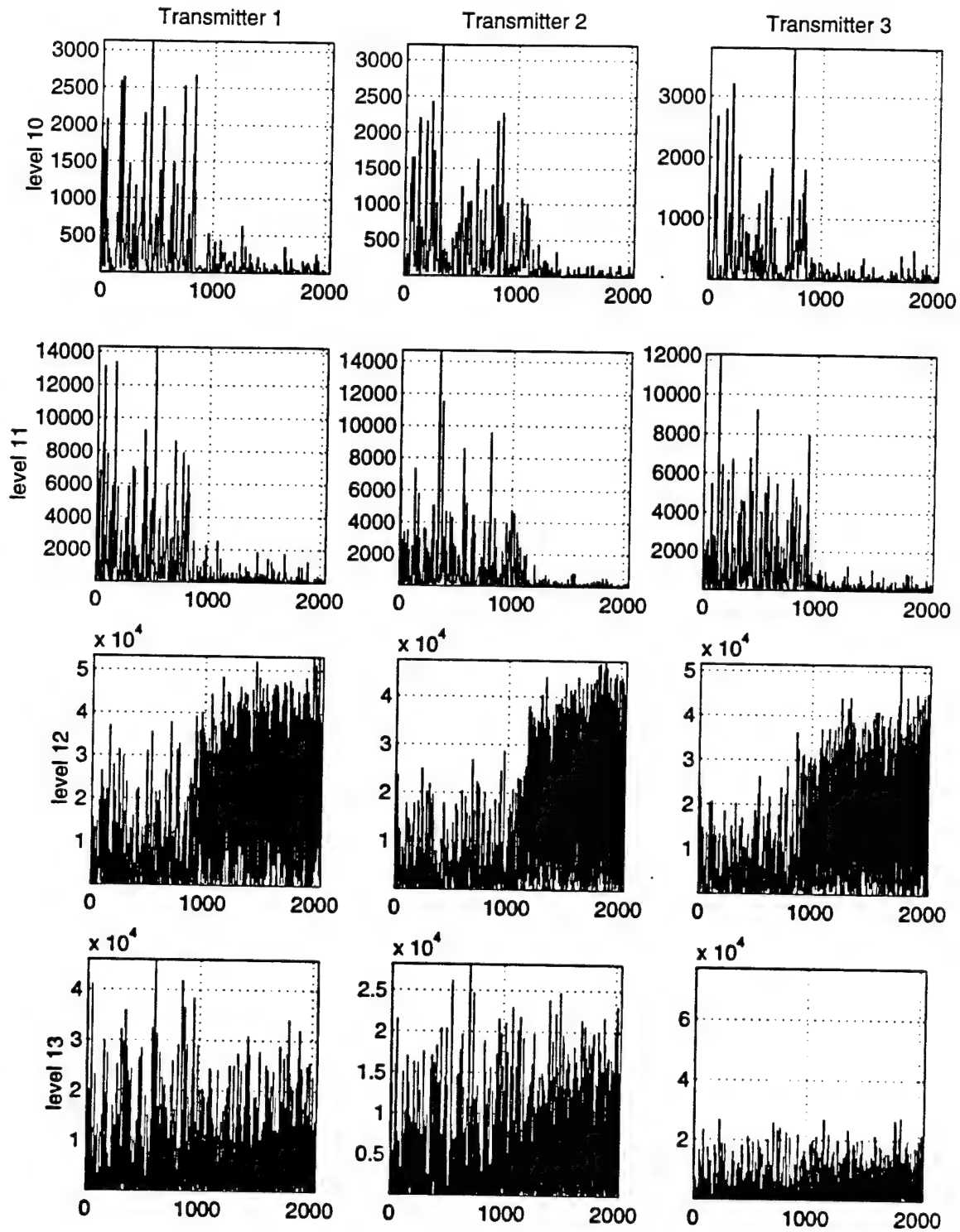


Figure 49. DWT of the First Record of the Turn-Off of Transmitters 1, 2 and 3

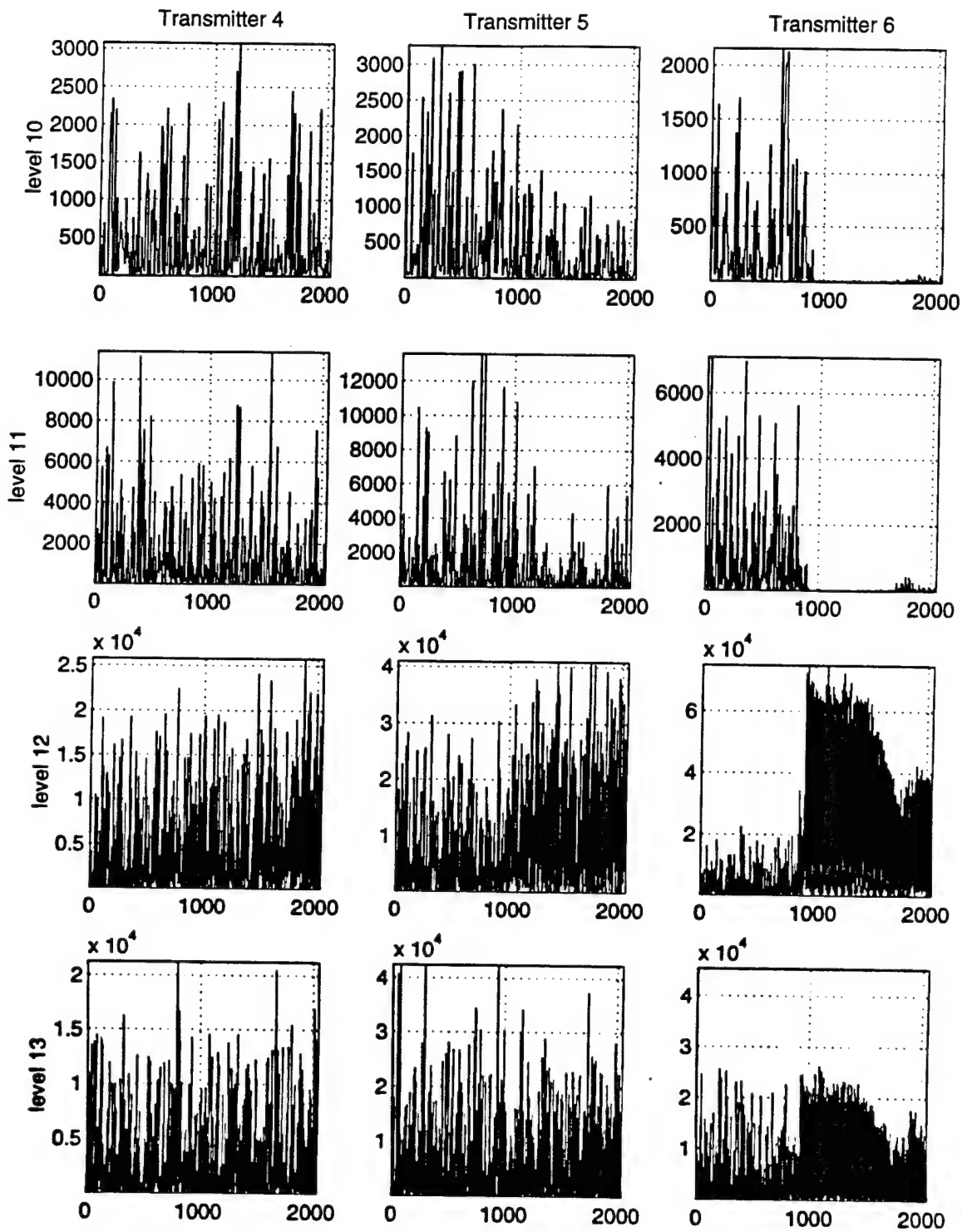


Figure 50. DWT of the First Record of the Turn-Off of Transmitters 4, 5 and 6

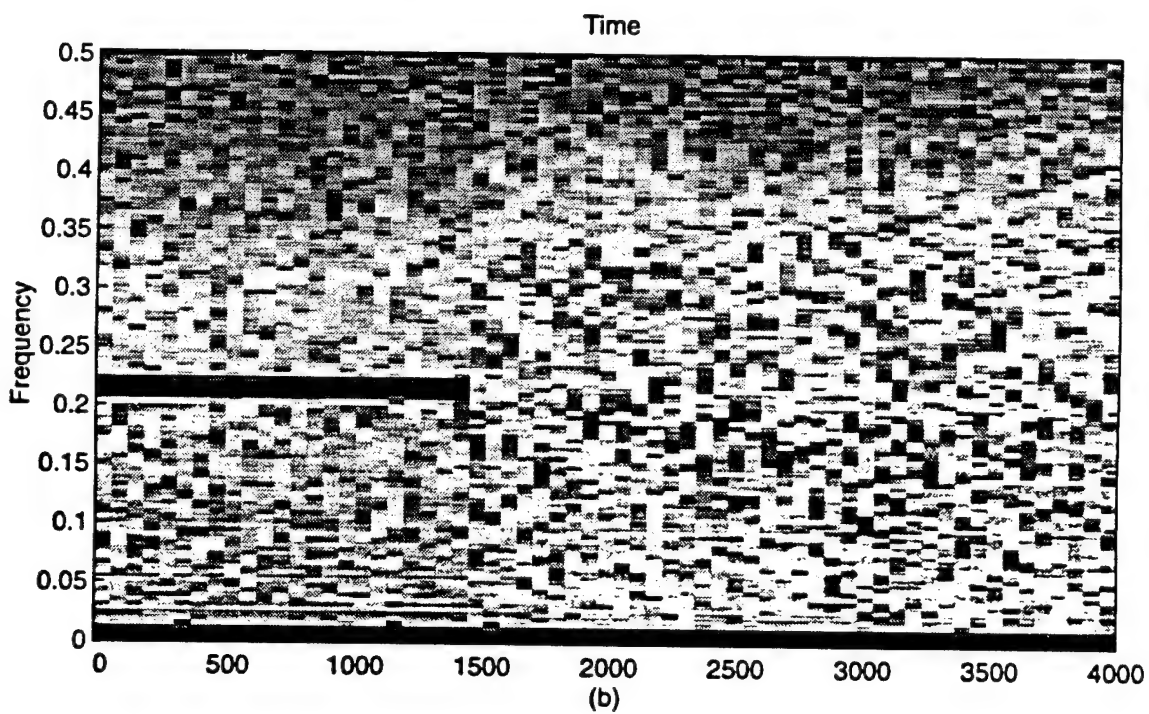
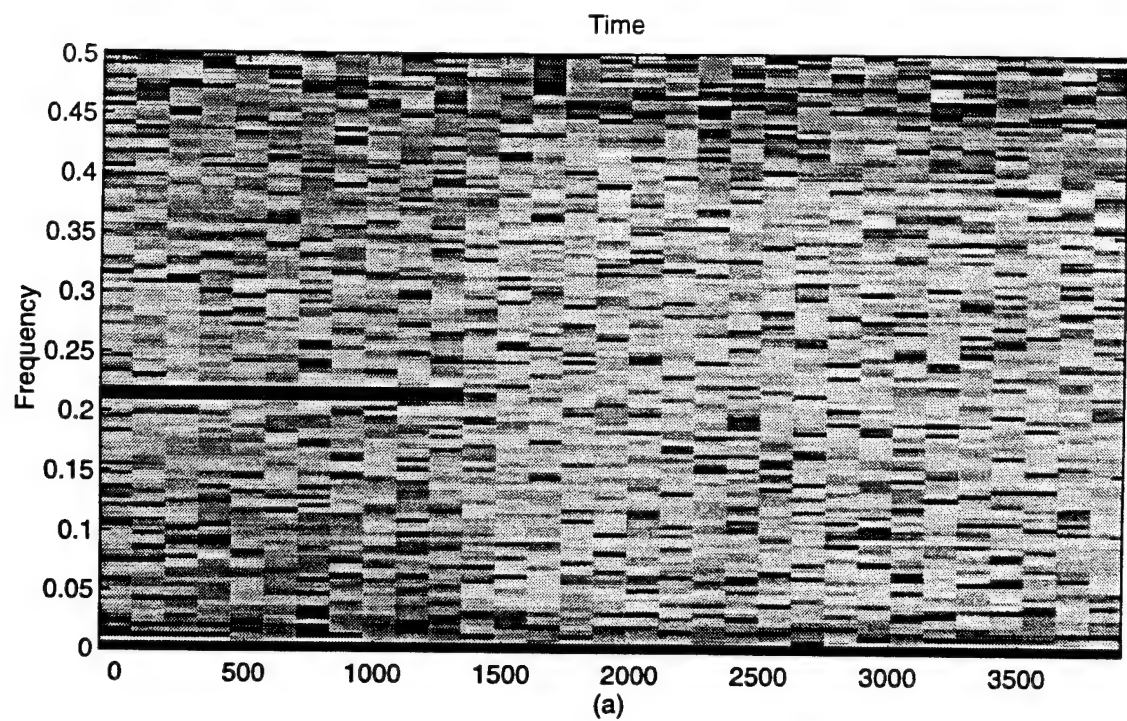


Figure 51. Spectrogram of Transmitter 4 First Turn-On Record:  
(a) No Windowing  
(b) Using a 128 Points Hamming Window



## IV. CONCLUSIONS

### A. RESULTS

The identification of transient signals using the Discrete Wavelet Transform (DWT) provided mixed results. When the signals of interest have sharp variations in the time domain and the Signal-to-Noise-Ratio is positive, it is possible to identify these behavior changes in the scales. The wavelet used as a basis function determines the overall performance of the algorithm. The use of the *ad hoc* wavelet as a basis function improved the identification of the test signals in low SNR, possibly because it matched the signal characteristics better and enhanced them relative to the noise.

The DWT of the sounds produced by metallic objects indicated that it might be possible to use the wavelet transform for classification purposes. Also, the latch sound analysis showed that the exact instant of the transient occurrences can be established.

The question of what should be the scale of interest was brought up during the simulation and the test phase. The higher scales have more energy and better time resolution and should; therefore, have more importance than the lower scales.

A transient detection algorithm for the transmitters turn-on / turn-off based on the energy of the scales was implemented, but the results were inconclusive. The transformed signals have the same total energy at any given scale when compared between signals. This was perhaps due to the transmitters being manufactured by the same maker.

The DWT is simple to implement and is very fast. Its speed depends on the number of scaling function coefficients that is being used.

### B. RECOMMENDATIONS FOR FUTURE STUDIES

The implementation of an automatic transient detection algorithm based on the scales of the signal is the goal. Further studies, focused on finding an optimum wavelet function, are necessary. The use of a larger number of actual transient signals with known characteristics is recommended to make the conclusions statistically more reliable. An



additional untapped source of information is the phase of the DWT, which should be investigated if the signals of interest are complex.

## APPENDIX A. DEVELOPMENT OF NECESSARY CONDITIONS

### Necessary Condition 1:

Integrating both sides of Equation 2.27

$$\begin{aligned}\int \varphi(t)dt &= \int \sum_k h_0(k)\varphi(2t-k)dt \\ &= \sum_k h_0(k) \int \varphi(2t-k)dt.\end{aligned}\tag{A.1}$$

Let  $z = 2t - k$ , so  $dz = dt/2$ , substituting into Equation A.1

$$\int \varphi(t)dt = \frac{1}{2} \sum_k h_0(k) \int \varphi(z)dz,\tag{A.2}$$

$$\frac{\int \varphi(t)dt}{\int \varphi(z)dz} = \frac{1}{2} \sum_k h_0(k).\tag{A.3}$$

The left hand side of Equation A.3 is equal to 1 and so

$$\frac{1}{2} \sum_k h_0(k) = 1,$$

or

$$\sum_k h_0(k) = 2.\tag{A.4}$$

**Necessary Condition 2:**

Substituting Equation 2.27 in Equation 2.39 we obtain

$$\begin{aligned}\langle \varphi(t)\varphi(t-k) \rangle &= \int \sum_n h_0(n)\varphi(2t-n) \sum_m h_0(m)\varphi(2(t-k)-m)dt \\ &= \sum_n \sum_m h_0(n)h_0(m) \int \varphi(2t-n)\varphi(2t-2k-m)dt = \delta(k) . \quad (\text{A.5})\end{aligned}$$

The integral of Equation 2.44 is non-zero only if

$$2t-n = 2t-2k-m \Rightarrow n = 2k+m .$$

That leads to

$$\int \varphi(2t-n)\varphi(2t-2k-m)dt = \frac{1}{2}\delta(n-m-2k) . \quad (\text{A.6})$$

Substituting in equation A.5 we obtain

$$\sum_n \sum_m h_0(n)h_0(m) \frac{1}{2}\delta(n-m-2k) = \delta(k) . \quad (\text{A.7})$$

The Kronecker delta on the left hand side exists only if  $m = n - 2k$  and Equation A.7 is now

$$\frac{1}{2} \sum_n h_0(n)h_0(n-2k) = \delta(k) ,$$

or

$$\sum_n h_0(n)h_0(n-2k) = 2\delta(k) . \quad (\text{A.8})$$

**Necessary Condition 3:**

Reproducing Equation A.8

$$\sum_n h_0(n)h_0(n-2k) = 2\delta(k).$$

Let  $k = 0$ , and substitute in Equation A.8

$$\sum_n h_0(n)h_0(n) = 2\delta(0) = 2. \quad (\text{A.9})$$

**Necessary Condition 4:**

Substituting Equation 2.47 and summing over  $k$  we get

$$\sum_k \sum_n h_0(n)h_0(n-2k) = 2. \quad (\text{A.10})$$

Splitting Equation A.10 in even and odd terms

$$\sum_k \left[ \sum_m h_0(2m)h_0(2k+2m) + \sum_m h_0(2k+2m+1)h_0(2m+1) \right] = 2, \quad (\text{A.11})$$

rearranging terms

$$\sum_m \left[ \sum_k h_0(2k+2m) \right] h_0(2m) + \sum_m \left[ \sum_k h_0(2k+2m+1) \right] h_0(2m+1) = 2. \quad (\text{A.12})$$

Substituting Equations 2.41 and 2.42 into Equation A.12

$$S_1 \sum_m h_0(2m) + S_2 \sum_m h_0(2m+1) = 2. \quad (\text{A.13})$$

Applying the same equations again in Equation A.13

$$S_1^2 + S_2^2 = 2. \tag{A.14}$$

Solving for  $S_1$  and  $S_2$  in Equations A.10 and A.13 we obtain

$$S_1 = \sum_n h_0(2n) = 1. \tag{A.15}$$

$$S_2 = \sum_n h_0(2n+1) = 1. \tag{A.16}$$

## APPENDIX B. DWT OF THE ARTIFICIAL SIGNALS IN NOISE

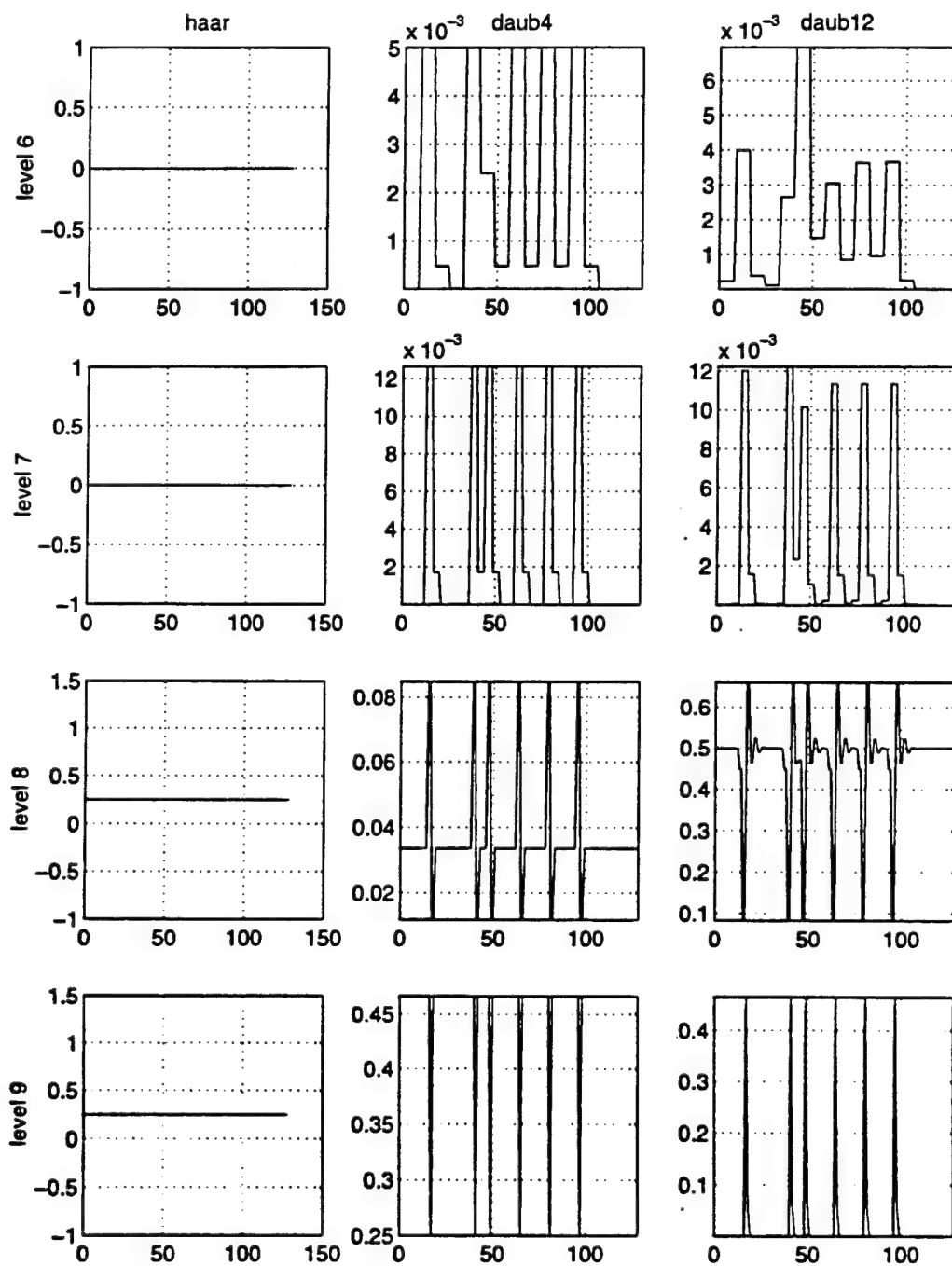


Figure B1. DWT of BPSK, SNR = 20dB

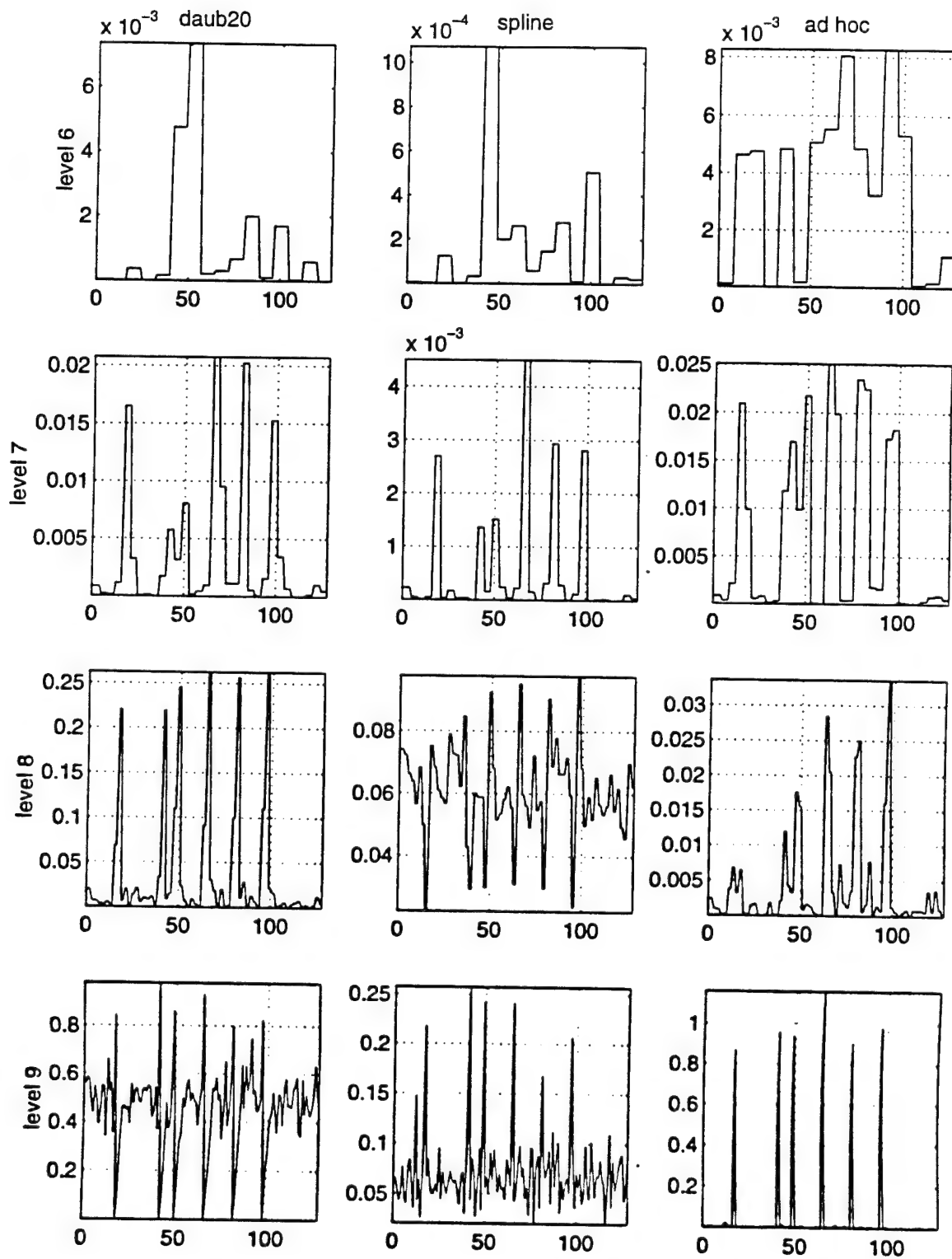


Figure B2. DWT of BPSK, SNR = 20dB

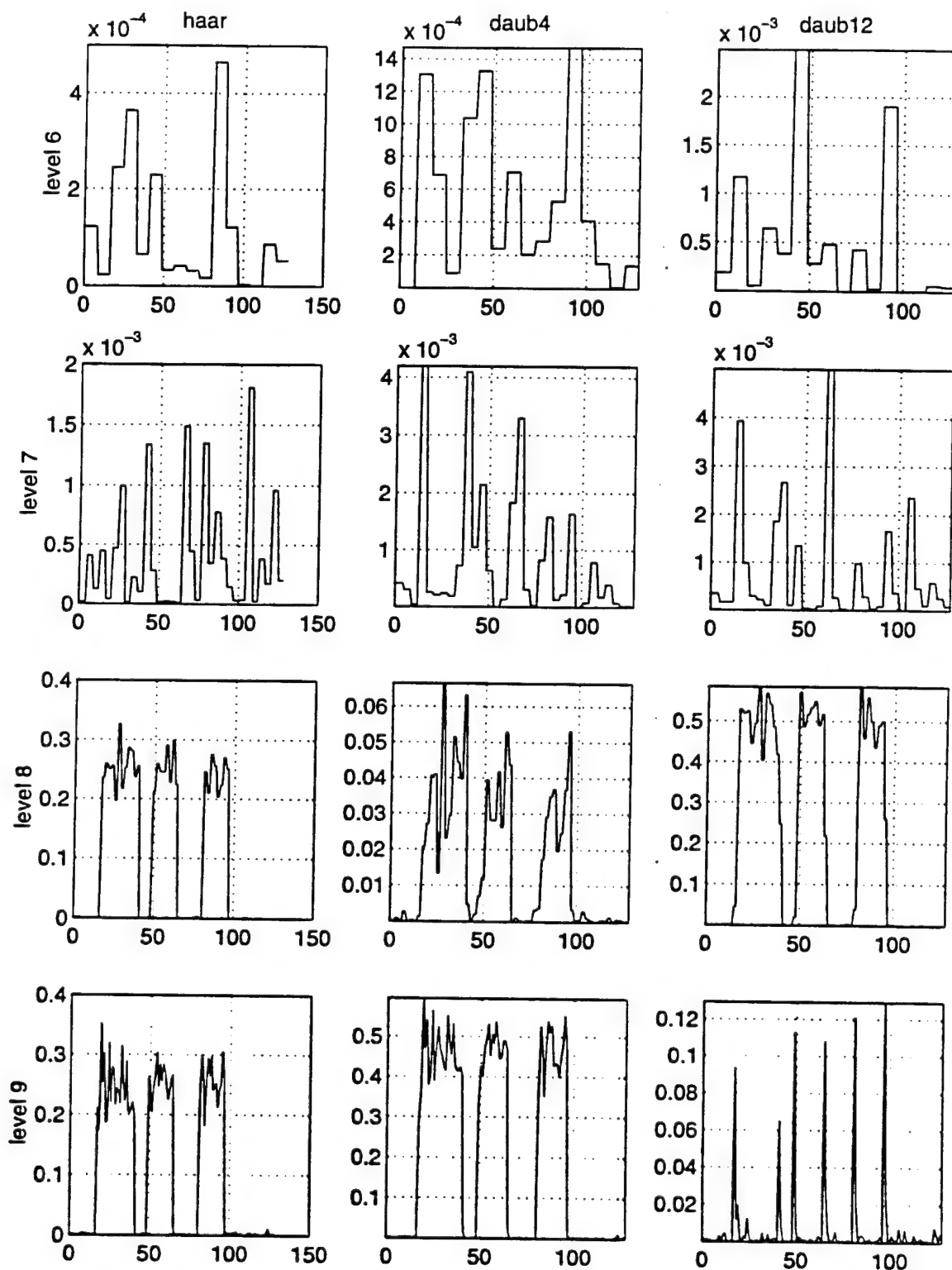


Figure B3. DWT of OOK, SNR = 20 dB



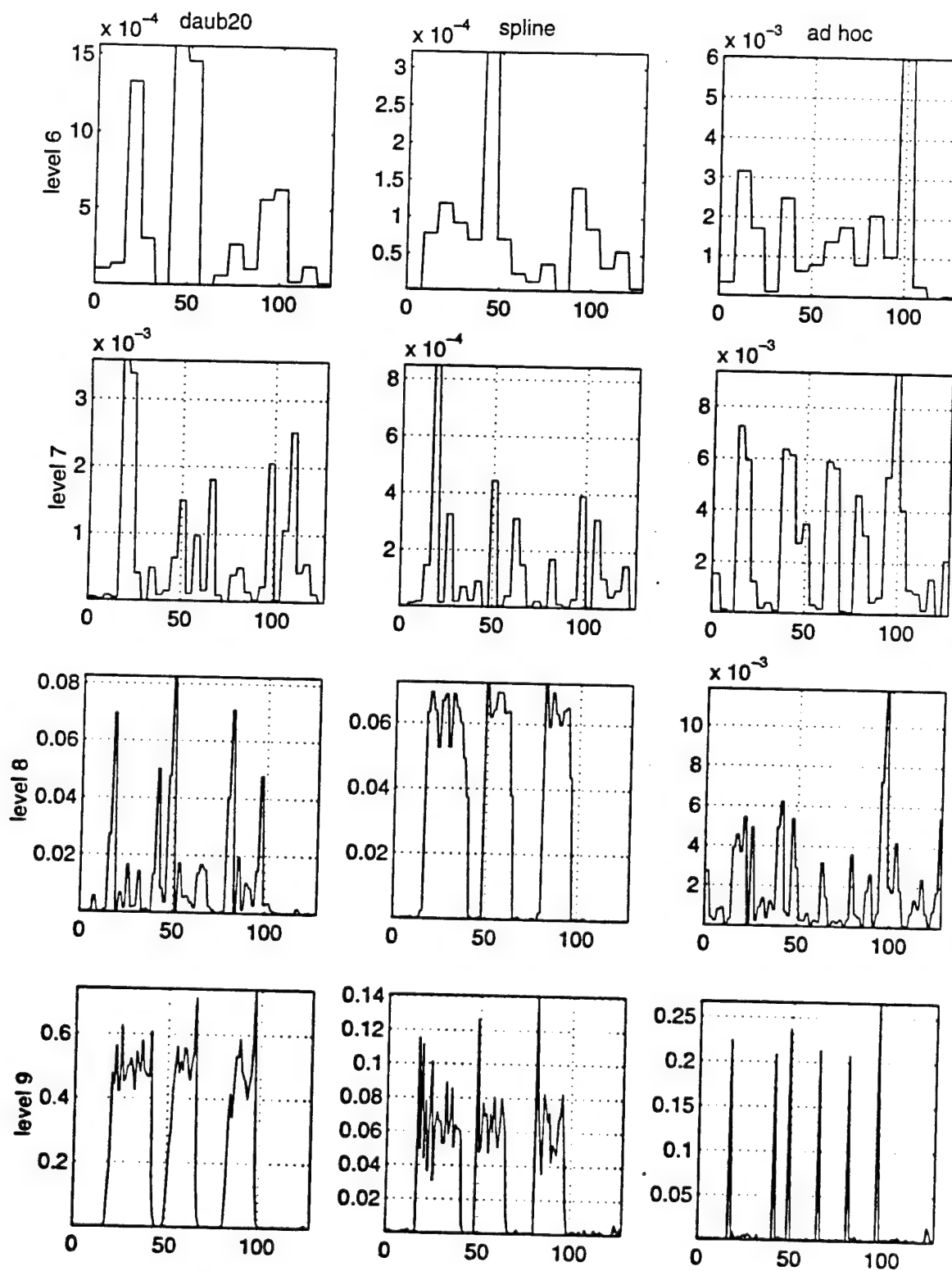


Figure B4. DWT of OOK, SNR = 20 dB

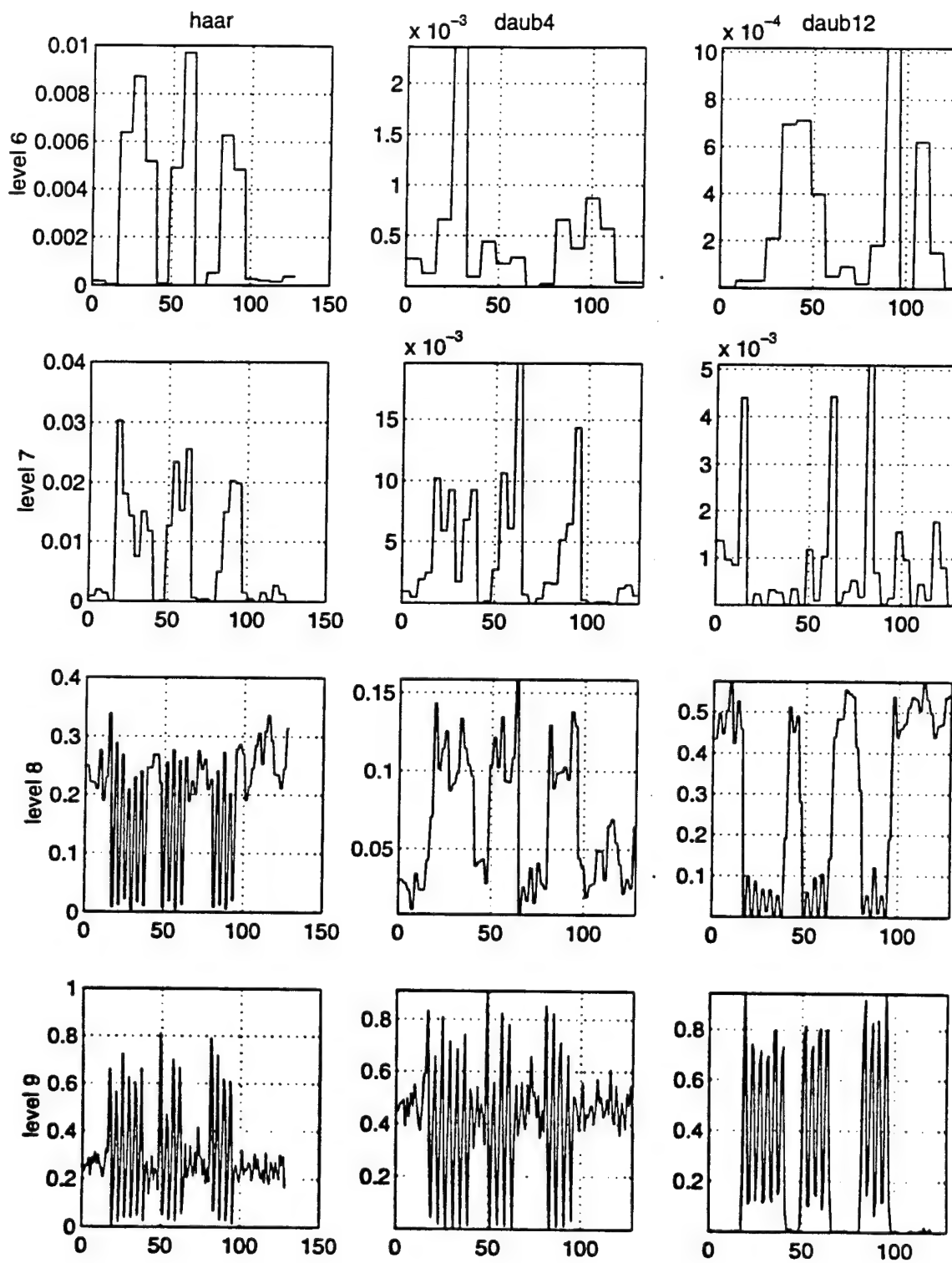


Figure B5. DWT of FSK, SNR = 20 dB

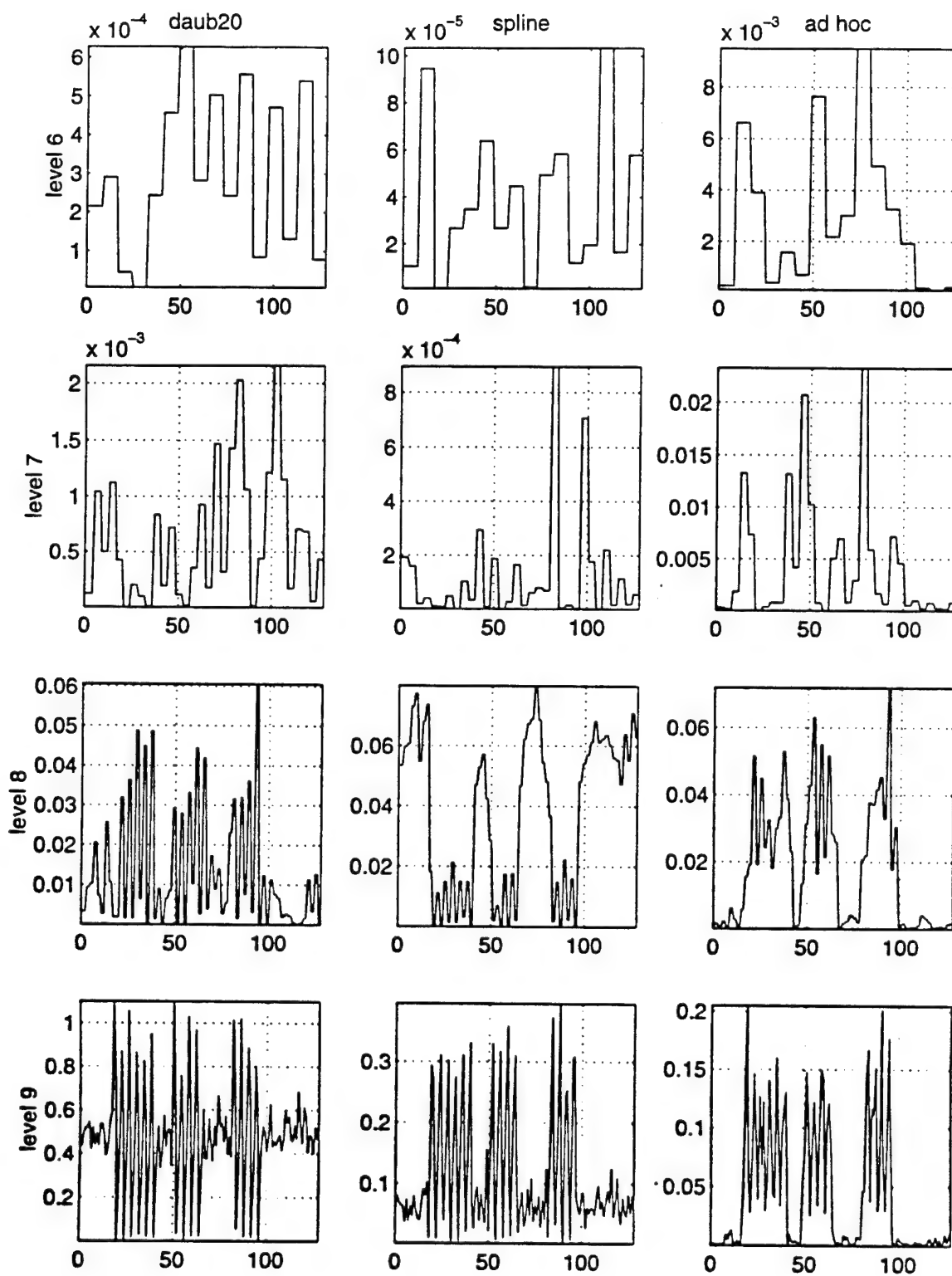


Figure B6. DWT of FSK, SNR = 20 dB

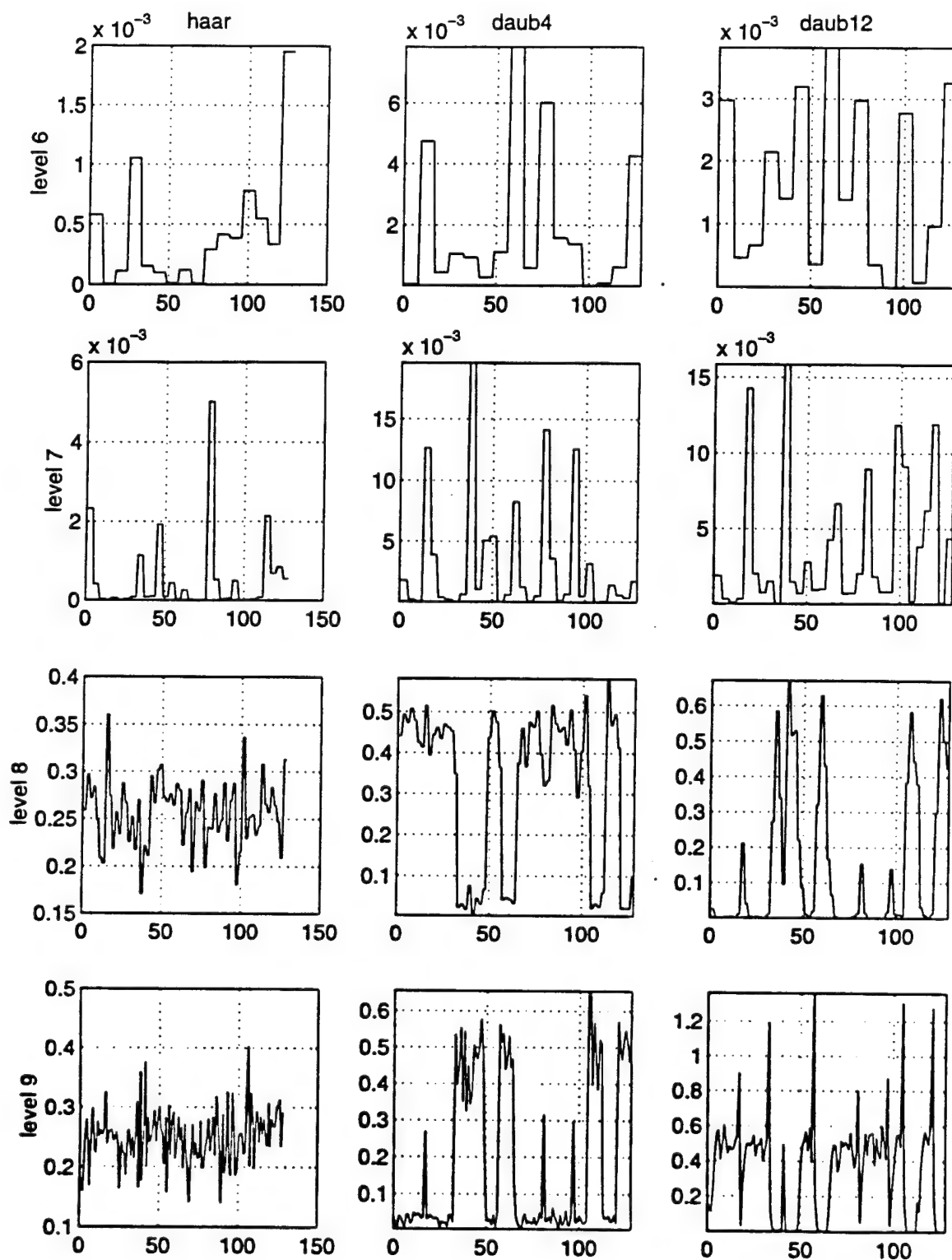


Figure B7. DWT of QPSK, SNR = 20 dB

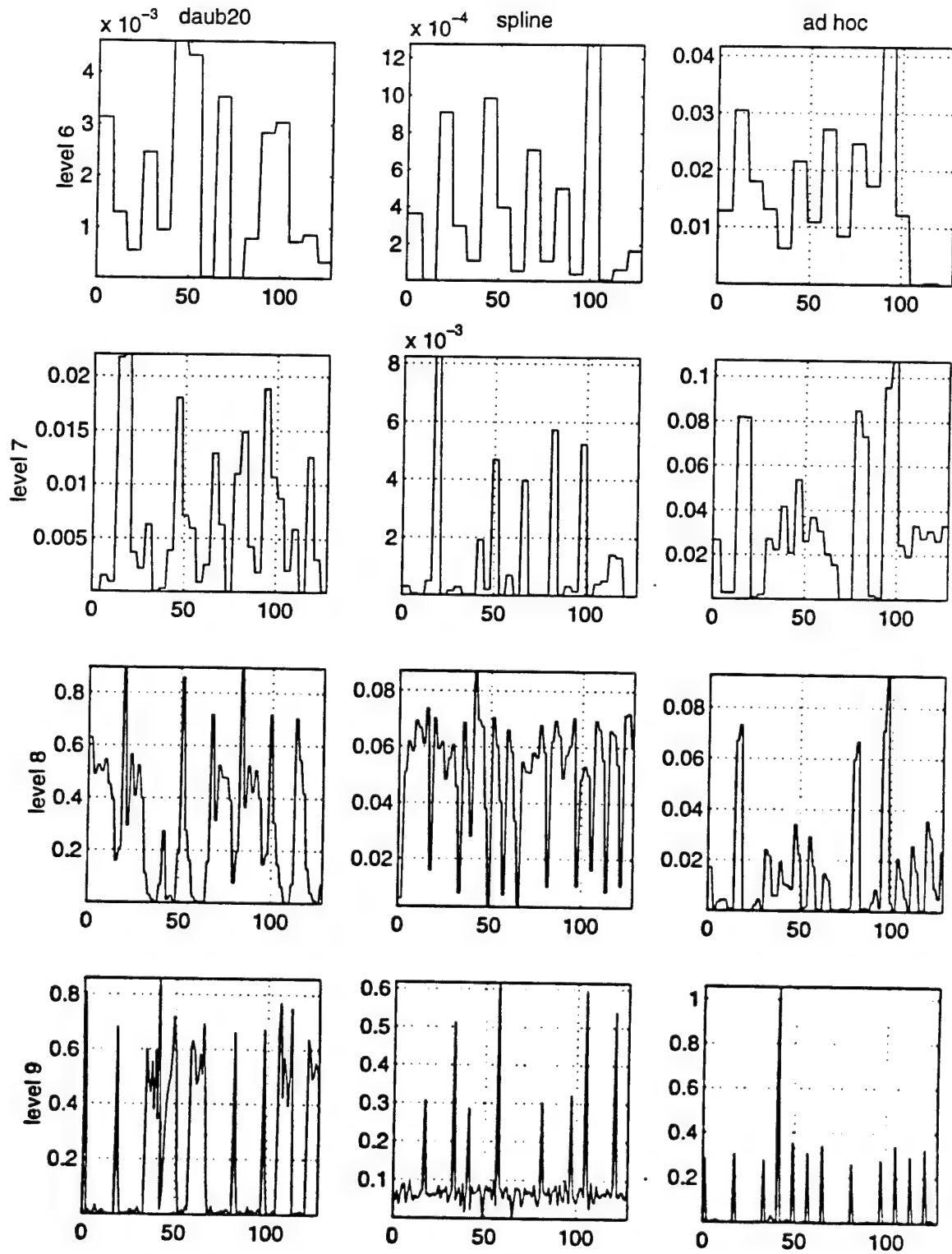


Figure B8. DWT of QPSK, SNR = 20 dB

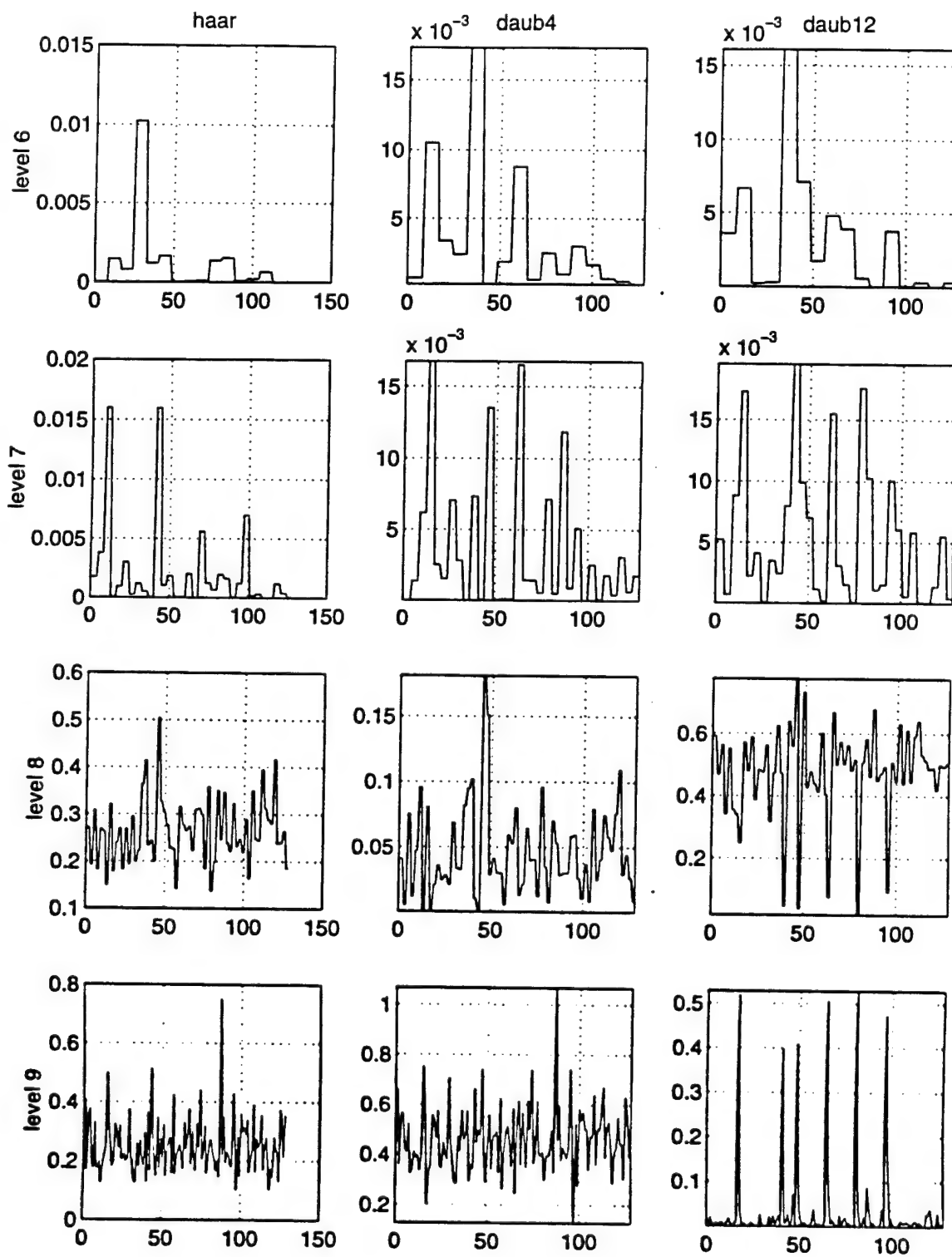


Figure B9. DWT of BPSK, SNR = 15 dB

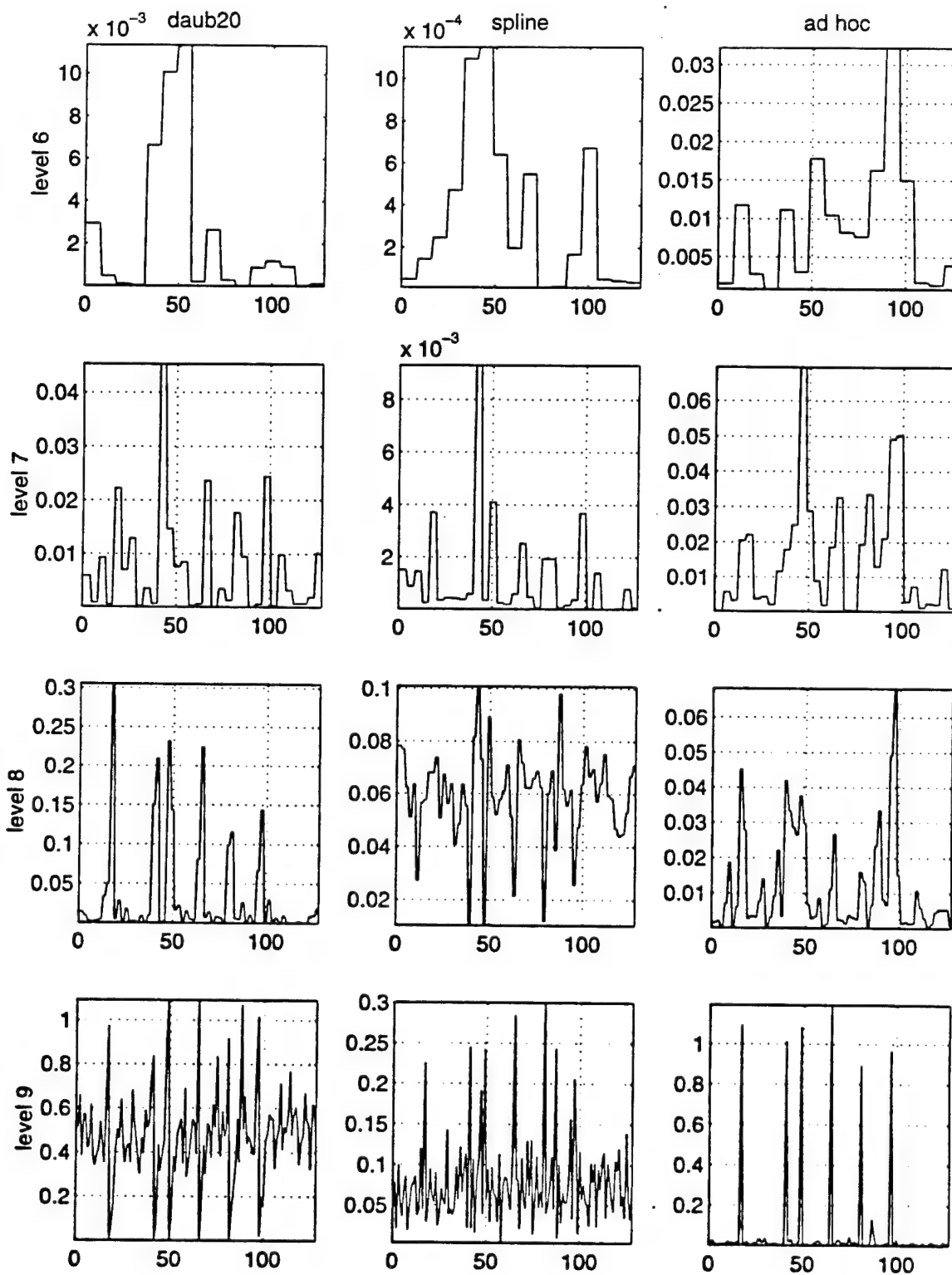


Figure B10. DWT of BPSK, SNR = 15 dB

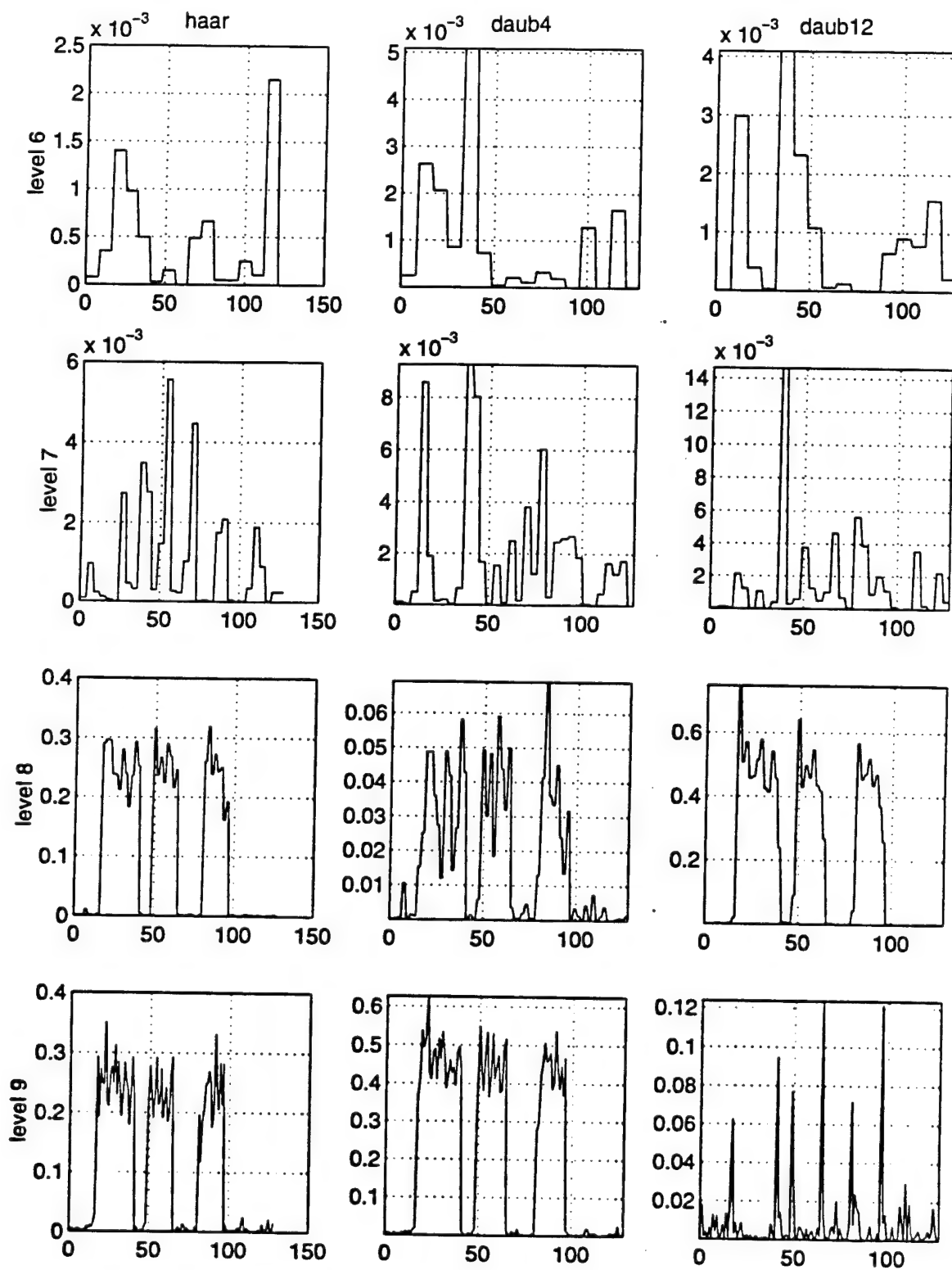


Figure B11. DWT of OOK, SNR = 15 dB



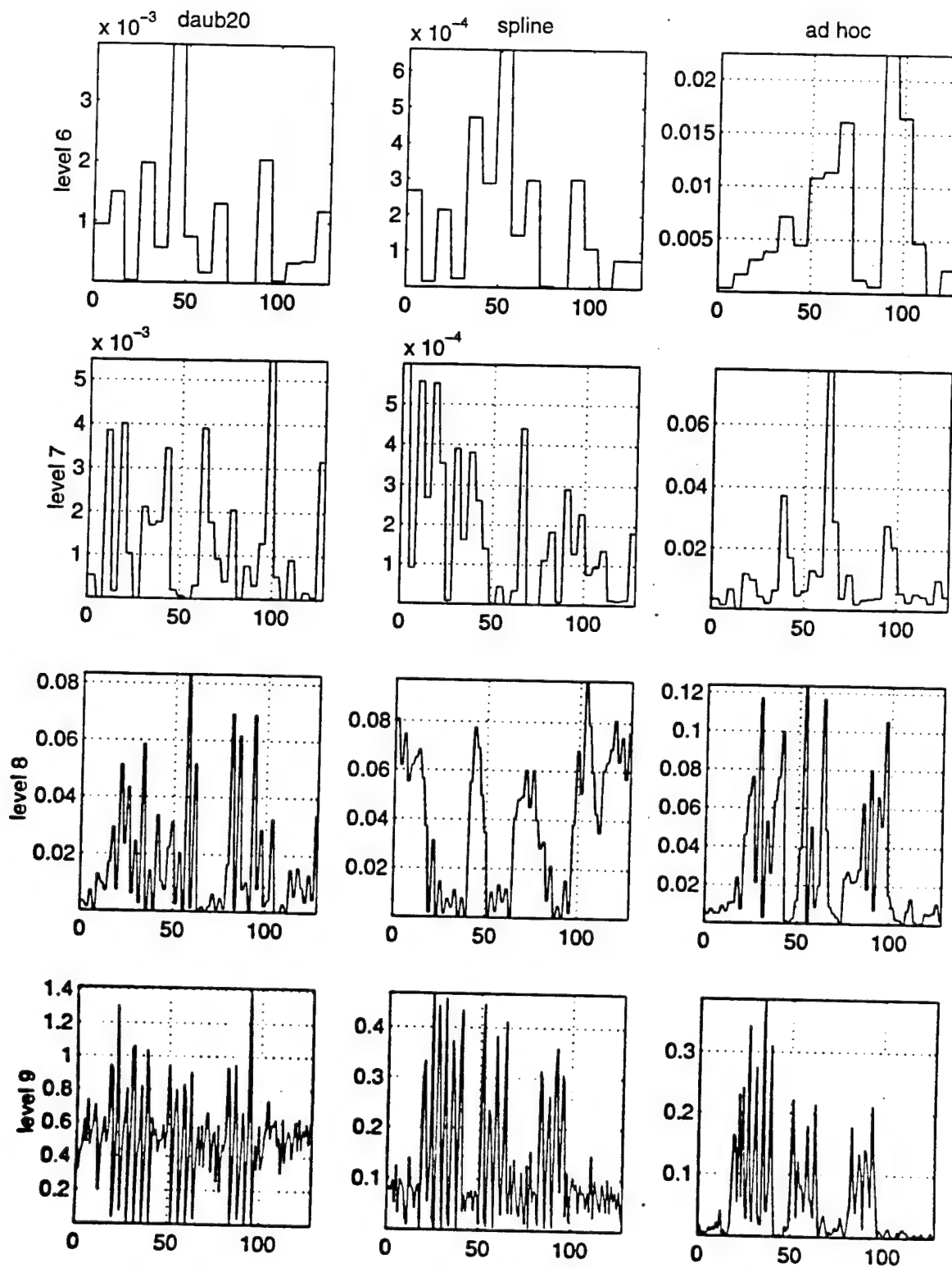


Figure B12. DWT of OOK, SNR = 15 dB

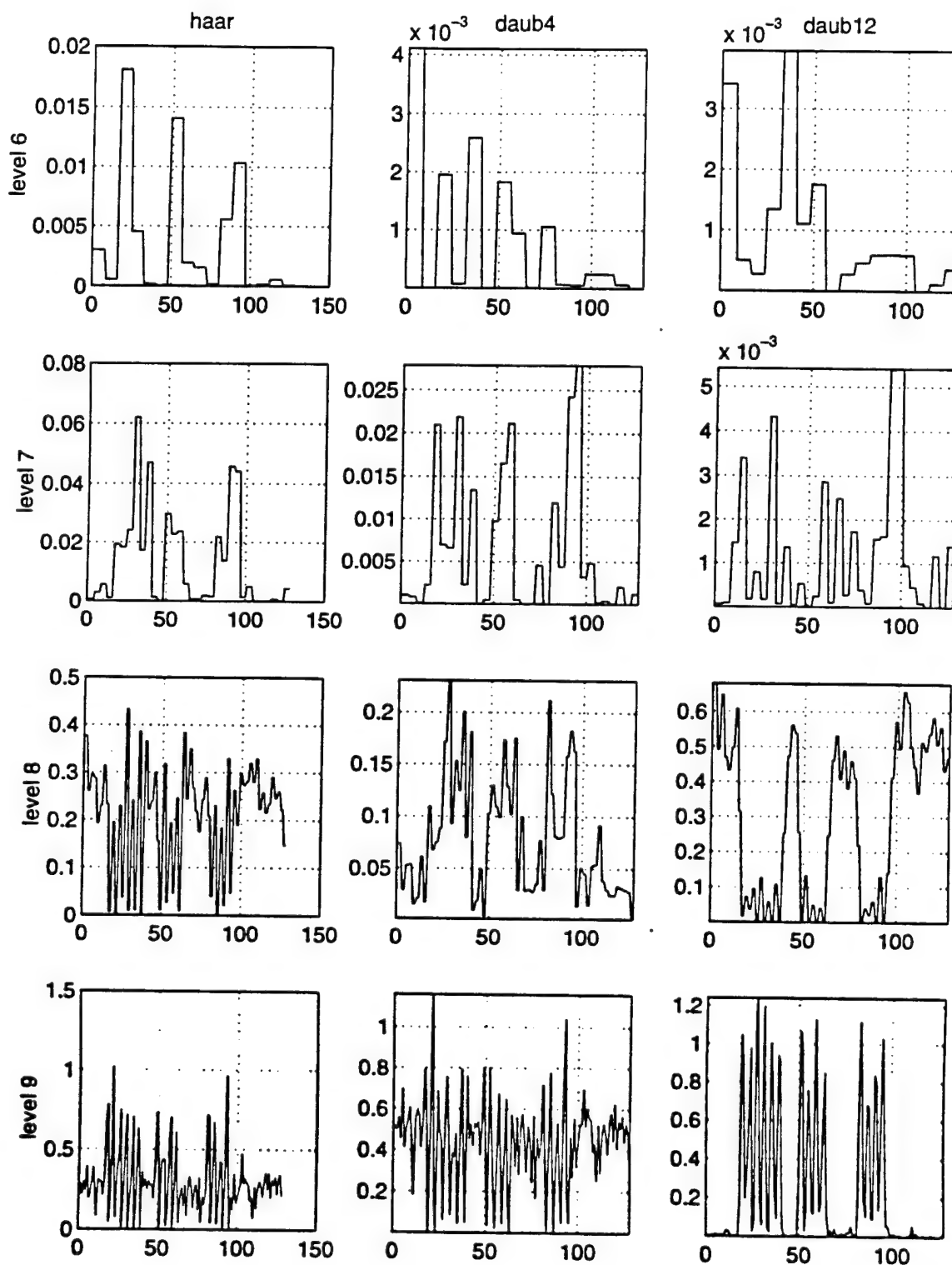


Figure B13. DWT of FSK, SNR = 15 dB

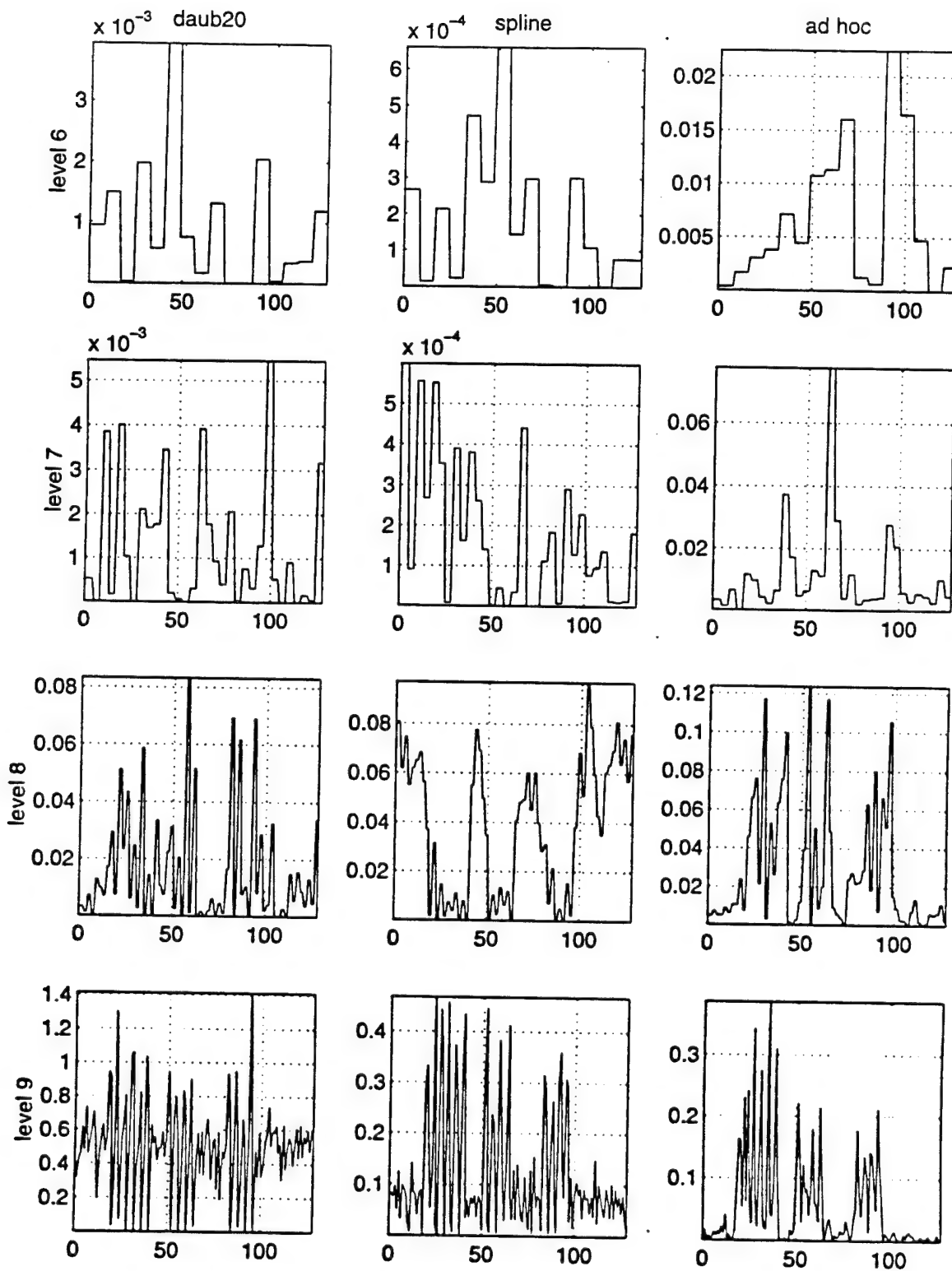


Figure B14. DWT of FSK, SNR = 15 dB

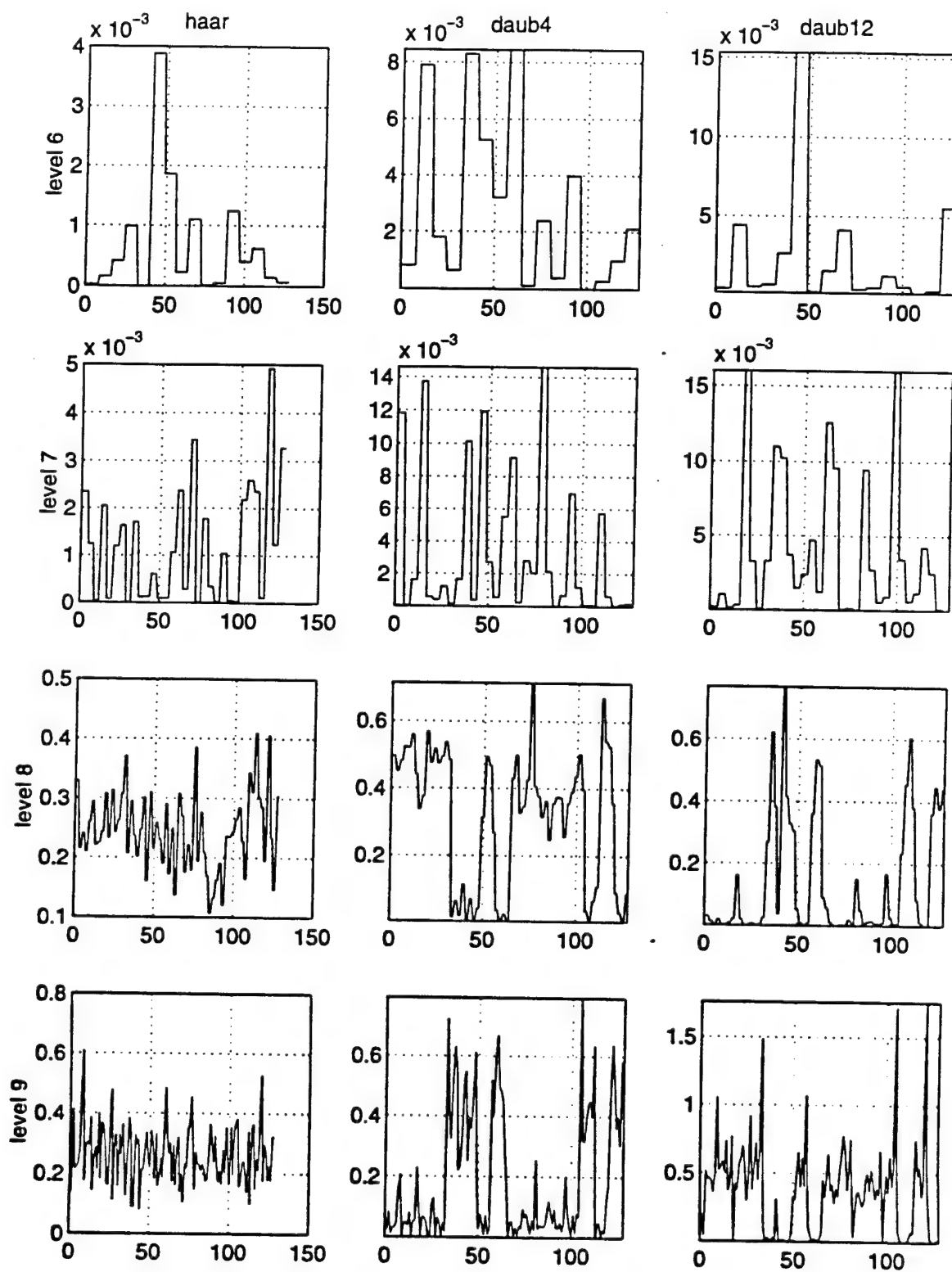


Figure B15. DWT of QPSK, SNR = 15 dB

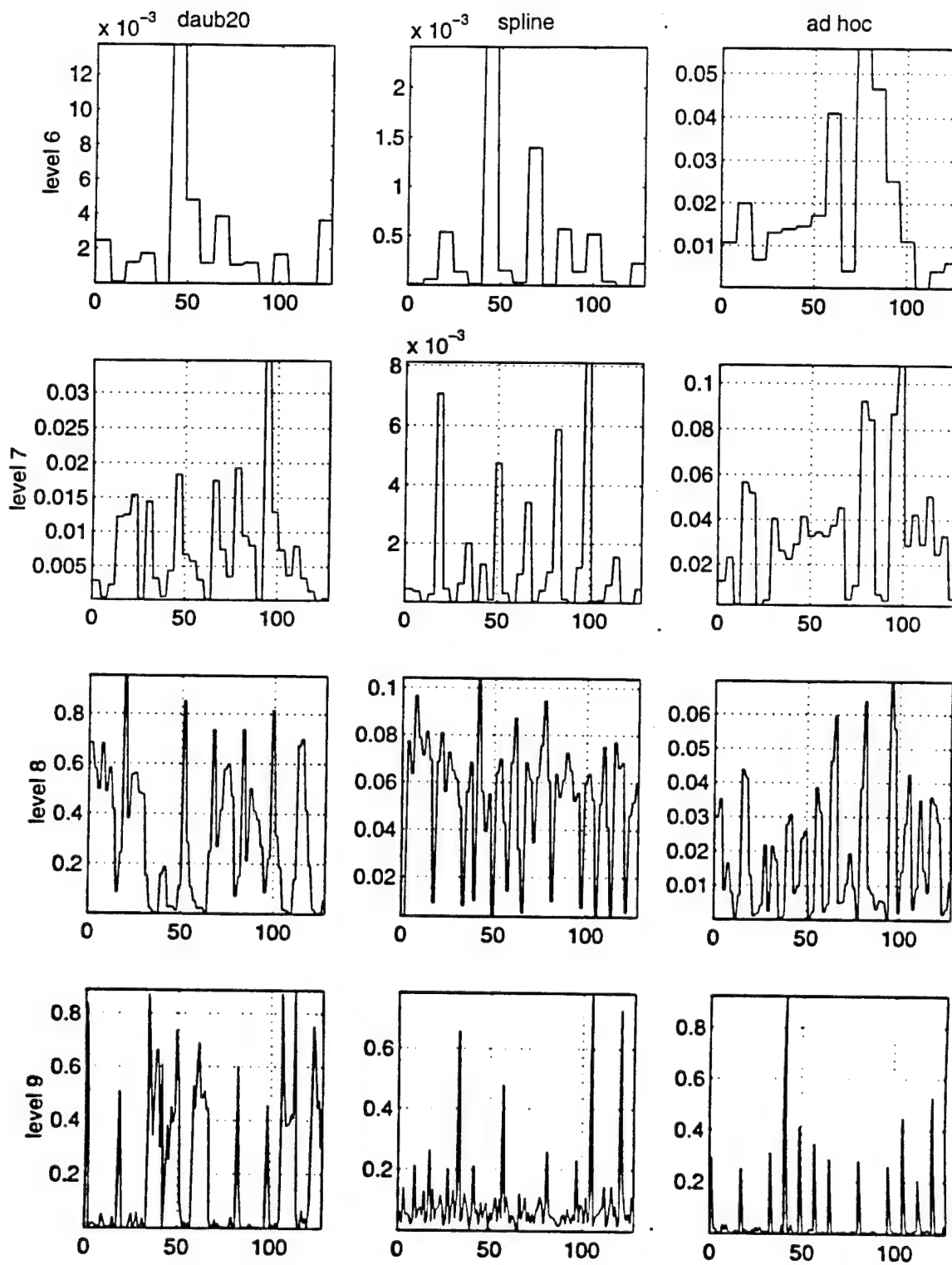


Figure B16. DWT of QPSK, SNR = 15 dB

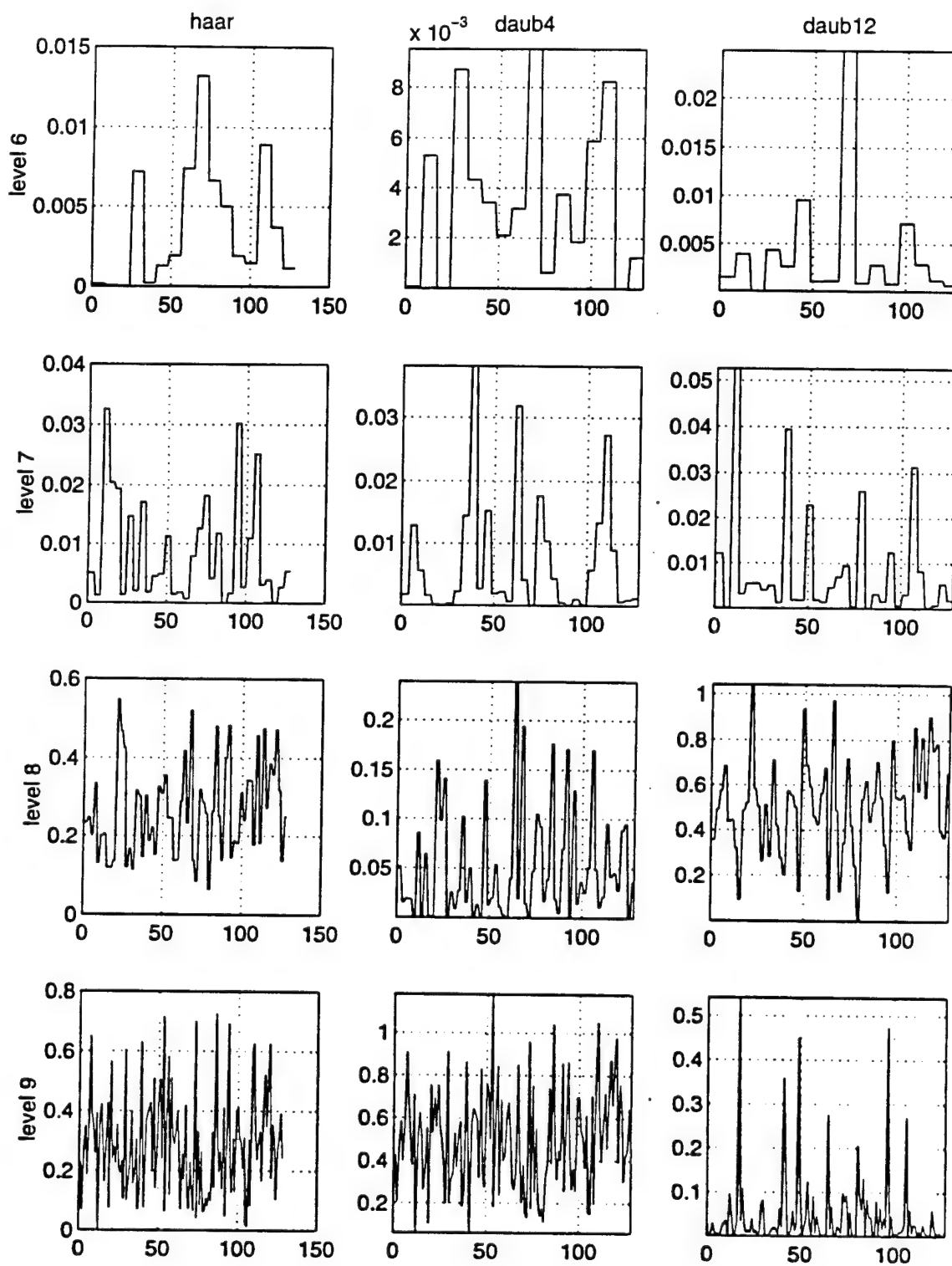


Figure B17. DWT of BPSK, SNR = 9 dB

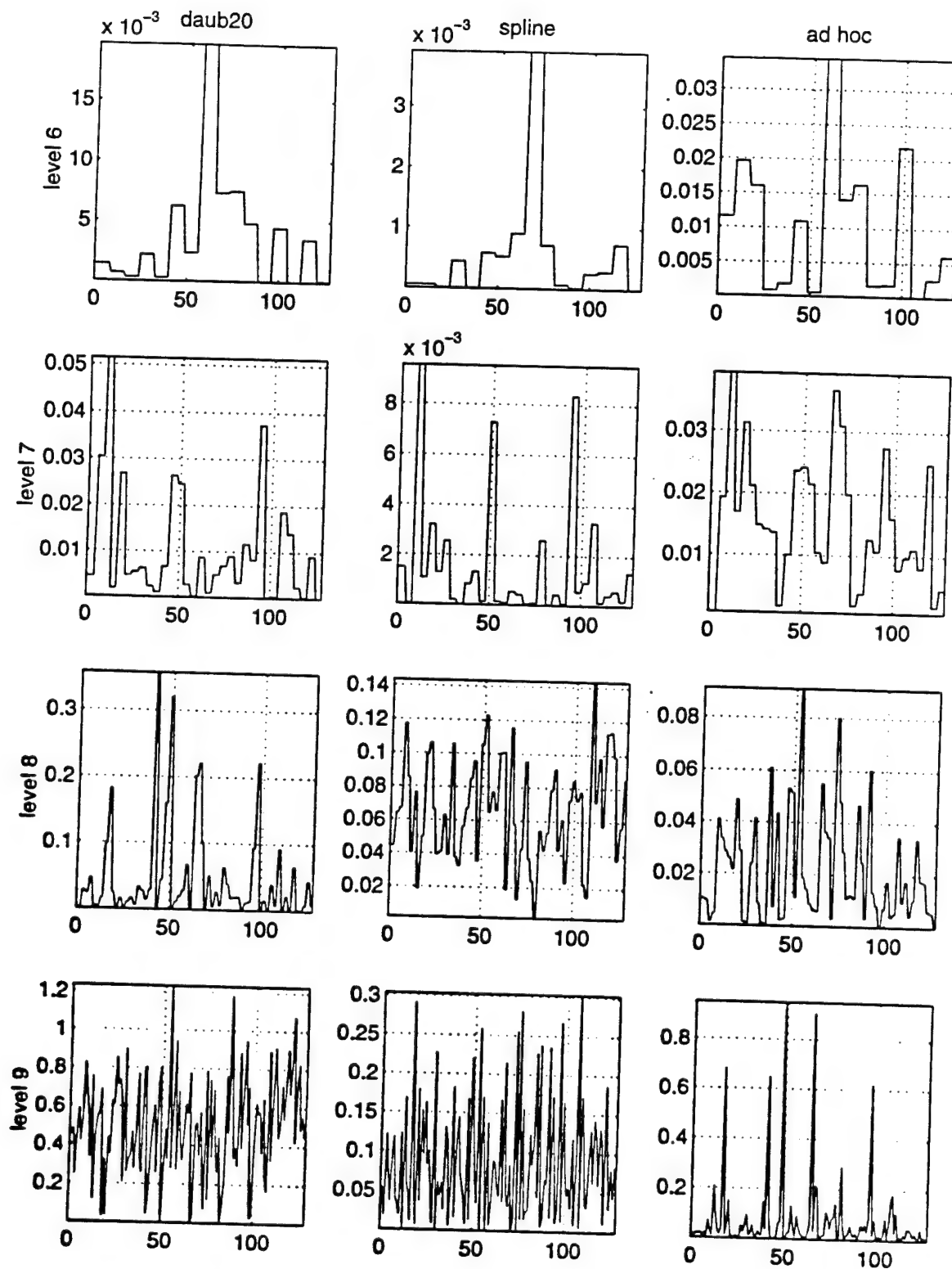


Figure B18. DWT of BPSK, SNR = 9 dB

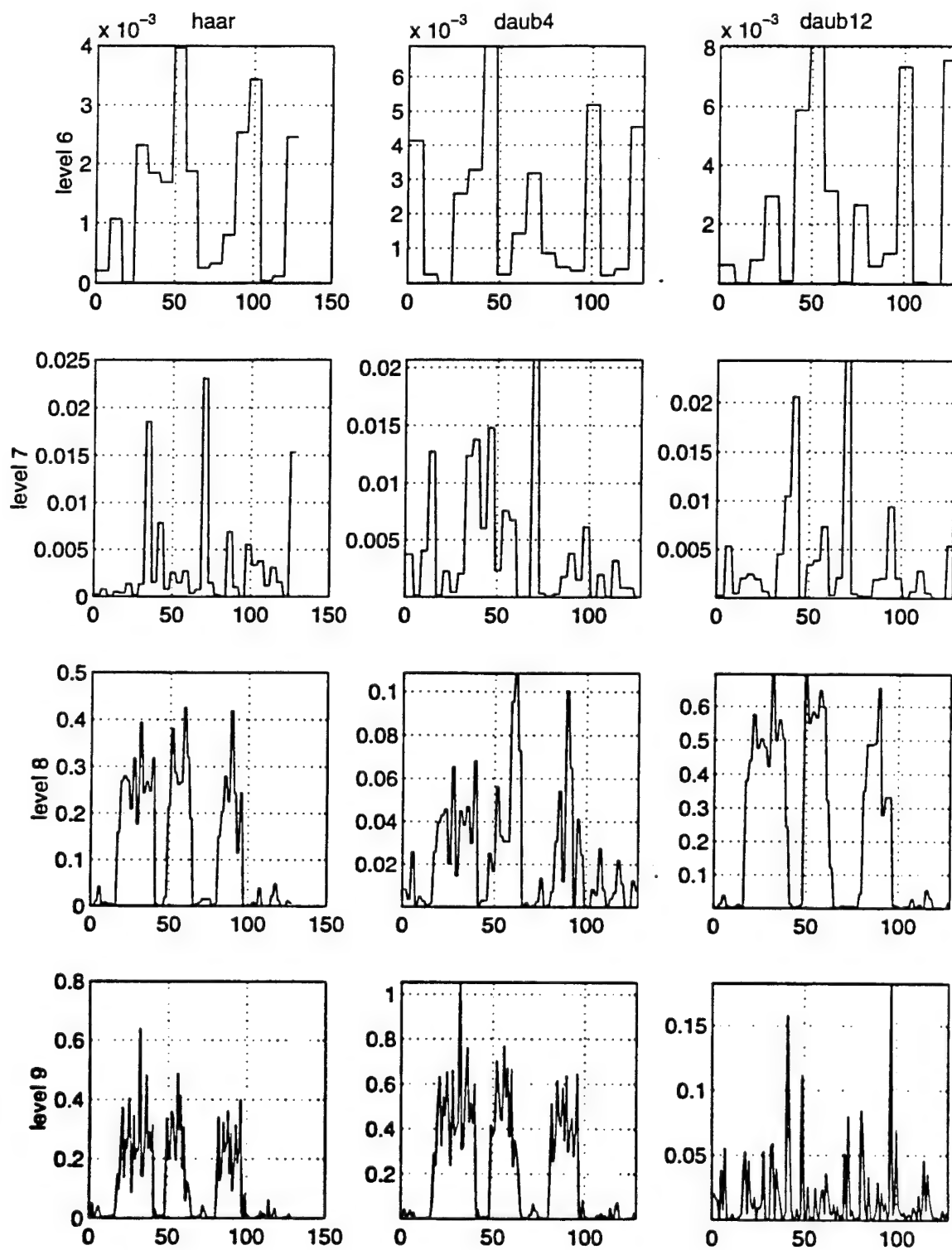


Figure B19. DWT of OOK, SNR = 9 dB



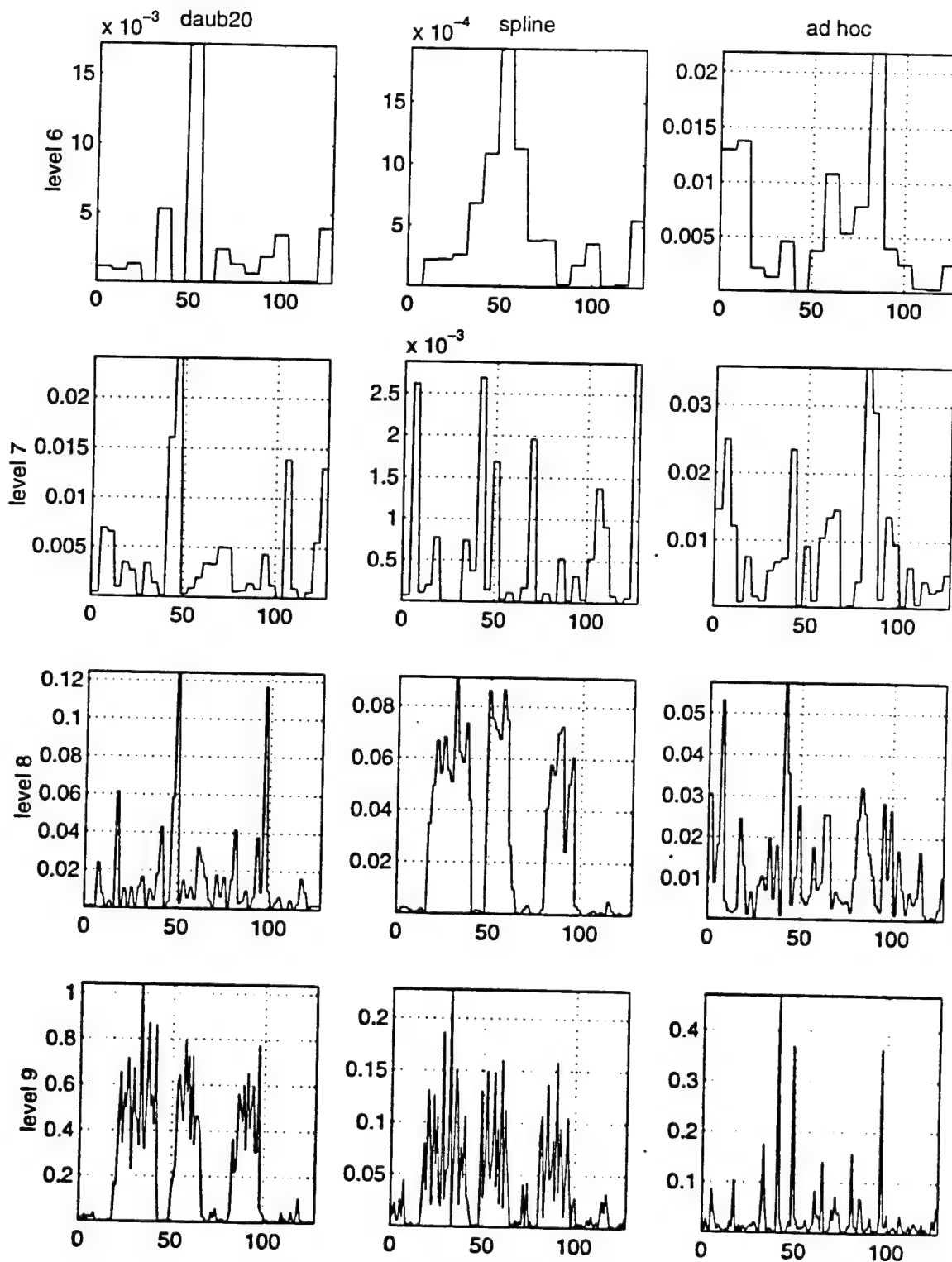


Figure B20. DWT of OOK, SNR = 9 dB

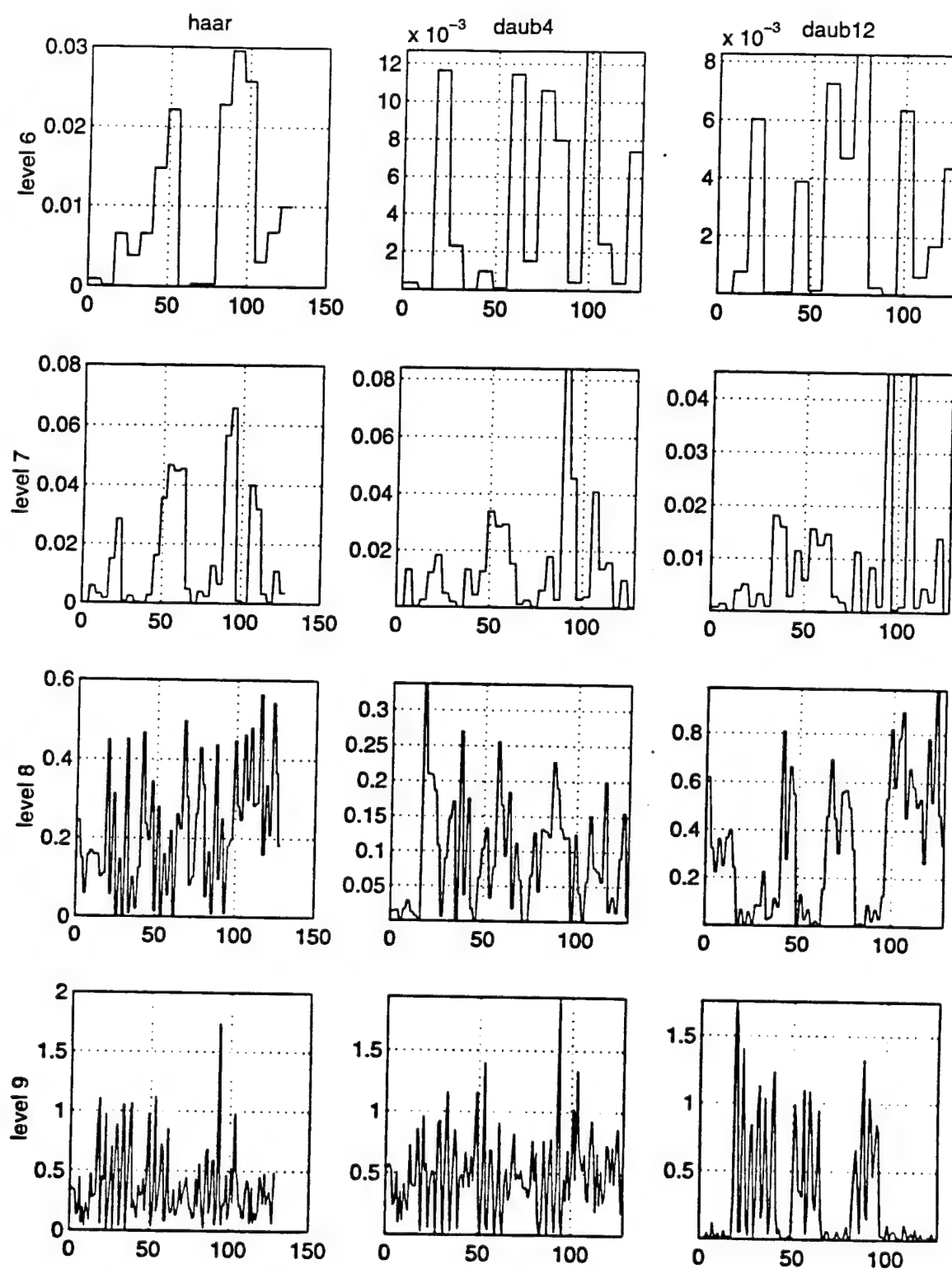


Figure B21. DWT of FSK, SNR = 9 dB

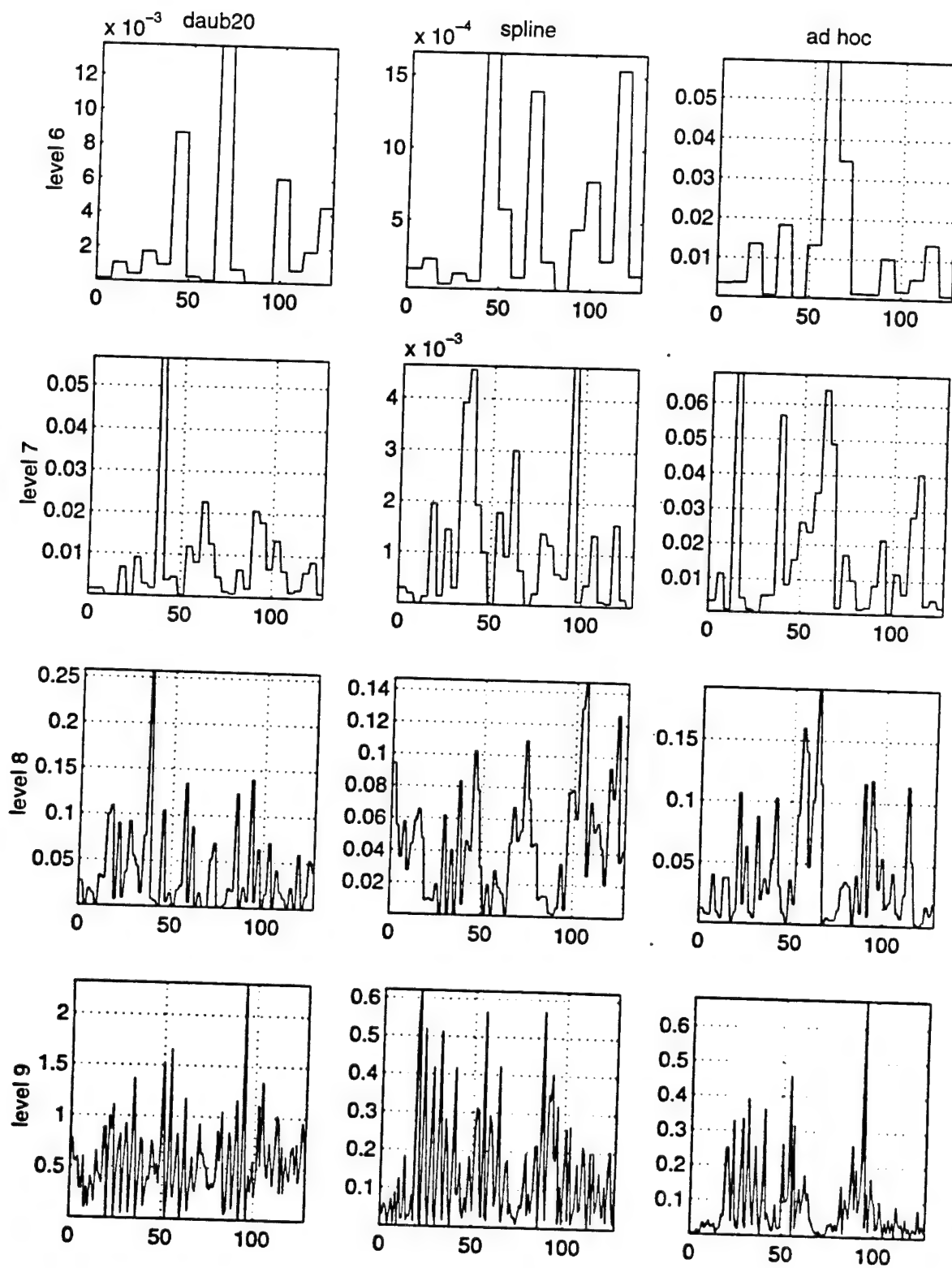


Figure B22. DWT of FSK, SNR = 9 dB

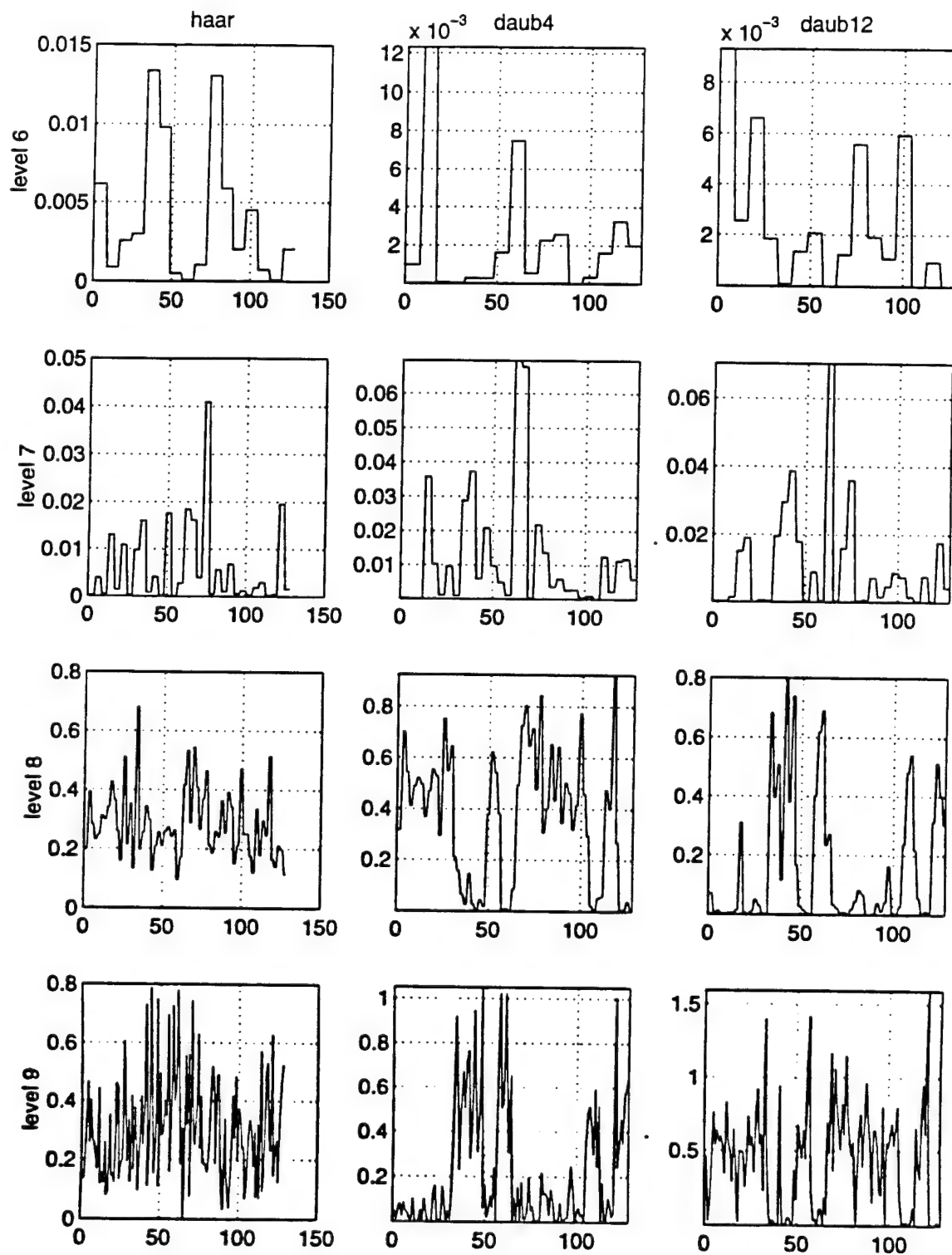


Figure B23. DWT of QPSK, SNR = 9 dB

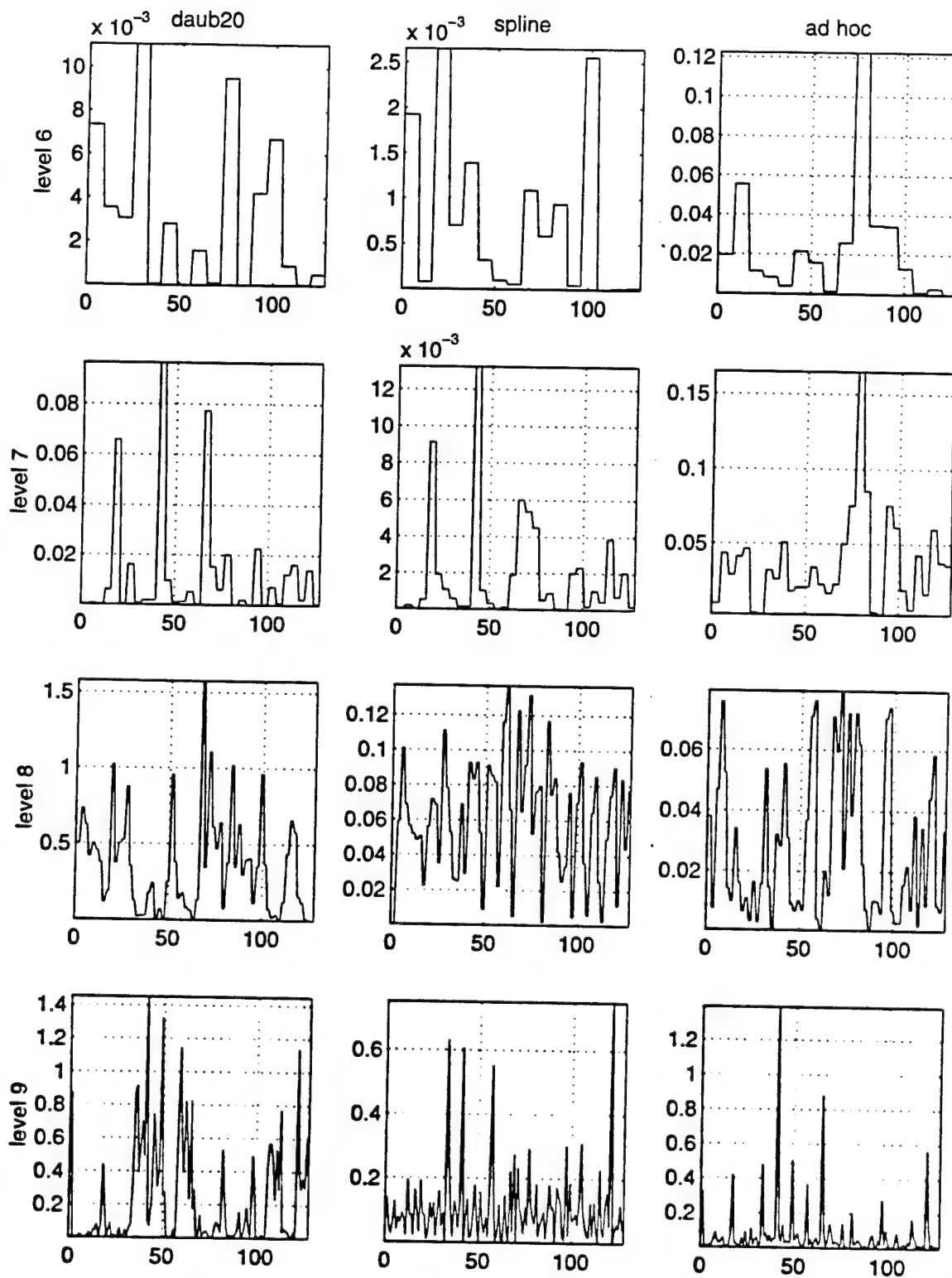


Figure B24. DWT of QPSK, SNR = 9 dB

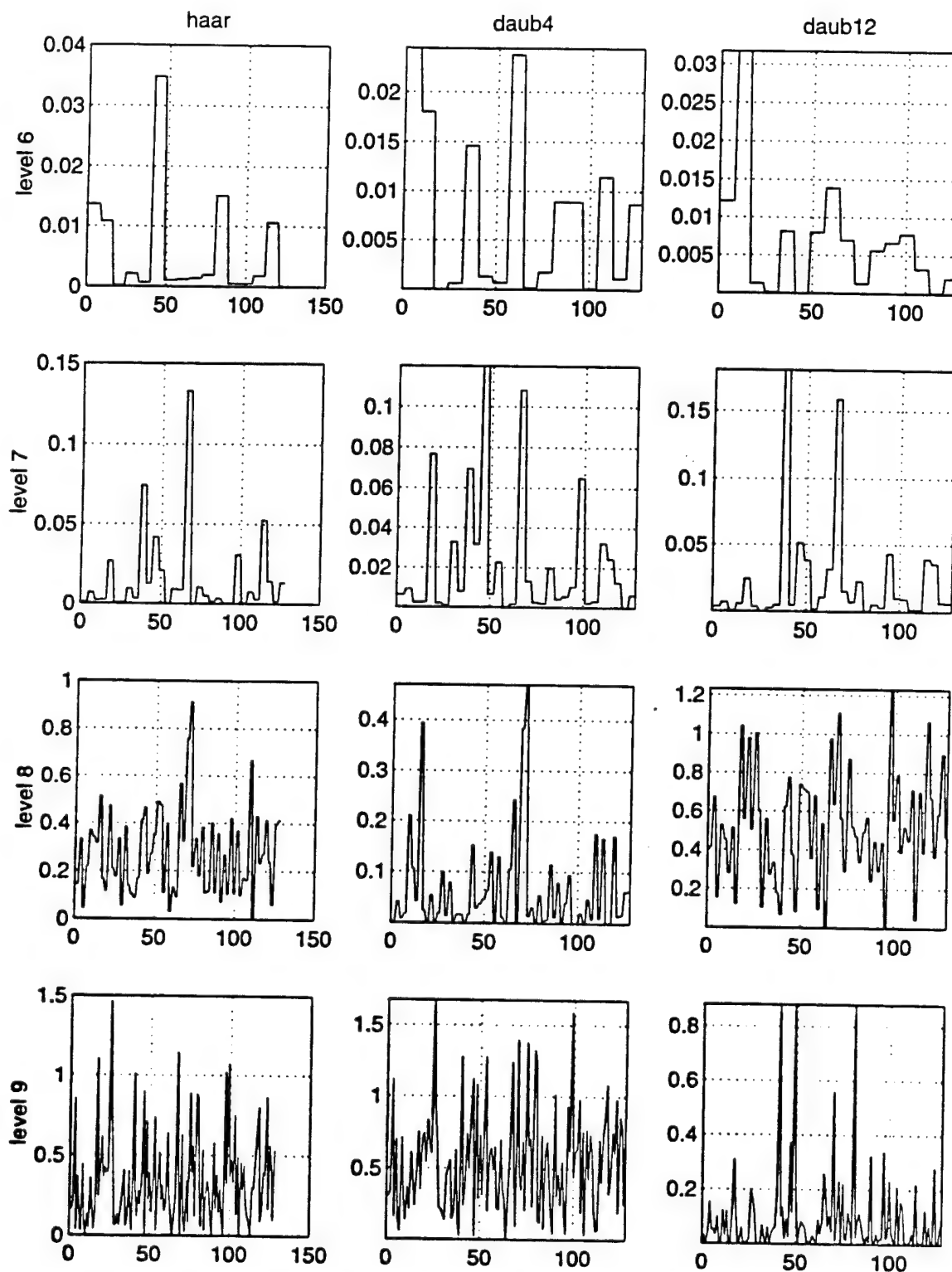


Figure B25. DWT of BPSK, SNR = 6 dB

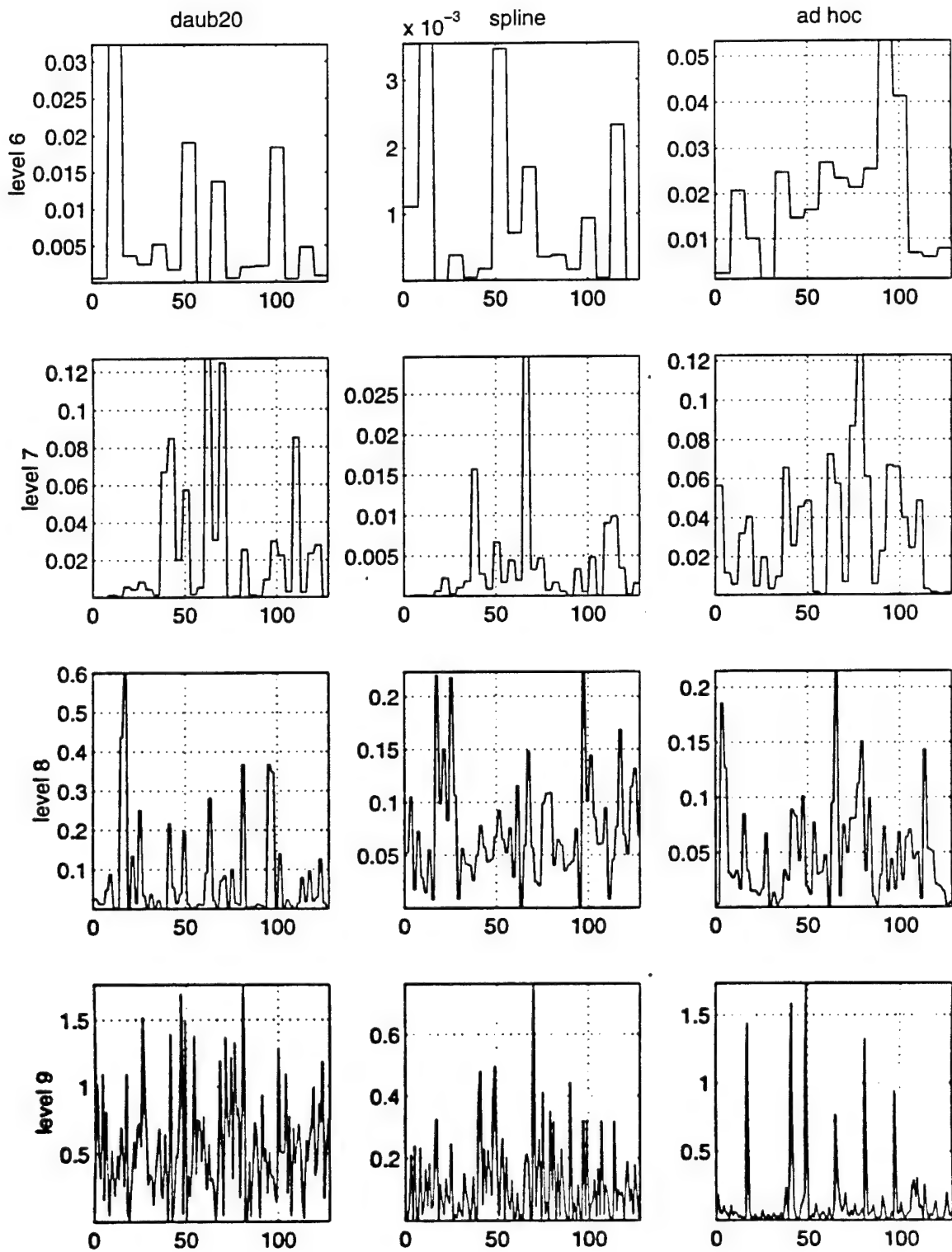


Figure B26. DWT of BPSK, SNR = 6 dB

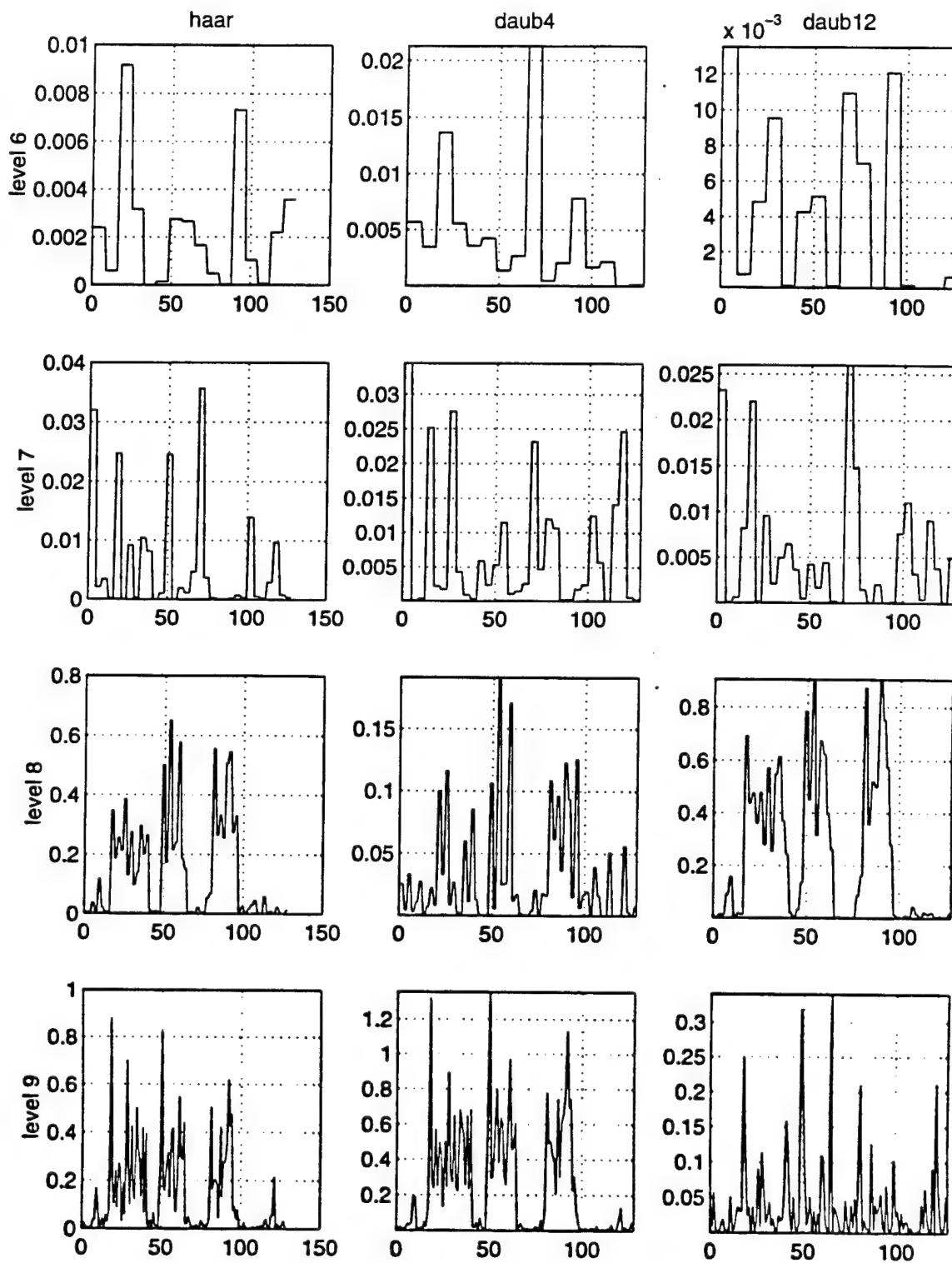


Figure B27. DWT of OOK, SNR = 6 dB



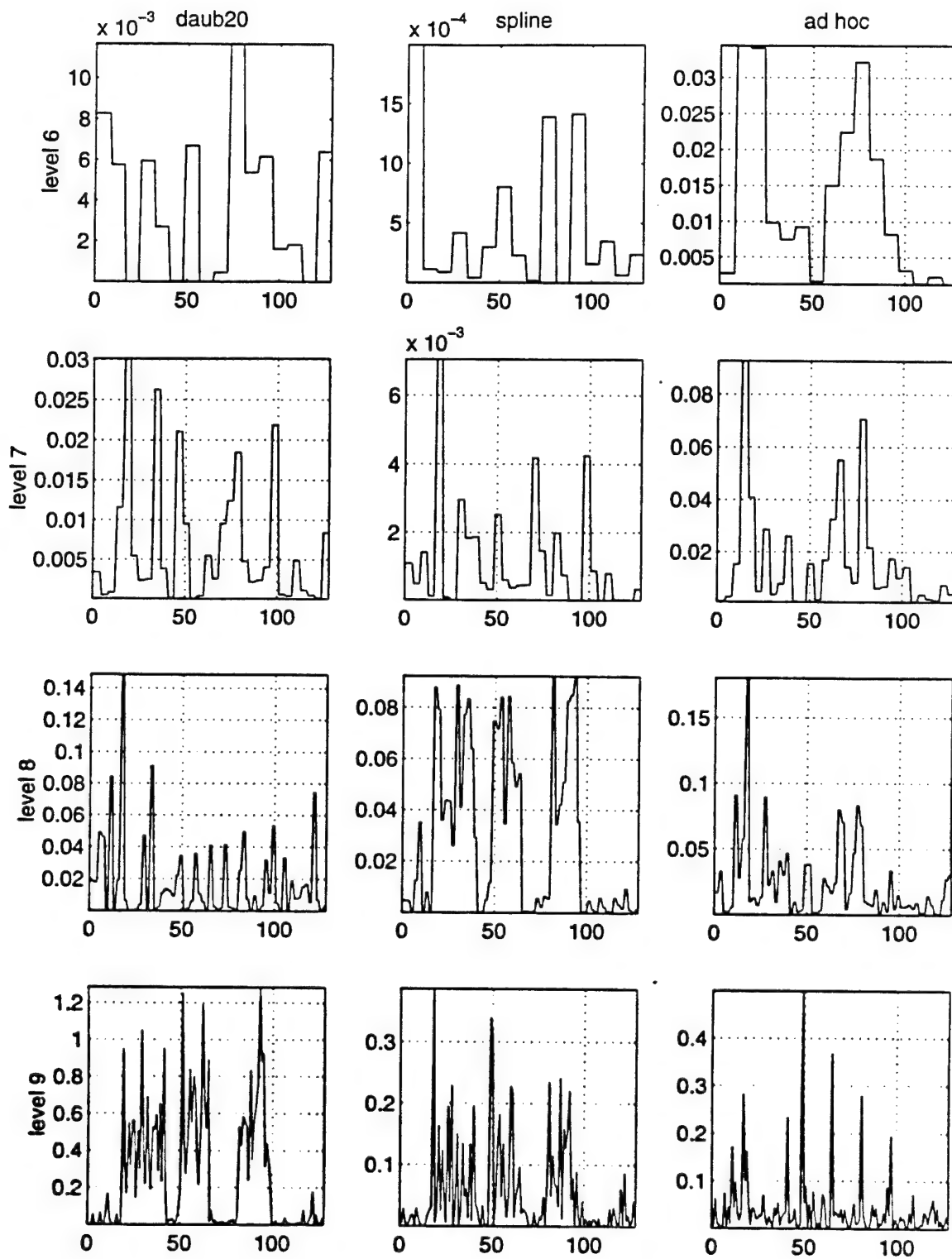


Figure B28. DWT of OOK, SNR = 6 dB

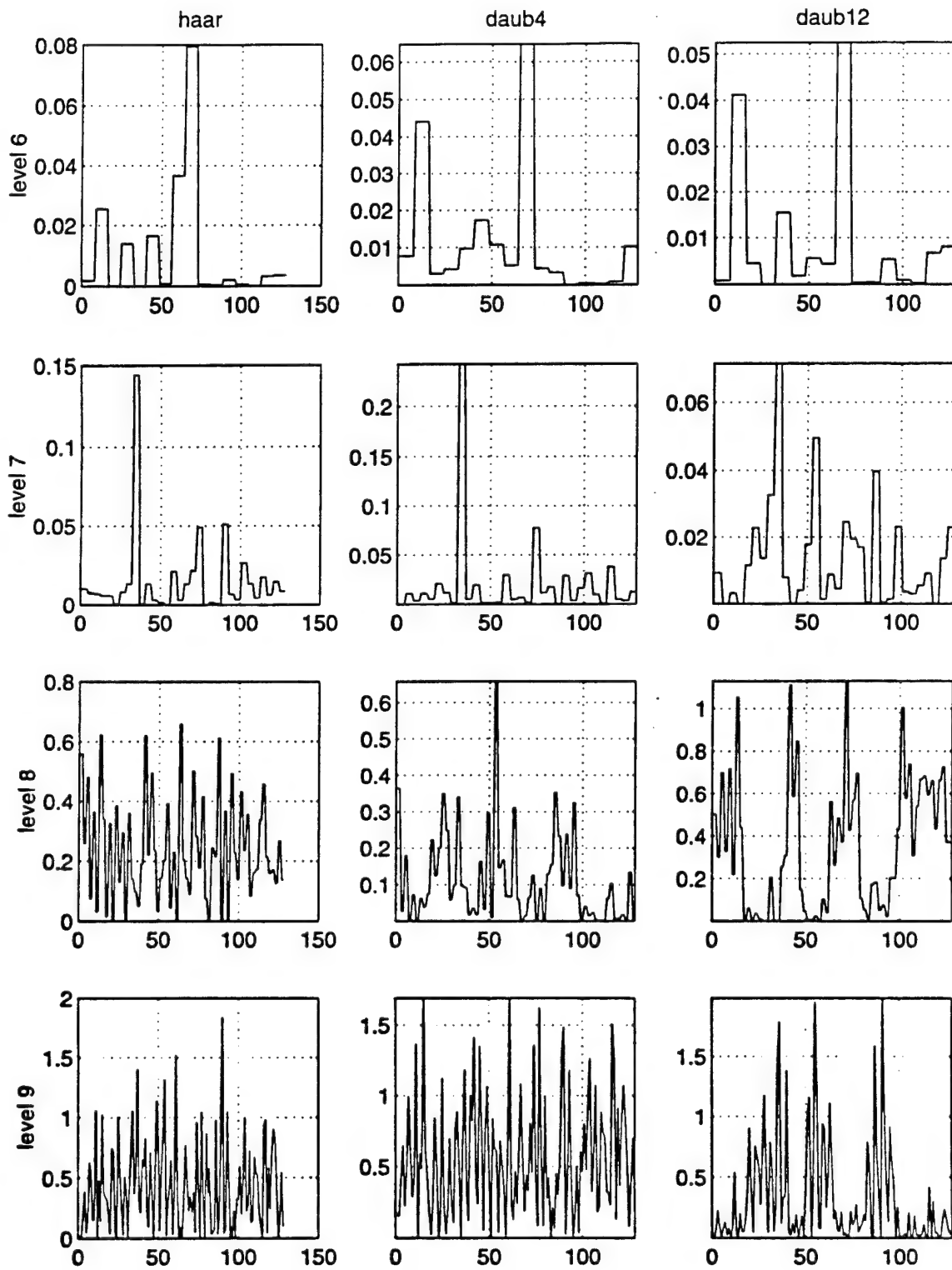


Figure B29. DWT of FSK, SNR = 6 dB

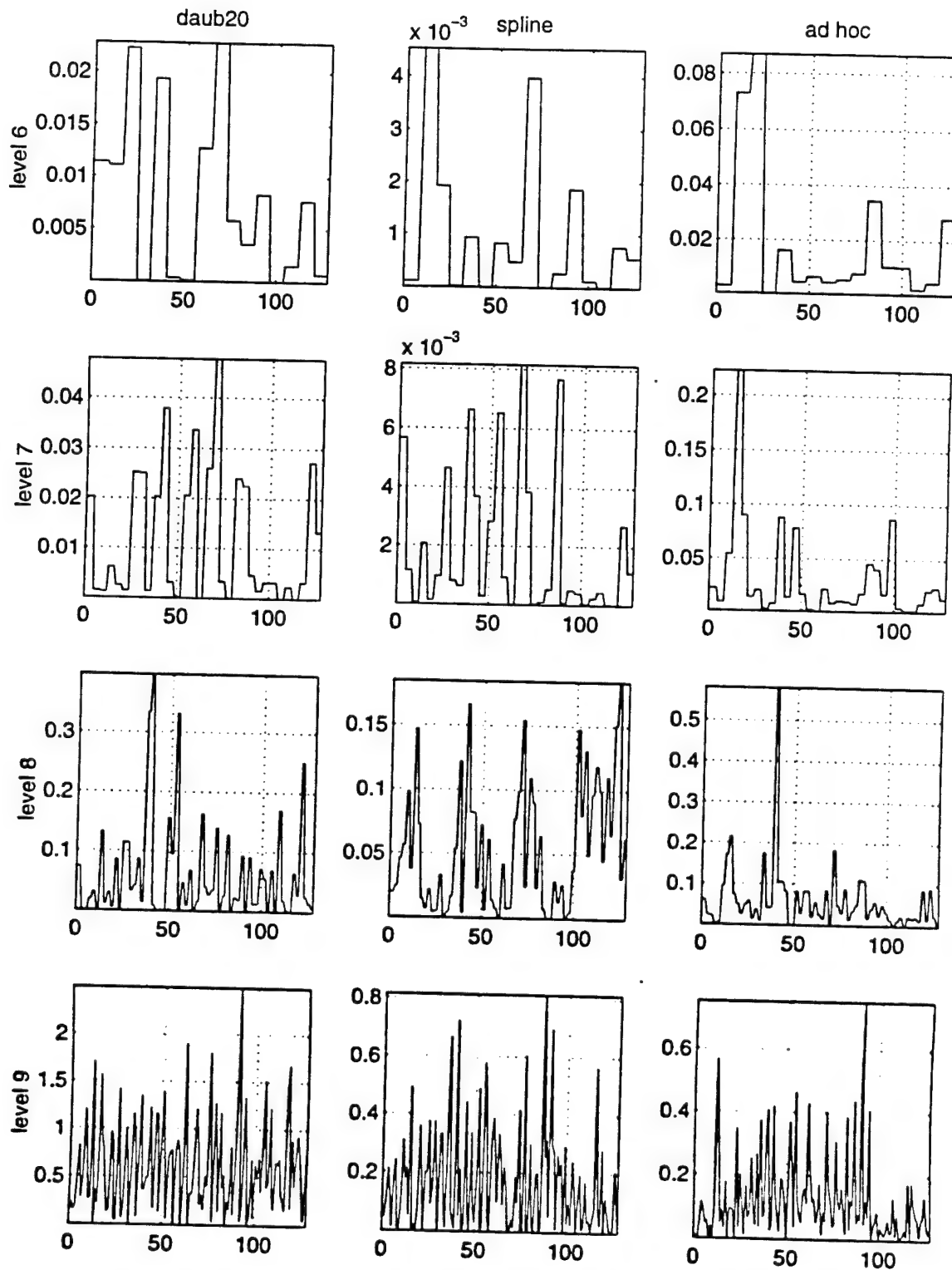


Figure B30. DWT of FSK, SNR = 6 dB

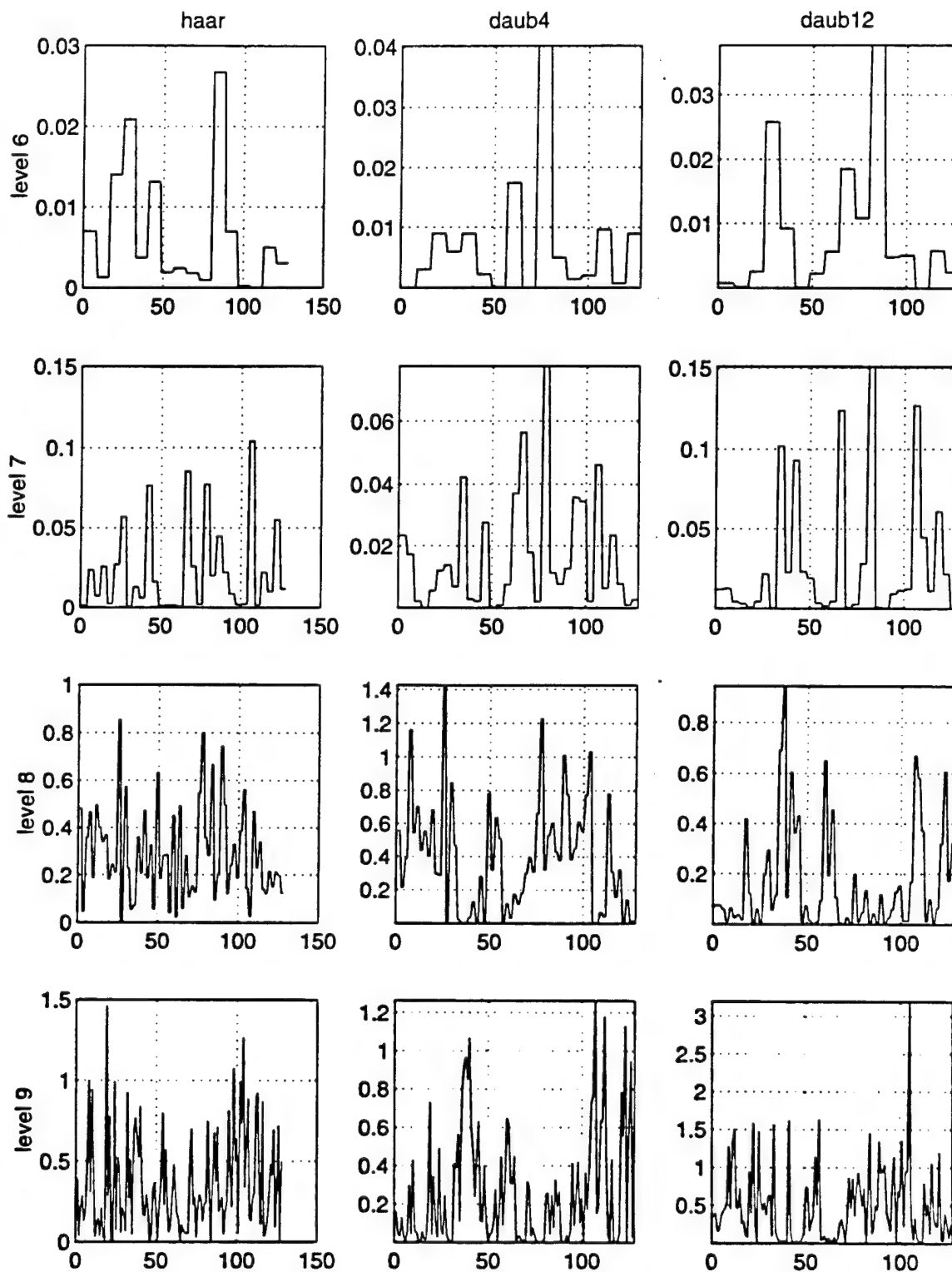


Figure B31. DWT of QPSK, SNR = 6 dB

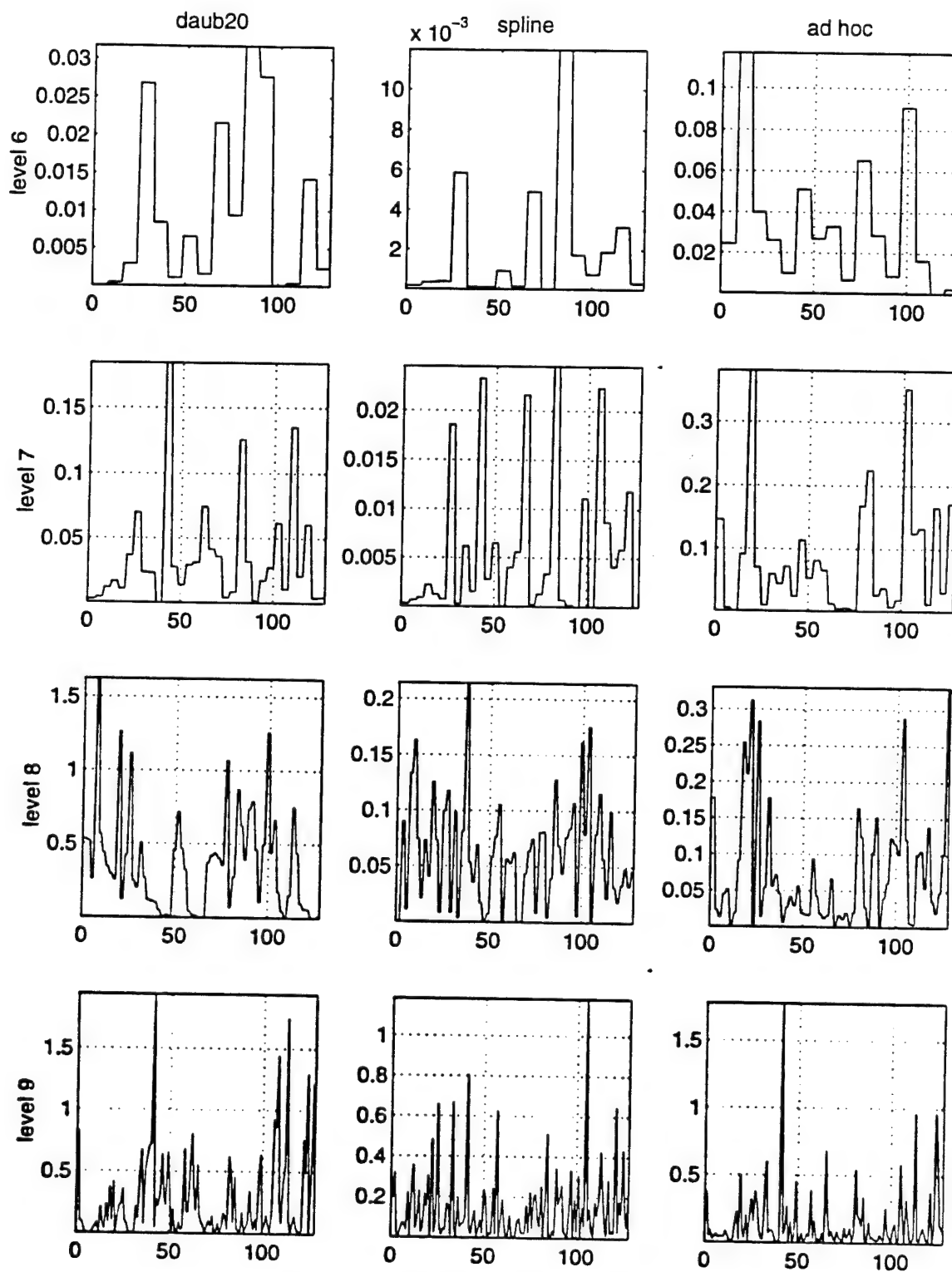


Figure B32. DWT of QPSK, SNR = 6 dB

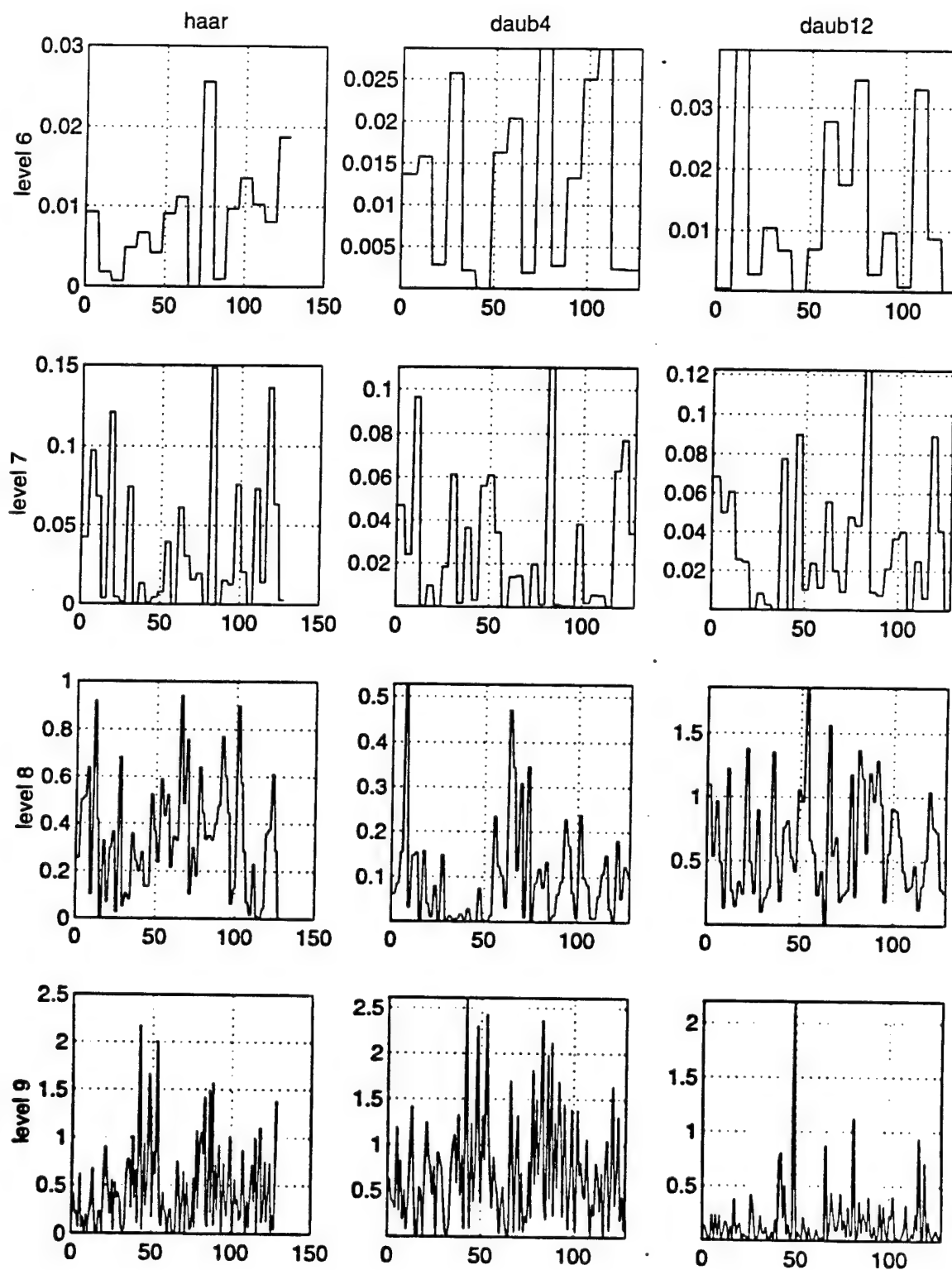


Figure B33. DWT of BPSK, SNR = 3 dB

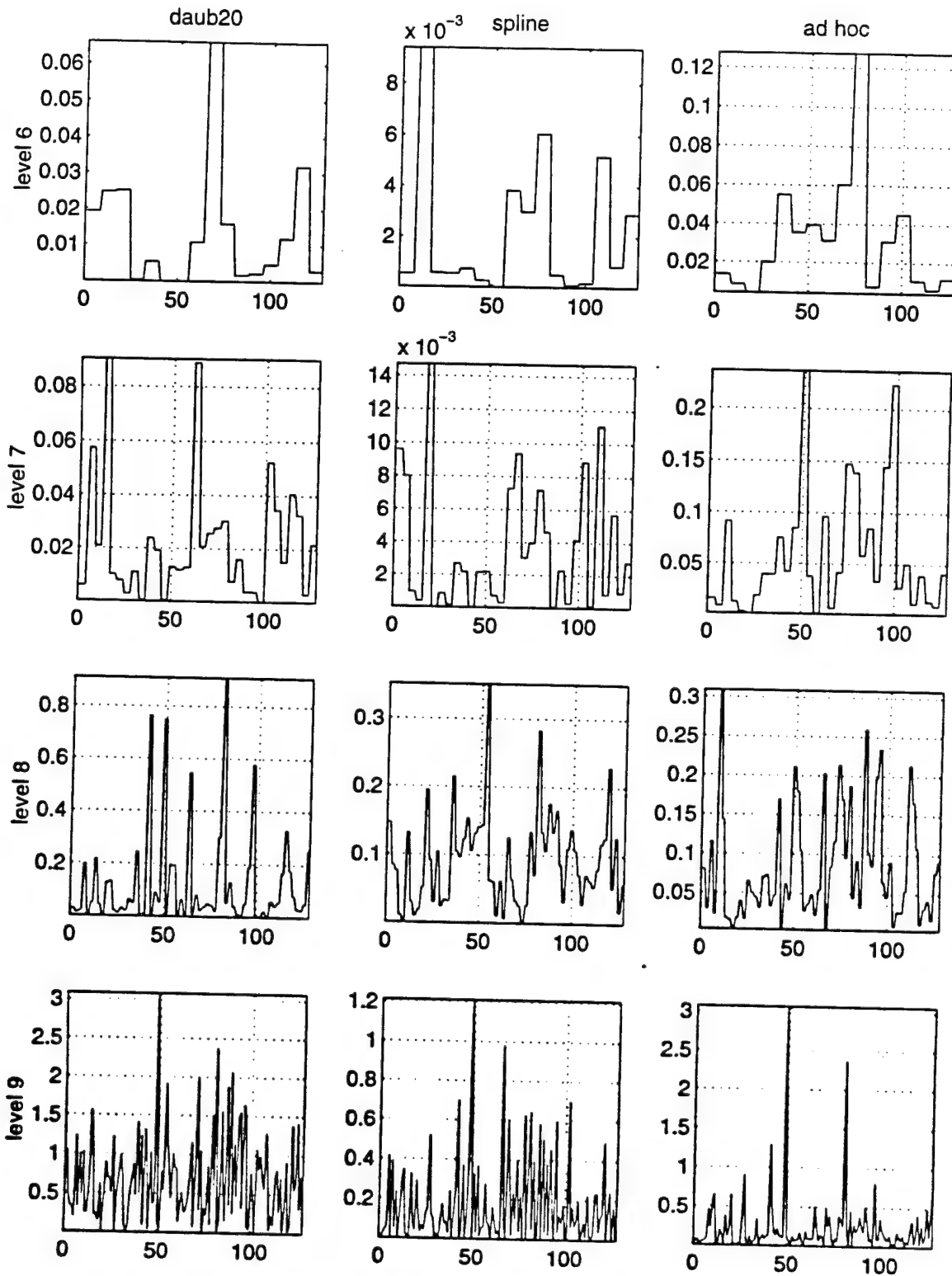


Figure B34. DWT of BPSK, SNR = 3 dB

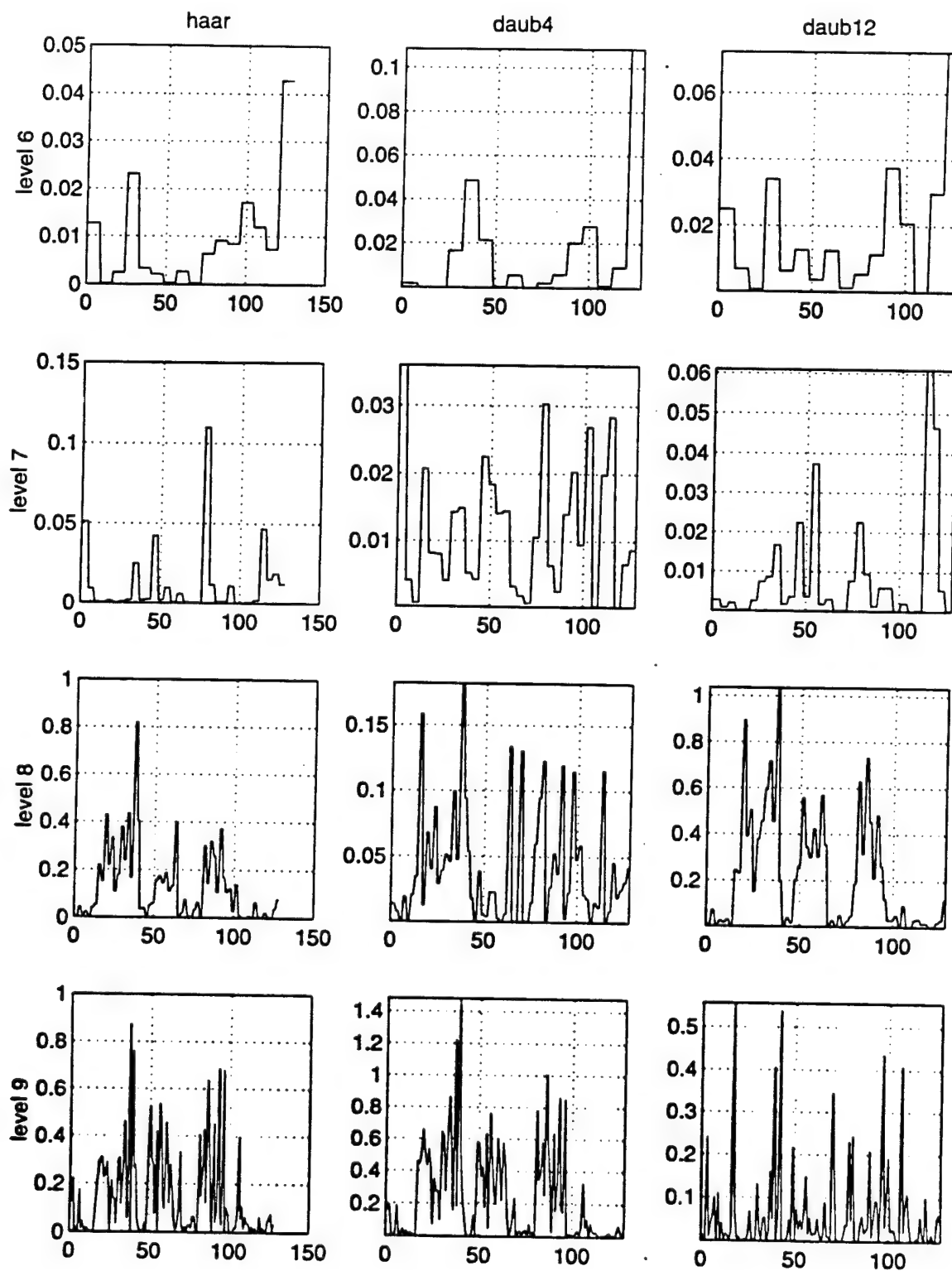


Figure B35. DWT of OOK, SNR = 3 dB



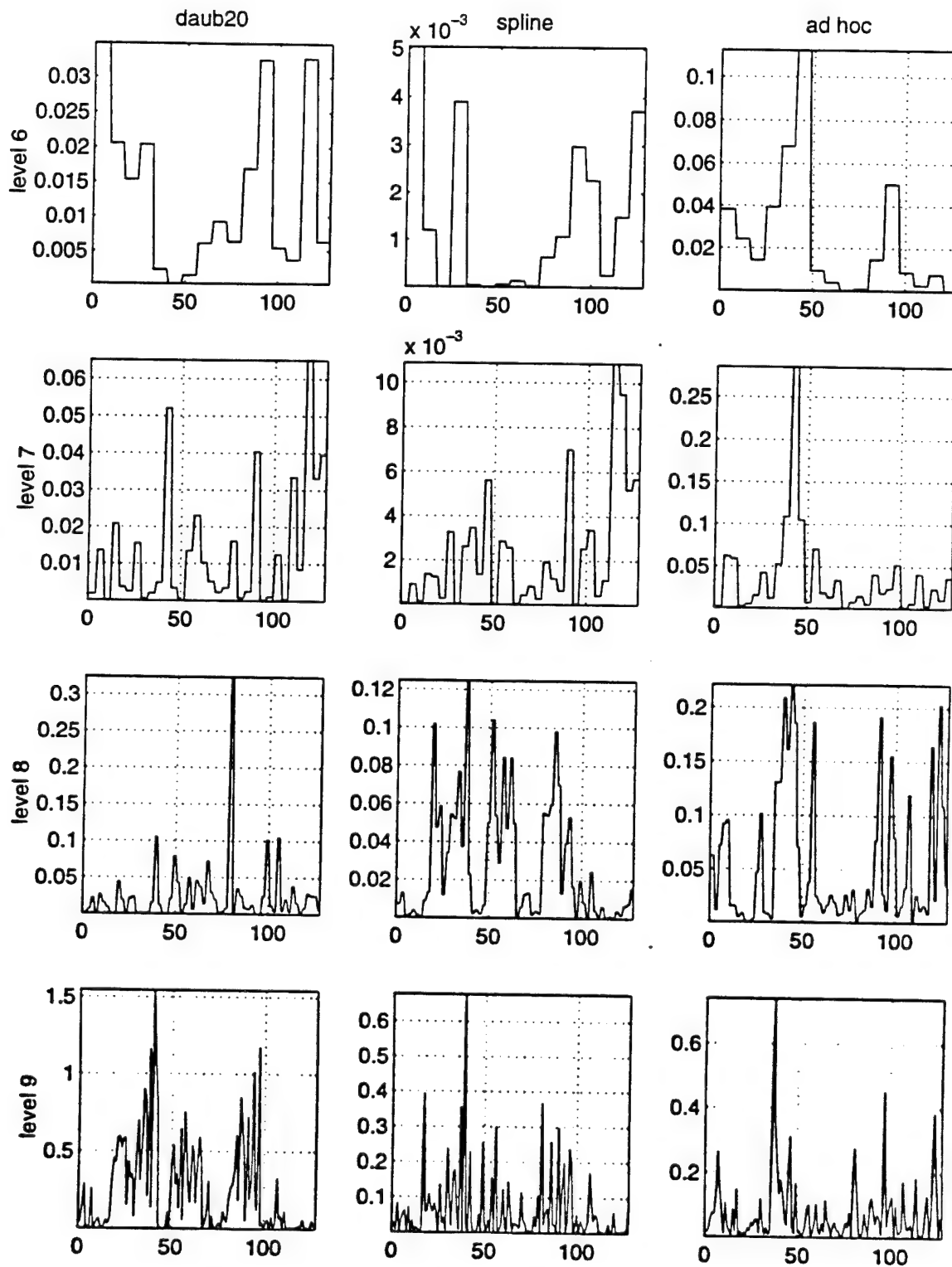


Figure B36. DWT of OOK, SNR = 3 dB

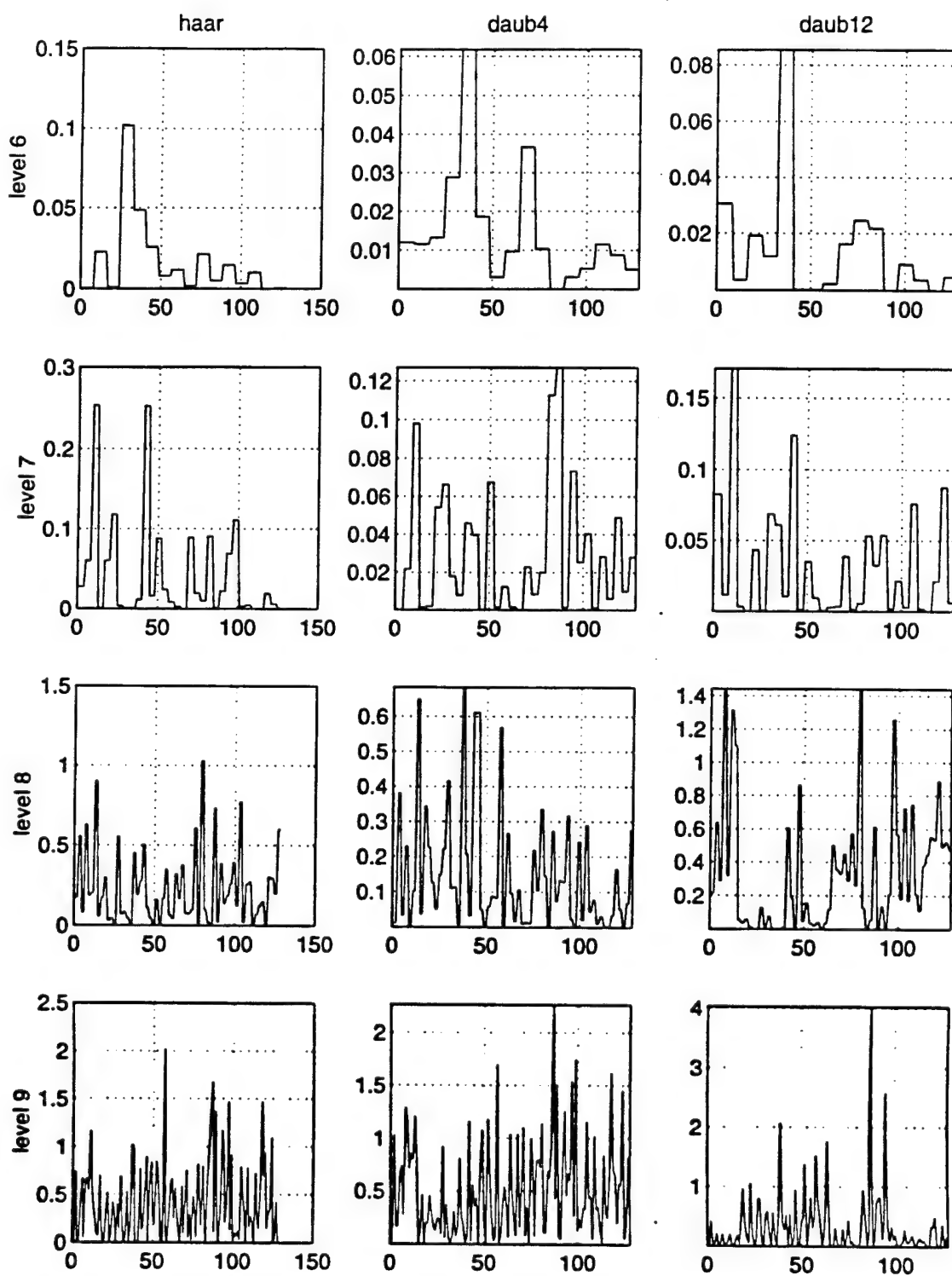


Figure B37. DWT of FSK, SNR = 3 dB

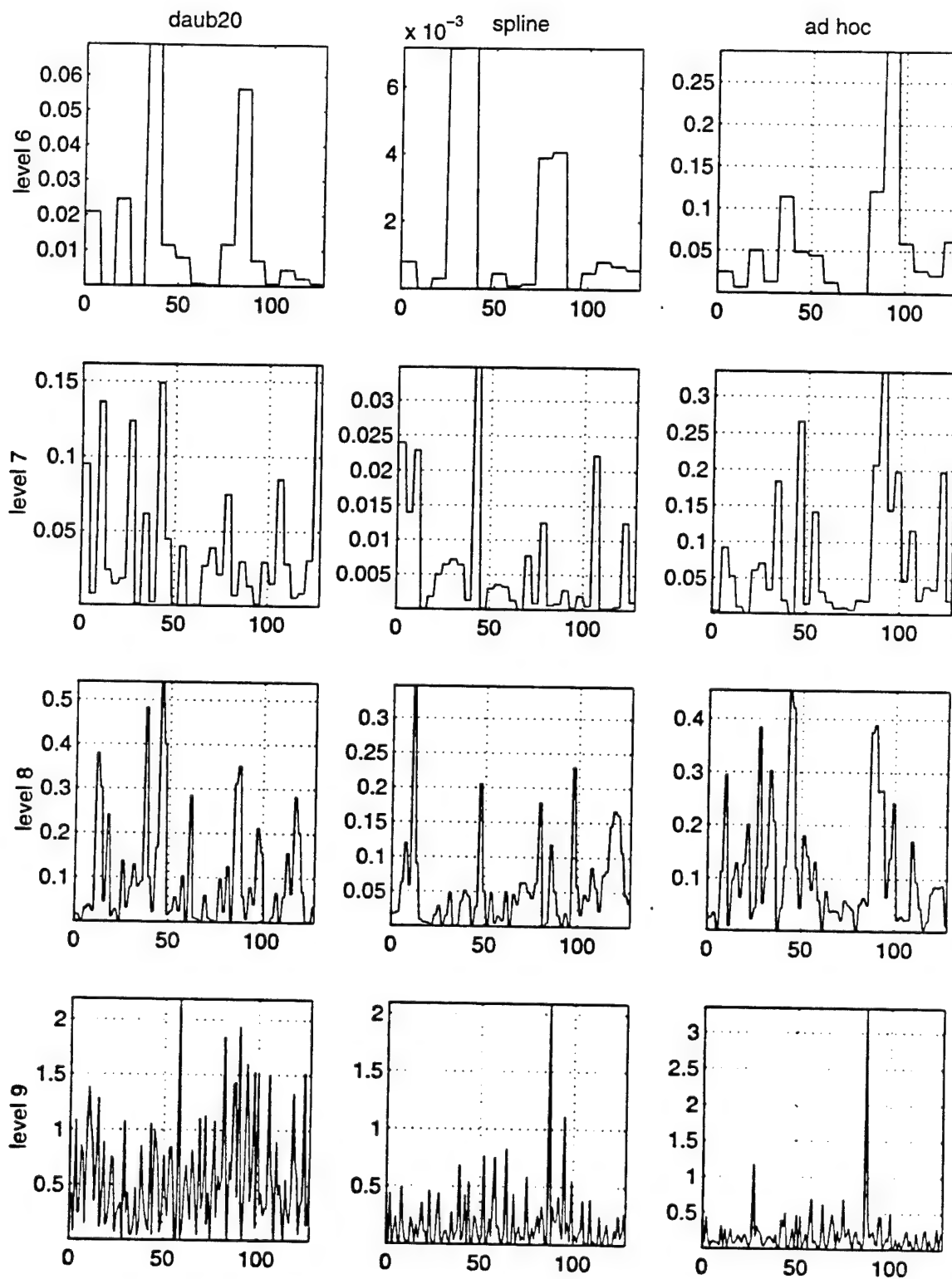


Figure B38. DWT of FSK, SNR = 3 dB

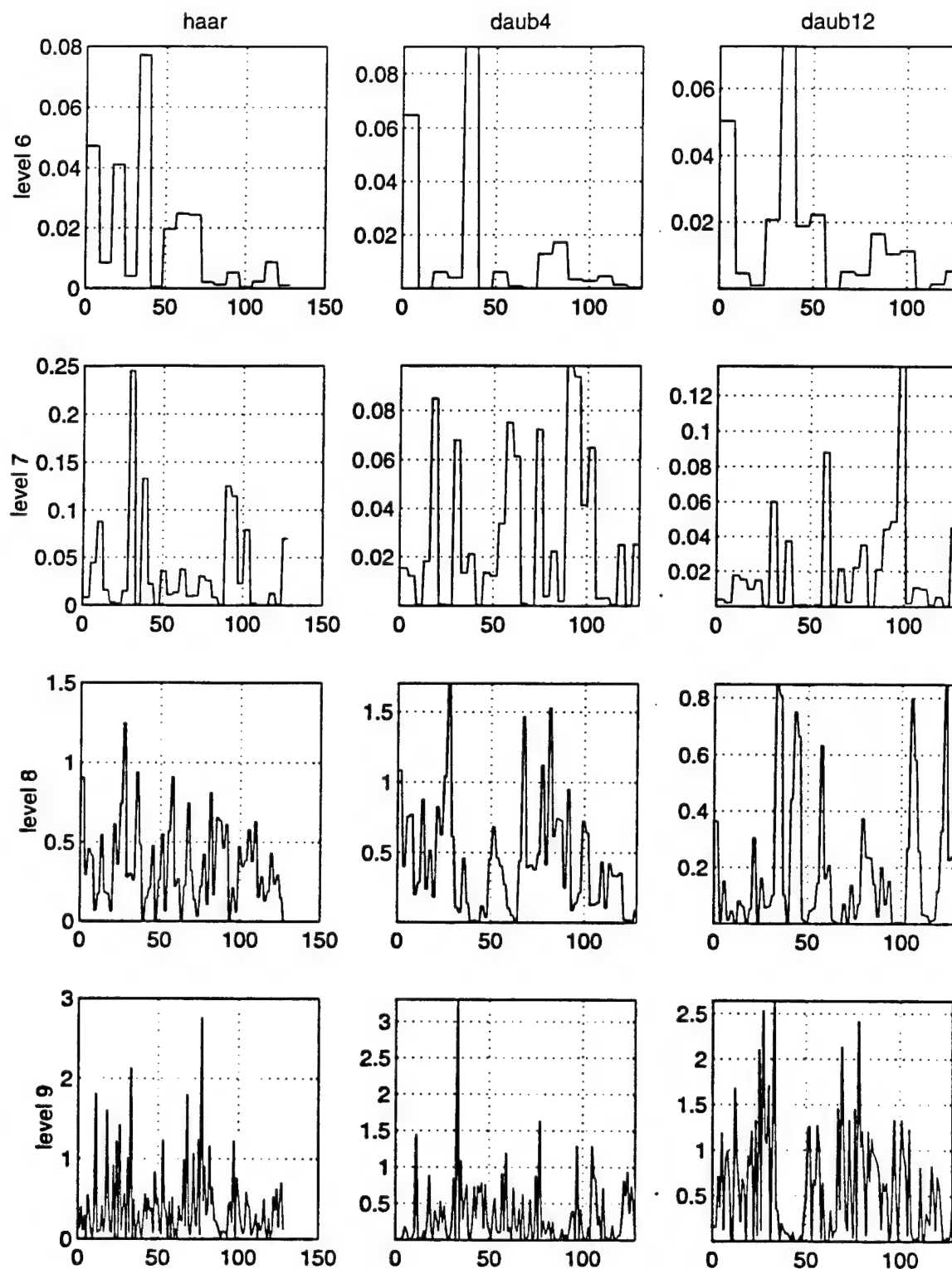


Figure B39. DWT of QPSK, SNR = 3 dB

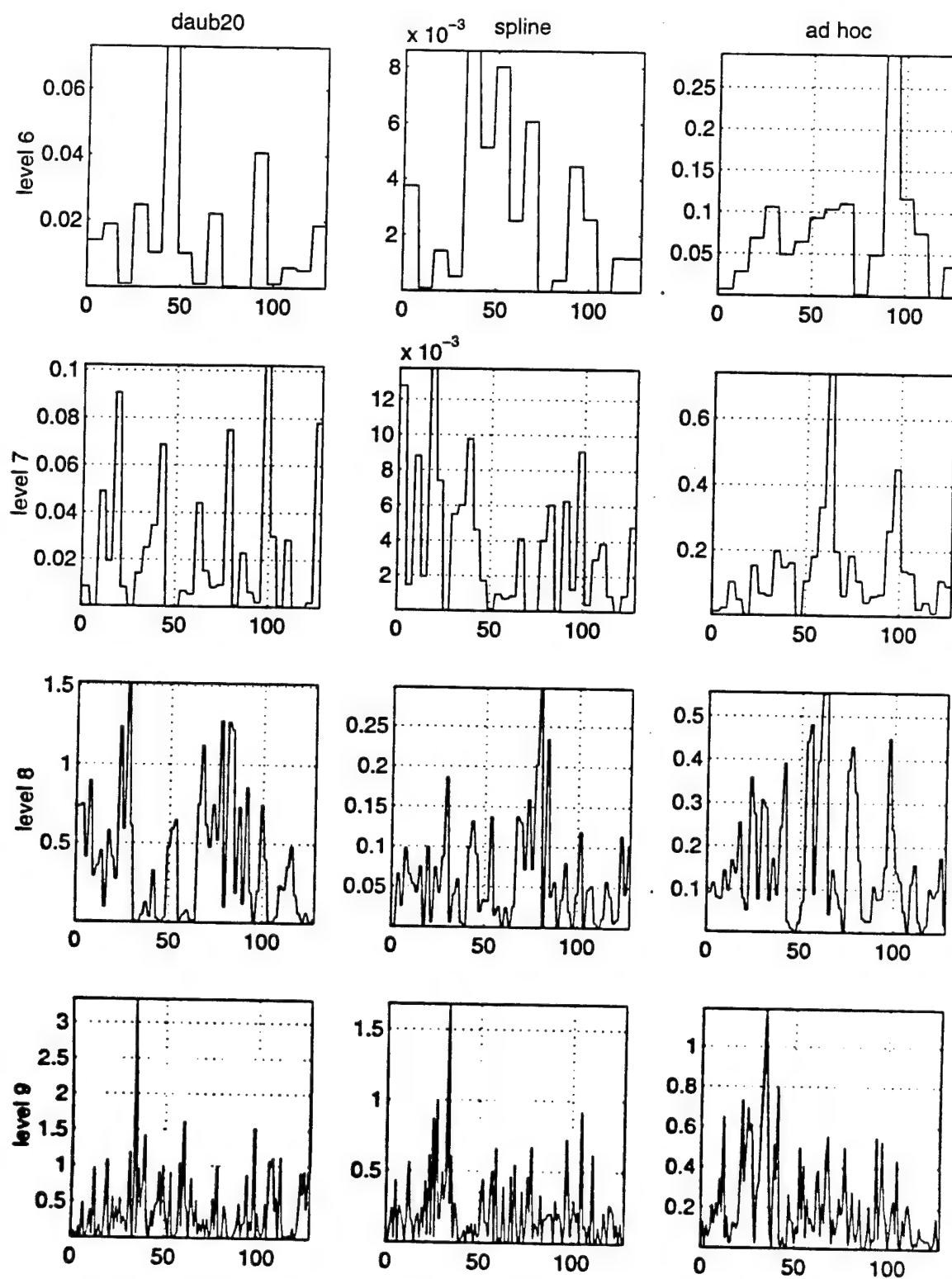


Figure B40. DWT of QPSK, SNR = 3 dB

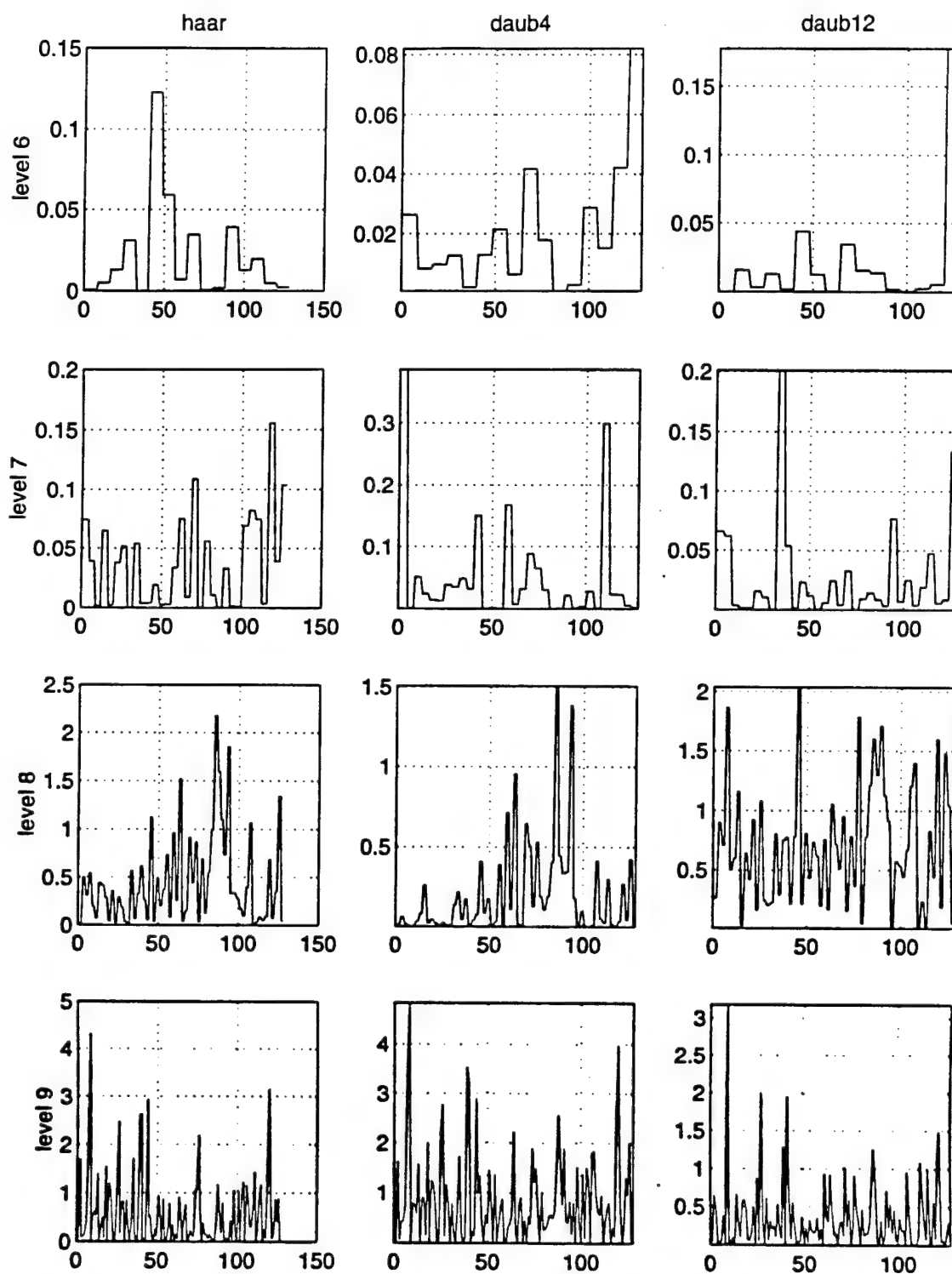


Figure B41. DWT of BPSK, SNR = 0 dB

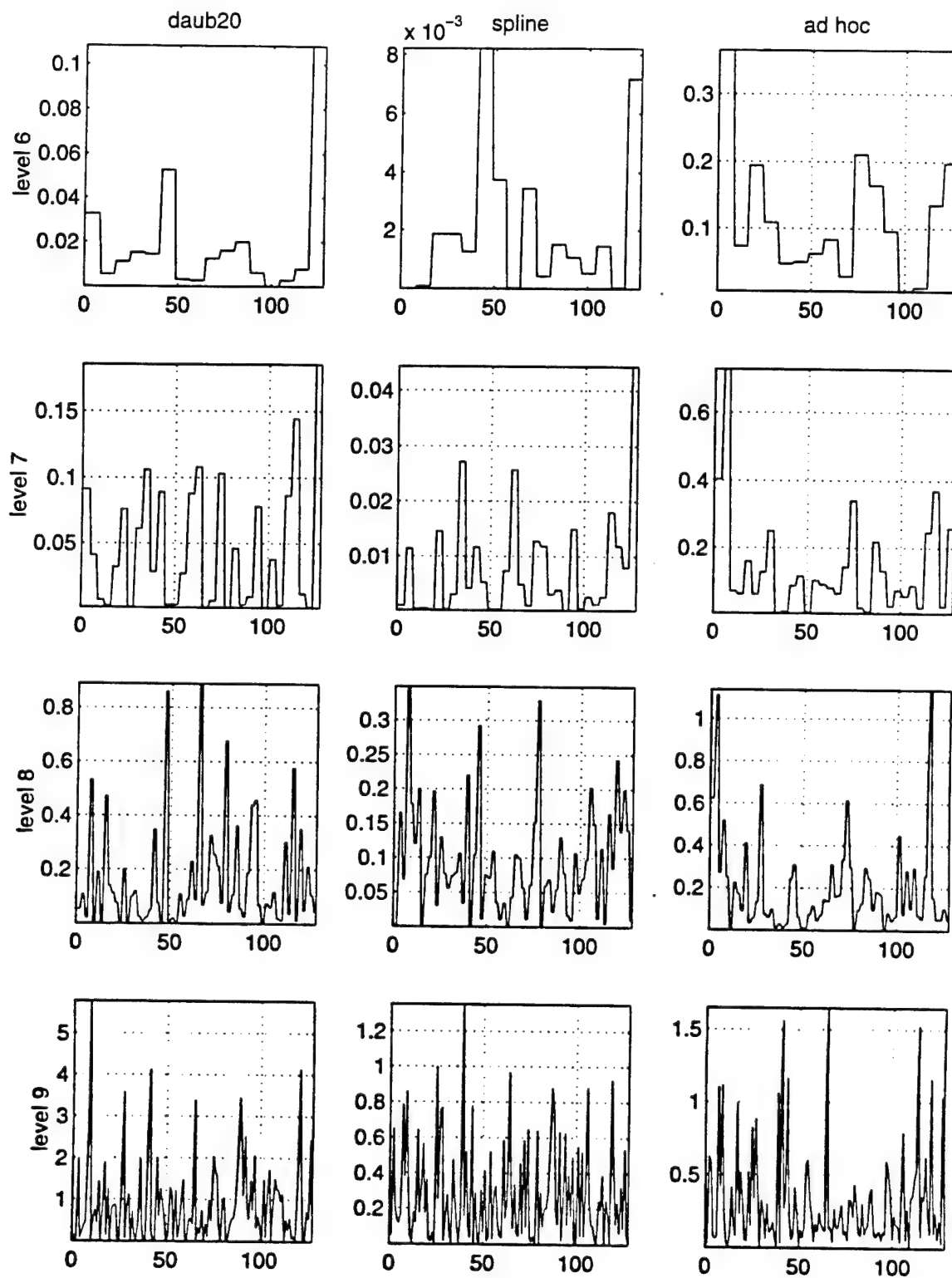


Figure B42. DWT of BPSK, SNR = 0 dB

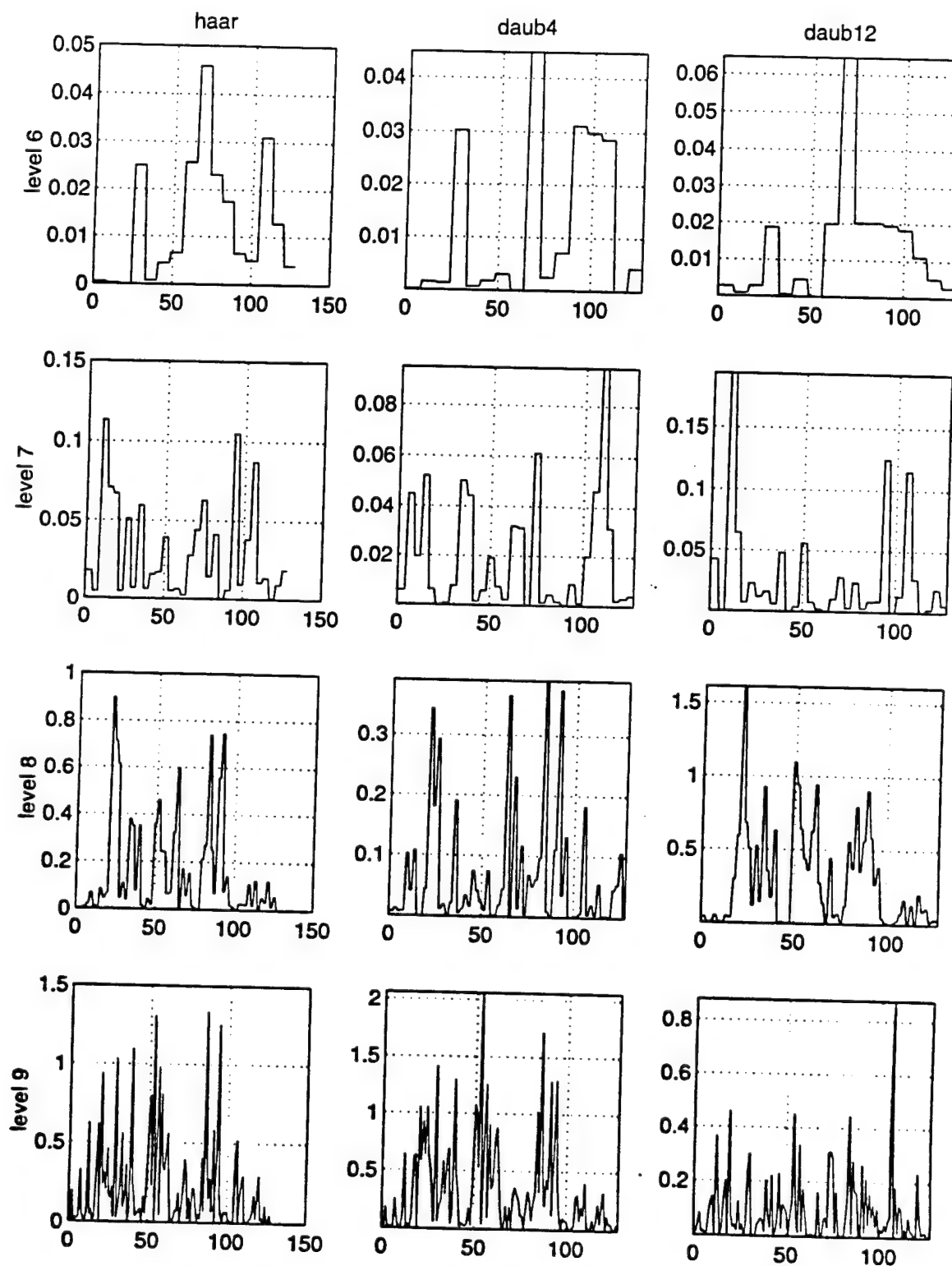


Figure B43. DWT of OOK, SNR = 0 dB



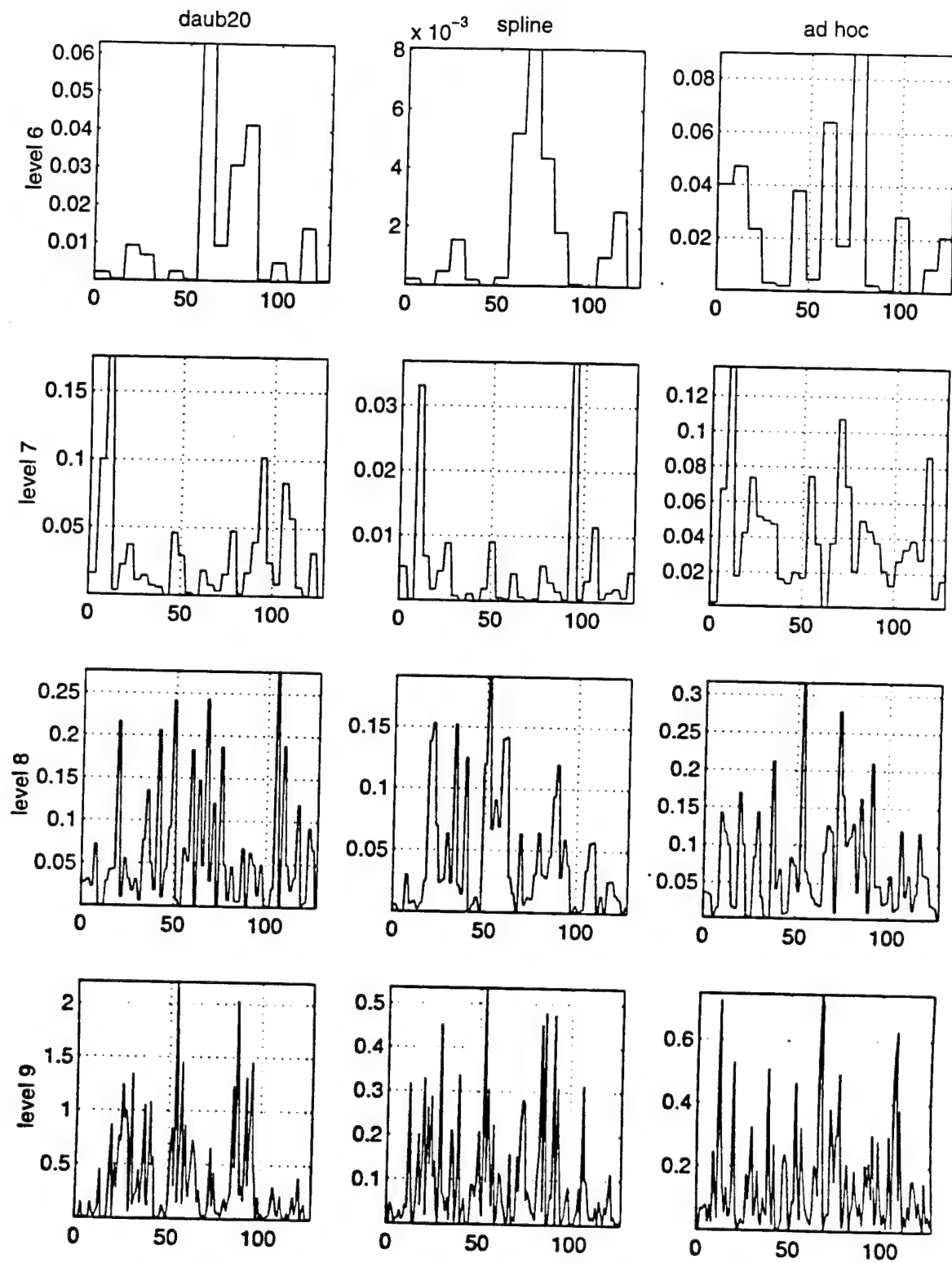


Figure B44. DWT of OOK, SNR = 0 dB

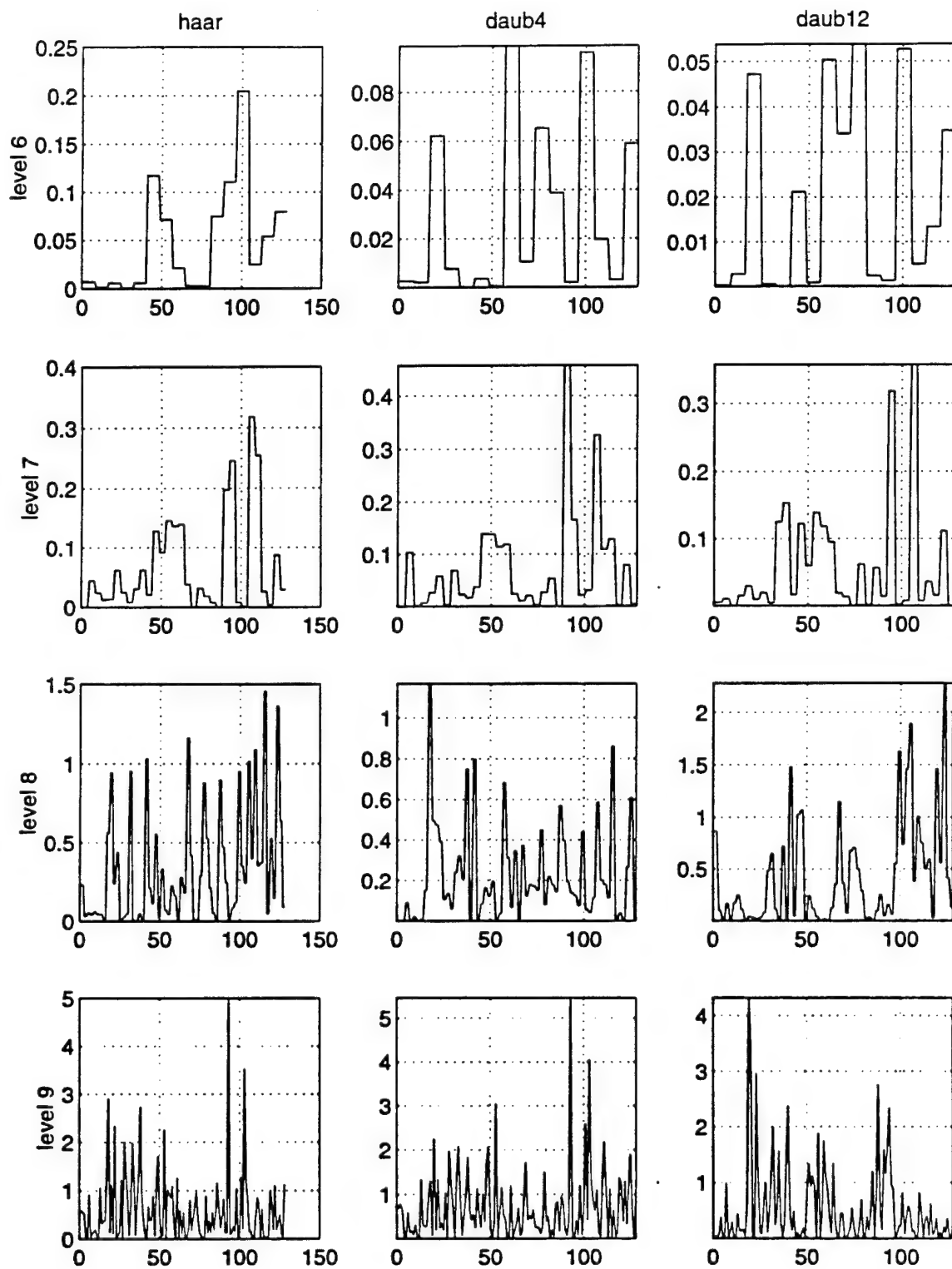


Figure B45. DWT of FSK, SNR = 0 dB

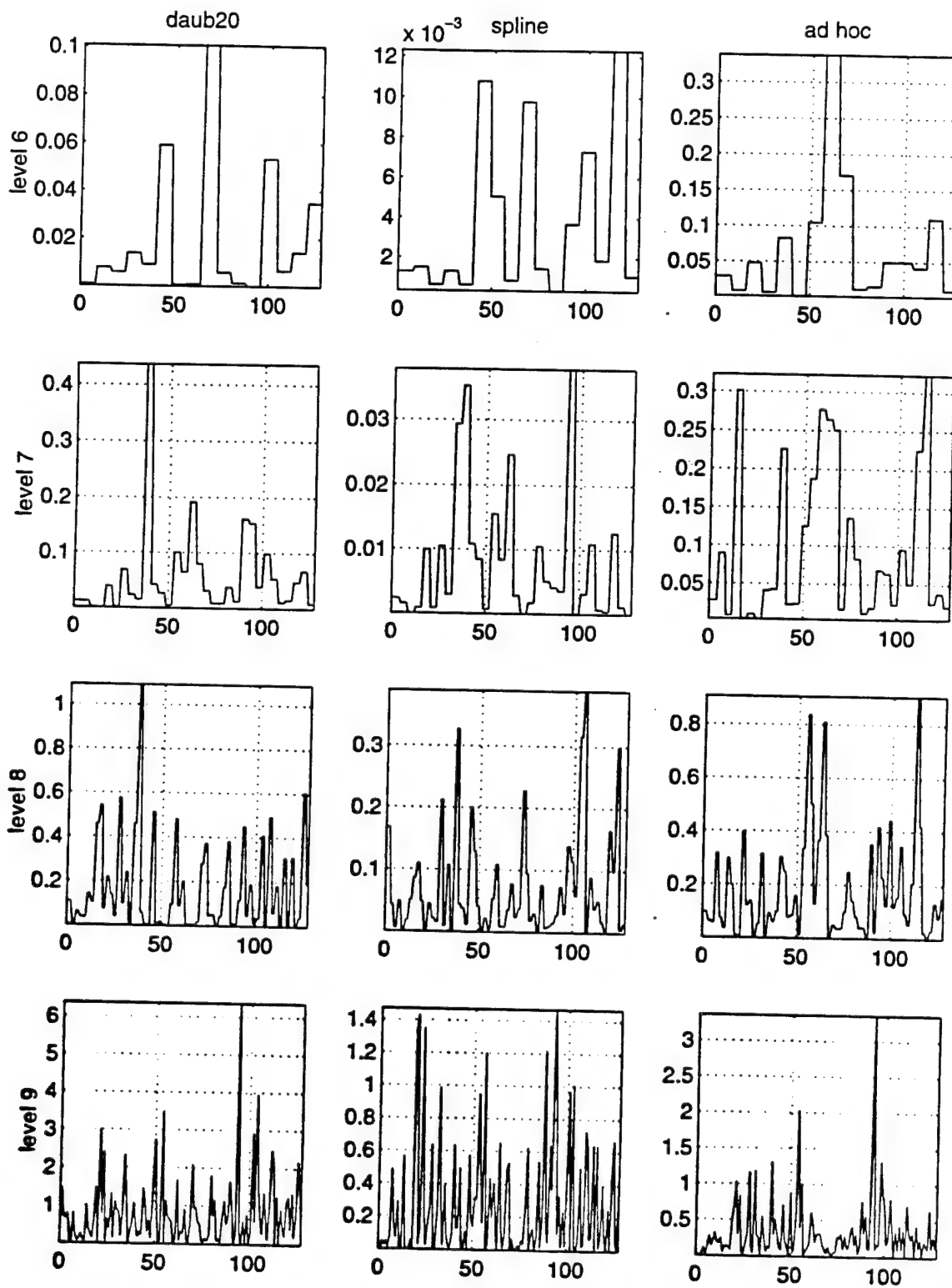


Figure B46. DWT of FSK, SNR = 0 dB

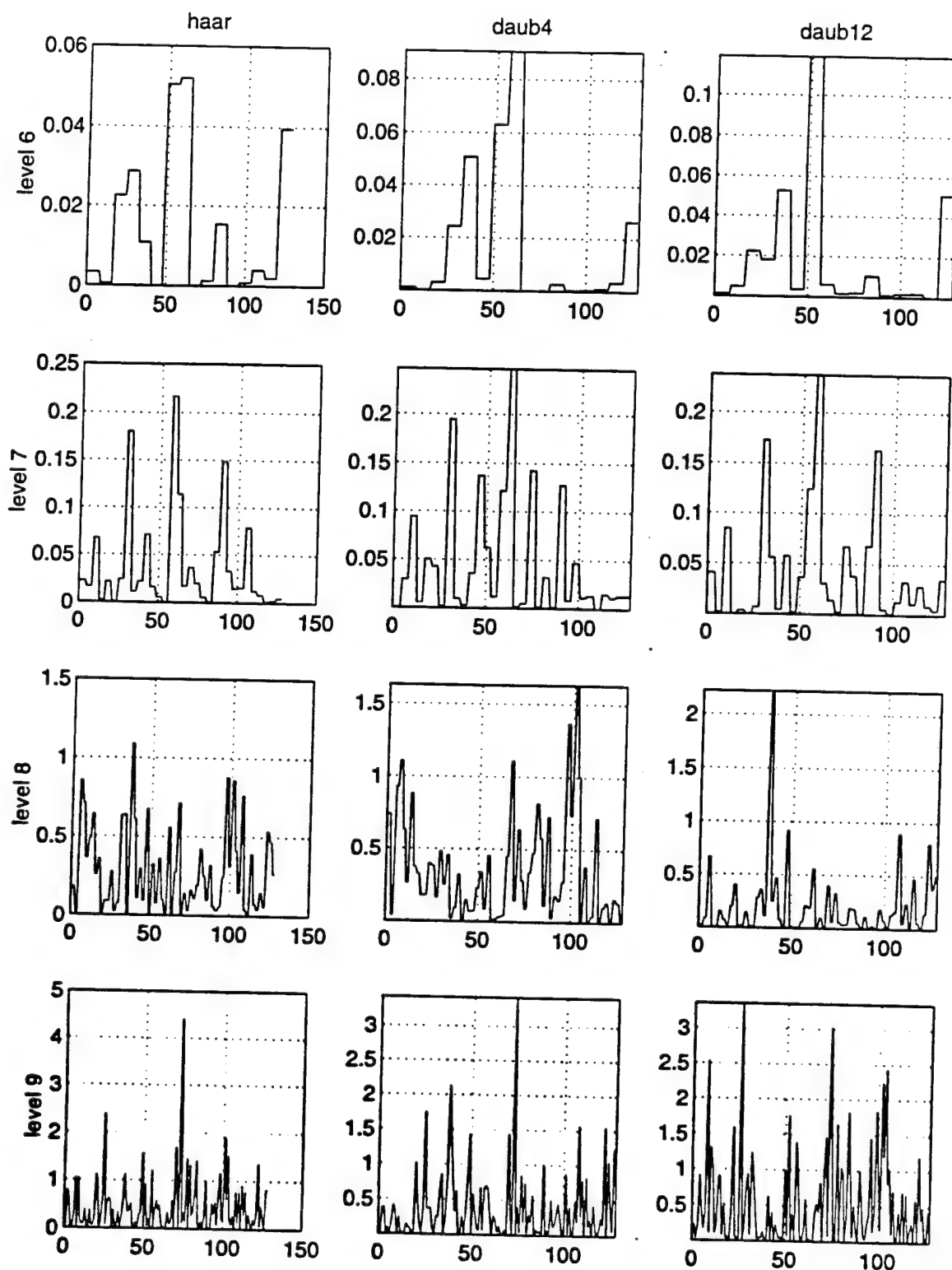


Figure B47. DWT of QPSK, SNR = 0 dB

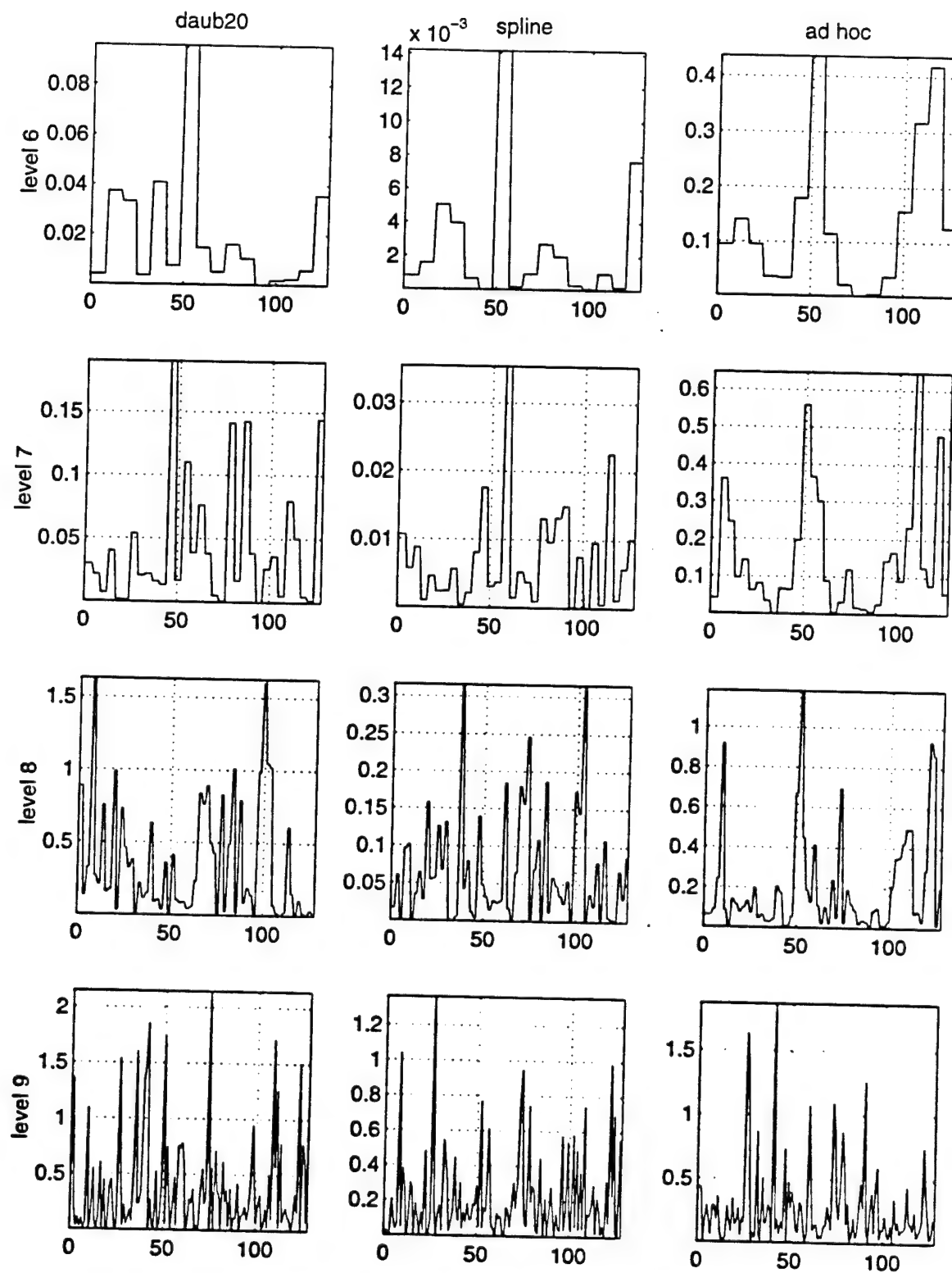


Figure B48. DWT of QPSK, SNR = 0 dB

## APPENDIX C. MATLAB CODES

### **mapdn.m**

#### **Purpose:**

Computes a two-dimensional array  $A$  which defines the mean square map for a dimensional function  $f$ .

#### **Synopsis:**

$A = \text{mapdn}(f, N, \text{type})$ .

#### **Description:**

Uses  $a = \text{wavedn}(f, N, \text{type})$  to compute the wavelet transform of  $f$ , which is a sequence of length  $2n$ ; then reorders and arranges the square of elements (  $1:2n$  ) to form the two-dimensional array  $A$ , which has  $n+1$  rows and  $2(n-1)$  columns; the volume under this surface is proportional to the mean-square value of  $f$ , using four mother wavelets: Haar, Daubechies, Spline and the *ad hoc*.

#### **Algorithm:**

The elements of the wavelet transform  $a$  are recorded according to the strategy described in Ref. 12, Chapter 17, so that when the matrix  $A$  is formed each element (squared) is located at the center of the wavelet it represents.

#### **Limitations:**

Restricted to even values of  $N$  in the range 2 to 20 for Daubechies' wavelet functions, being  $N = 2$  the call for the Haar wavelet function and  $N = 4$  to the *ad hoc* wavelet function. No limitation for the number of spline function coefficients.

**Modifications:**

Addition of two other types of wavelet functions to be used: spline and *ad hoc*.

Plotting subroutine appended to the end of the program.

```
function A = mapdn(f,N,type)
%
% Copyright (c) D. E. Newland 1992
% All rights reserved
%
% Modified by Jorge Pitta, by permission from the author.
%
M = length(f);
n = round(log(M)/log(2))
a = wavedn(f,N,type);
b(1) = a(1);b(2) = a(2);
for j = 1:n-1
    for k = 1:2^j
        index = 2^j+k+N/2-1;
        while index > 2^(j+1),index = index-2^j;end
        b(index) = a(2^j+k);
    end
end
a = b;
for j = 1:2^(n-1)
    A(1,j) = a(1);
end
for j = 2:n+1
    for k = 1:2^(j-2)
        for m = 1:2^(n-j+1)
```

```

    A(j,(k-1)*2^(n-j+1)+m) = a(2^(j-2)+k);
end
end
end
A = A.*conj(A);

%% Printing Subroutine

subplot((n+1)/2,2,1),plot(abs(f),'r'),title('signal-DAUB-COEFFS'),
ylabel('f(x)'),xlabel('x'); grid
hold on
for h = 2:1:n+1
    subplot((n+1)/2,2,h),plot(A(h,:), 'r'),grid,ylabel(['level ', num2str(h-2)])
end
hold off

```



## **wavedn**

### **Purpose:**

Wavelet Transform.

### **Synopsis:**

`a = wavedn(f,N,type).`

### **Description:**

Returns an array whose elements are the wavelet transform of the sequence of elements in *f*. The analysing wavelet has *N* even coefficients.

### **Algorithm:**

It is the Mallat's Pyramid Algorithm adapted to a circular form.

### **Limitations:**

It is necessary for the sequence *f* to have  $2n$  elements, where *n* is an integer number. Its transform *a* also has  $2n$  elements. The wavelet's coefficients are imported from the file `dcoeffs.m` ( for the Haar and Daubechies wavelets), `dcoeffs1.m` ( for the Spline wavelet ) and `dcoeffs2.m` ( for the *ad hoc* wavelet ).

If the sequence *f* is complex, then the transform *a* is also complex.

### **Modifications:**

Addition of a third local variable called *type* that determines the type of wavelet function.

Addition of three IF statements to use with the local variable *type*.

```
function a = wavedn(f,N,type)
```

```
%
```

```
% Copyright (c) D. E. Newland 1992
```

```
% All rights reserved
```

```

% Modified by Jorge Pitta, by permission from the author.
%
M = length(f);
n = round(log(M)/log(2));
if type == 1; c = dcoeffs(N); end
if type == 2; c = dcoeffs1(N); end
if type == 3; c = dcoeffs2(N); end
clr = fliplr(c);
for j = 1:2:N-1 , clr(j) = -clr(j) ; end
a = f;
for k = n:-1:1
    m = 2^(k-1);
    x = [0]; y = [0];
    for i = 1:m
        for j = 1:N
            k(j) = 2*i-2+j;
            while k(j) > 2*m , k(j) = k(j)-2*m ; end
        end
        z = a(k);
        [mr,nc] = size(z);
        if nc > 1 , z = z' ; end
        x(i) = c*z;
        y(i) = clr*z;
    end
    x = x/2 ; y = y/2 ;
    a(1:m) = x;
    a(m+1:2*m) = y;
end

```

## **dcoeffs.m**

### **Purpose:**

Generates the Haar wavelet coefficients for  $N = 2$  and the  $N$ th order Daubechies' wavelet coefficients up to  $N = 20$ .

### **Synopsis:**

`c = dcoeffs(N).`

### **Description:**

It is called by `a = wden(f,N,type)` for providing the  $N$  Daubechies wavelet coefficients.

### **Limitations:**

Restricted to even values of  $N$  in the range 2 to 20.

%

% Copyright (c) D. E. Newland 1992

%

% All rights reserved

%

function c = dcoeffs(N)

%

if N == 2

c = [1 1];

end

if N == 4

c = [(1+sqrt(3))/4 (3+sqrt(3))/4 (3-sqrt(3))/4 (1-sqrt(3))/4];

end

if N == 6

q = sqrt(10);s = sqrt(5+2\*q);

c = [(1+q+s)/16 (5+q+3\*s)/16 (5-q+s)/8 (5-q-s)/8 (5+q-3\*s)/16 (1+q-s)/16];

end

if N == 8

c = [.3258030428051 ,1.010945715092 .892200138246,-.039575026236, -  
.264507167369,.043616300475,.046503601071,-0.14986989330];

end

if N == 10

c = [.226418982583,.853943542705,1.024326944260,.195766961347,-.342656715382,  
-.045601131884,.109702658642,-.008826800109,-.017791870102,.004717427938];

end

if N == 12

c = [.157742432003, .699503814075, 1.062263759882, .445831322930,  
-.319986598891,-.183518064060,.137888092974,.038923209708,  
-.044663748331,.000783251152,.006756062363,-.001523533805];

end

if N == 14

c = [.110099430746,.560791283626,1.031148491636,.664372482211,  
-.203513822463,-.316835011281,.100846465010,.114003445160,  
-.053782452590;-.023439941565,.017749792379,.000607514996,  
-.002547904718,.000500226853];

end

if N == 16

```
c = [.076955622108,.442467247152,.955486150427,.827816532422,  
    -.022385735333,-.401658632782,.000668194093,.182076356847,  
    -.024563901046,-.062350206651,.019772159296,.012368844819,-  
    .006887719256,-.000554004548,.000955229711,-.000166137261];
```

end

if N == 18

```
c = [.053850349589,.344834303815,.855349064359,.929545714366,  
    .188369549506,-.414751761802,-.136953549025,.210068342279,  
    .043452675461,-.095647264120,.000354892813,.031624165853,  
    -.006679620227,-.006054960574,.002612967280,.000325814672,  
    -.000356329759,.000055645514];
```

end

if N == 20

```
c=[.037717157593,.266122182794,.745575071487,.973628110734,.39763774177;,  
    -.353336201794,.277109878720,.180127448534,.131602987102,.100966571196,  
    .041659248088,.046969814097,.005100436968,.015179002335,.001973325365,  
    .002817686590,-.000969947840,-.000164709006,.000132354366,-.000018758416];
```

end

## **dcoeffs1.m**

### **Purpose:**

Generates spline wavelet coefficients for any integer  $N > 1$ .

### **Synopsis:**

`c = dcoeffs1(N).`

### **Description:**

It is called by `a = waden(f,N,type)` for providing the  $N$  spline wavelet coefficients.

### **Limitations:**

None.

%

% Created by Jorge Pitta, 1994

`function c = dcoeffs1(N)`

%

`c = triang(N)';`

## **dcoeffs2.m**

### **Purpose:**

Generates the *ad hoc* wavelet coefficients for any integer  $N = 4$ .

### **Synopsis:**

`c = dcoeffs2(N).`

### **Description:**

It is called by `a = waden(f,N,type)` for providing the fourth order *ad hoc* wavelet coefficients.

### **Limitations:**

Limited to only a fourth order *ad hoc* wavelet function.

%

% Created by Jorge Pitta, 1994

function c = dcoeffs2(N)

%

`c = [.5 1 .5 1];`

## **filtspec.m**

### **Purpose:**

Generates the spectrum response plot of the Haar,  $n^{\text{th}}$  order Daubechies', spline and *ad hoc* wavelet function and their dilations.

### **Synopsis:**

filtspec.

### **Description:**

It calls subroutines t1.m ( for the Haar and Daubechies' wavelets ), t2.m ( for Spline wavelets ), t3.m ( for the Ad Hoc wavelet ).

Created by Jorge Pitta, 1994.

```
F = menu('Wavelet','Daubechies','Spline','Ad Hoc','Own');
```

```
if F == 1;t1;end
```

```
if F == 2;t2;end
```

```
if F == 3;t3;end
```

```
x=[1 zeros(1,1023)];n=0:511;
```

```
N=length(G);
```

```
for nn=1:N
```

```
H(nn)=((-1)^nn)*G(N+1-nn);
```

```
end
```

```
w=filter(H,1,x);e=filter(G,1,x);
```

```
W=abs(fftshift(fft(w,1024)));E=abs(fftshift(fft(e,1024)));
```

```
W1=W(513:1024);E1=E(513:1024);
```

```
H2=upsam(H,2);
```



```

A1=fft(H2,1024);
B1=fft(G,1024);
C1=A1.*B1;
H2G=fftshift(C1);
H2G1=abs(H2G(513:1024));

```

```

H4=upsam(H,3);
G2=upsam(G,2);
A2=fft(H4,1024);
B2=fft(G2,1024);
C2=A2.*B2.*B1;
H4G2G=fftshift(C2);
H4G2G1=abs(H4G2G(513:1024));

```

```

H8=upsam(H,5);
G4=upsam(G,3);
A3=fft(H8,1024);
B3=fft(G4,1024);
C3=A3.*B3.*B2.*B1;
H8G4G2G=fftshift(C3);
H8G4G2G1=abs(H8G4G2G(513:1024));

```

```

H16=upsam(H,7);
G8=upsam(G,5);
A4=fft(H16,1024);
B4=fft(G8,1024);
C4=A4.*B4.*B3.*B2.*B1;
H16G8G4G2G=fftshift(C4);
H16G8G4G2G1=abs(H16G8G4G2G(513:1024));

```

```

H32=upsam(H,9);
G16=upsam(G,7);
A5=fft(H32,1024);
B5=fft(G16,1024);
C5=A5.*B5.*B4.*B3.*B2.*B1;
H32G16G8G4G2G=fftshift(C5);
H32G16G8G4G2G1=abs(H32G16G8G4G2G(513:1024));

H64=upsam(H,11);
G32=upsam(G,9);
A6=fft(H64,1024);
B6=fft(G32,1024);
C6=A6.*B6.*B5.*B4.*B3.*B2.*B1;
H64G32G16G8G4G2G=fftshift(C6);
H64G32G16G8G4G2G1=abs(H64G32G16G8G4G2G(513:1024));
m=max(H64G32G16G8G4G2G1);

y=linspace(0,pi,512);subplot(211)
plot(y,H64G32G16G8G4G2G1/m,'k'),hold on
plot(y,H32G16G8G4G2G1/m,'k'),
plot(y,H16G8G4G2G1/m,'k'),
plot(y,H8G4G2G1/m,'k'),
plot(y,H4G2G1/m,'k');
plot(y,H2G1/m,'k');
plot(y,W1/m,'k')
plot(y,E1/m,'k');
hold off

```

## **t1**

### **Purpose:**

Calls the m.file dcoeffs.m for supplying filtspec.m with the Haar and Daubechies wavelet coefficients.

### **Synopsis:**

t1.

### **Description:**

Produces a *pop-up* menu on screen with the order of the Daubechies' wavelet to be used, if the order equals two, it calls Haar wavelet coefficients.

Created by Jorge Pitta, 1994.

```
O = menu('Order','2','4','6','8','10','12','14','16','18','20');
ZZ = 2*O;
G = dcoeffs(ZZ)/sqrt(2);
for zz = 1:ZZ
H(zz) = ((-1)^zz)*G(ZZ+1-zz);
end
KK = 'Daub';
```

## **t2**

### **Purpose:**

Calls the m.file dcoeffs1.m for supplying filtspec.m with the Spline wavelet coefficients.

### **Synopsis:**

t2.

### **Description:**

Produces a *pop-up* menu on screen with the order of the Spline wavelet to be used, if the

Created by Jorge Pitta, 1994..

```
O = menu('Order','2','4','6','8','10','12','14','16','18','20');
ZZ = 2*O;
G = dcoeffs1(ZZ)/sqrt(2);
for zz = 1:ZZ
H(zz) = ((-1)^zz)*G(ZZ+1-zz);
end
KK = 'Spline';
```

**t3**

**Purpose:**

Calls the m.file dcoeffs2.m for supplying filtspec.m with *ad hoc* wavelet coefficients.

**Synopsis:**

t3.

**Description:**

Produces a *pop-up* menu on screen with the order of the *ad hoc* wavelet to be used.

However, it is limited to an order 4.

Created by Jorge Pitta, 1994.

```
ZZ = 4;
G = dcoeffs2(ZZ)/sqrt(2);
for zz = 1:ZZ
H(zz) = ((-1)^zz)*G(ZZ+1-zz);
end
KK = 'Weird';
```



## LIST OF REFERENCES

- [1] D. Gabor, "Theory of Communication," *Journal of IEE*, Vol. 93, pp. 429-457, 1946.
- [2] A. N. Akansu and R. A. Haddad, *Multiresolution Signal Decomposition*, Academic Press, Inc., San Diego, CA, 1992.
- [3] J. S. Lim and A. V. Oppenheim, *Advanced Topics in Signal Processing*, Prentice Hall, Englewood Cliffs, NJ, 1988.
- [4] O. Rioul and M. Vetterli, "Wavelets and Signal Processing," *IEEE SP Magazine*, pp. 14-38, October, 1991.
- [5] H. J. Barnard, "Image and Video Coding Using a Wavelet Decomposition," Ph.D. Thesis, Technische Universitet Delft, 1994.
- [6] R. J. Duffin and A. C. Schaeffer, "A Class of Nonharmonic Fourier Series," *Transactions of American Mathematics Society*, Vol. 72, pp. 341-366, 1952.
- [7] I. Daubechies, "The Wavelet Transform, Time-Frequency Localization and Signal Analysis," *IEEE Transactions on Information Theory*, Vol. 36, pp. 961-1005, September, 1990.
- [8] I. Daubechies, "Ten Lectures on Wavelets," *SIAM*, Philadelphia, PA, 1992.
- [9] B. Jawerth and W. Sweldens, "An Overview of Wavelet Based Multiresolution Analysis," Department of Mathematics, University of South Carolina, SC, 1994.
- [10] C. S. Burrus and R. A. Gopinath, "Introduction to Wavelets and Wavelet Transforms," notes from the ICASSP 93, Minneapolis, MN, April 1993.
- [11] W. A. Brooks, Jr., "Ultra Wideband Radar Transient Signal Detection Using Time-Frequency and Wavelet Transforms," Master's Thesis, Naval Postgraduate School, Monterey, CA, December, 1992.

- [12] D. E. Newland, *An Introduction to Random Vibrations, Spectral and Wavelet Analysis*, Longman Scientific & Technical, John Wiley & Sons Inc., New York, NY, 1992.
- [13] S. Mallat, "A Theory for Multiresolution Signal Decomposition: The Wavelet Representation," *IEEE Transactions in Pattern Analysis and Machine Intelligence*, Vol. 11, pp. 674-693, 1989.
- [14] P. G. Battle, "A Block Spin Construction of Ondelettes. Part I: Lemarié Functions," *Comm. Math. Physics*, Vol. 110, pp. 601-615, 1987.
- [15] W. H. Press, S. A. Teukolski, W. T. Vetterling, and B. P. Flannery, *Numerical Recipes in C, The Art of Scientific Computing*, Second Edition, Cambridge University Press, New York, NY, 1992.
- [16] C.Yayci, "Higher Order Spectra and Their Use in Digital Communication Signal Estimation," Master's Thesis, Naval Postgraduate School, Monterey, CA, September, 1994.
- [17] Mathworks, *MATLAB Reference Guide*, August, 1992.
- [18] M. J. Smith and T. P. Barnwell, "Exact Reconstruction Techniques for Tree Structure Subband Coders," *IEEE Transactions on ASSP*, Vol. 34, pp. 434-441, 1986.

## INITIAL DISTRIBUTION LIST

- |    |   |            |
|----|---|------------|
| 1. | Defense Technical Information Center<br>Cameron Station<br>Alexandria, Virginia 22304-6145  | 2          |
| 2. | Library, Code 52<br>Naval Postgraduate School<br>Monterey, California 93943-5101  | 2<br><br>1 |
| 3. | Chairman, Code EC<br>Department of Electrical and<br>Computer Engineering<br>Naval Postgraduate School<br>Monterey, California 93943-5121                       | 1          |
| 4. | Professor Ralph Hippenstiel, Code EC/Hi<br>Department of Electrical and<br>Computer Engineering<br>Naval Postgraduate School<br>Monterey, California 93943-5121 | 3          |
| 5. | Professor Monique Fargues, Code EC/Fa<br>Department of Electrical and<br>Computer Engineering<br>Naval Postgraduate School<br>Monterey, California 93943-5121   | 1          |
| 6. | Professor Gurnam Gill, Code EC/GI<br>Department of Electrical and<br>Computer Engineering<br>Naval Postgraduate School<br>Monterey, California 93943-5121       | 1          |
| 7. | LCDR Jorge Pitta<br>Brazilian Naval Commission<br>4706 Wisconsin Avenue, N.W.<br>Washington, D.C., 20016  | 1          |